The surface-atmosphere exchange of ammonia and sulphur dioxide

Daniela Famulari

Doctor of Philosophy

The University of Edinburgh

2005

Acknowledgements

I'd like to acknowledge funding of this work from NERC through the GANE project. The work was carried out jointly between the University of Edinburgh and Centre for Ecology and Hydrology (CEH), Scotland, UK.

Many people have contributed in different ways to this work, and I would like to thank them.
First of all, thanks to both my supervisors, David Fowler and Keith Weston, for having given me the opportunity to do this, for all the inspiration, enthusiasm, patience and encouragement they gave me through these years.

I would also like to thank Mhairi Coyle, Ken Hargreaves and Eiko Nemitz for their help, support and advice on instrumentation and data analysis. Ron Smith and Massimo Vieno for their contribution and help with the modelling. George Rutherford for the precious teachings and kind assistance specially in the first stage of my work; Chiara Di Marco for the great help she gave me on the field and for the sisterhood that we share. Thanks to Robert Storeton-West and Sim Tang for the great field work and chemical analysis of the TAG data.

Thanks to Maeve O'Donoghue and Tim Lenton for bringing the sun everyday in the office despite the Scottish weather, and for their caring friendship.
A big thank-you to my colleagues and friends, for the various forms of support they showed me through these years, specially Marsailidh Twigg, Genevieve Patenaude, Stephanie Jones, Jennifer Muller, Cecile Bacles, Alan McDonald, Nicole Swiercowski, Tristan Bantock and Peter Levy.
And finally special thanks to my parents, and to my friends Gula and Bigio, for always being there, far-away and yet so close.

I'd like to dedicate this work to some exceptional people: Gabriella Tognoli, Anna Grando and Wei-Shin Chang, whose teachings always guide me through each step of my life.

Abstract

Field measurements of the surface-atmosphere exchange of SO_2 and NH_3 have been made using two very different micrometeorological methods, a long-term averaging method based on flux-gradient principles and an eddy covariance method, using a tunable diode laser fast response gas analysis system. The field data are then applied in surface-atmosphere models to calculate deposition of pollutant gases at the regional scale.

The Time Averaged Gradient system (TAG) has been developed following a prototype implemented during a pilot study in 1998. The main goal of the TAG is to provide direct long-term average (1 to 4 weeks) flux-gradient measurements for a range of trace gas species, between atmosphere and terrestrial surfaces. Over daily periods, atmospheric conditions can range from high stability, where the vertical gradients of ambient concentration are enhanced due to very small diffusivity, to highly unstable conditions, in which concentration gradients are small due to the intense turbulent activity of the surface layer.

By sampling continuously over a long-term period, the large vertical gradients generated by high stability would lead to an over-estimate of the actual flux; therefore it is necessary to avoid the bias due to these processes. To overcome this problem, the TAG system operates conditionally, sampling the micrometeorological variables within a carefully defined range of stability.

A data series of five years, from 1999 to 2003, for SO_2 and a data series of two years, from 2001 to 2003 for NH_3 has been obtained at Auchencorth Moss, a field site in Southern Scotland. The measurements provided a characterisation of the chemical climate, meteorology, turbulent characteristics, as well as deposition-emission rates at the field site. A comparison with a continuous flux-gradient system running in parallel on the same field site allowed the reliability of the TAG system to be quantified: the correlation coefficients for u_* and H show a very good

agreement (above 90% in both cases) between TAG protocol and continuous system suggesting the removal of stable conditions from the sampling period doesn't modify the evaluation of the turbulent fluxes, although it introduces a bias. The SO_2 fluxes calculated omitting stable conditions under-estimate the fluxes of SO_2 measured by the continuous system by providing fluxes that are the 77% of the values estimated with the continuous system.

A second TAG system has been implemented to improve estimates of gradients and reduce uncertainty on the fluxes and to increase the data coverage. It has been tested on the Easter Bush field site (Southern Scotland) measuring NH_3 fluxes from autumn 2001 to spring 2003.

Field measurements of NH_3 fluxes using an eddy covariance technique were made for a total of 60 days between July and October 2002 at intensively managed grassland in Southern Scotland. The collected data demonstrate the suitability of a Tuneable Diode Laser Absorption Spectroscopy (TDLAS) system coupled with a sonic anemometer for eddy covariance measurements. The novelty of these measurements is the application to ammonia, which has only become measurable using TDLAS techniques recently, because of its small ambient concentration.

Data presented in this work show typical features of the fluxes and concentration for the summer season. NH_3 concentration and flux values are in a similar range to previous studies using flux gradient methods at the same field site, although the particularly wet season reduced the concentration of NH_3 in the air. Measured NH_3 fluxes ranged between -139 and 198 ng m^{-2} s^{-1}, with an average value of 1.66 ng m^{-2} s^{-1} for the summer season in 2002, indicating a small net emission from the vegetation. Spectral analysis of the data shows that the percentage of flux carried by the small eddies (from 0.3 to 2 m) was on average 18%, suggesting that high detection frequency instruments are particularly suitable for estimating NH_3 fluxes between atmosphere and vegetation.

Field measurements of trace gas concentrations combined with a model of the atmosphere-vegetation exchange processes are used to provide regional and country scale deposition maps of a variety of airborne pollutants. The direct measurements of SO_2 and NH_3 fluxes using micrometeorological methods reported here were used to provide parameters for the models and a site specific validation tool. The flux data collected with the TAG instrument over three sites in the UK were used in

two comparisons with the output of process based models applied to national UK data; the first a semi-Lagrangian Long Range Transport model (FRAME) and the second a surface-atmosphere exchange model based on measured concentration fields and climatological meteorology.

Contents

Chapter 1

Background

1.1 Ammonia and sulphur dioxide in the atmosphere: recent history and current situation

Ammonia (NH_3) and sulphur dioxide (SO_2) are two of the most important primary gaseous pollutants present in the atmosphere. Both gases are reactive, soluble species and are emitted by natural as well as anthropogenic activity. They interact with the vegetation both at the external surface level and diffuse through stomata, as it is described in the following paragraphs.

Sulphur emissions mainly arise from combustion of fuels containing S used on a wide scale for domestic and industrial heating, electricity generation and transport. Starting from the 1960's, a concern regarding the impact of atmospheric pollution was raised, especially on sulphur oxidised compounds, depositing on surfaces and causing forest decline and acidification of freshwater.

The 1972 United Nations Conference on the Human Environment in Stockholm signalled the start for active international cooperation to tackle the problem of acidification. Between 1972 and 1977 several studies confirmed the hypothesis that air pollutants could travel several thousands of kilometres before deposition and damage occurred. This also implied that cooperation at the international level was necessary to solve problems such as acidification. In response to these acute problems, the Convention on Long-range Transboundary Air Pollution by 34 Governments and the European Community (EC) was signed in November 1979 in Geneva. The Convention was the first international legally binding instrument to deal with problems of air pollution on a broad regional basis; it lay down the general principles of international cooperation for air pollution abatement, bringing together research and policy. The Convention has been extended by eight protocols:

- The 1999 Protocol to Abate Acidification, Eutrophication and Ground-level Ozone; 31 Signatories and 18 ratifications. Entered into force on 17 May 2005: **Gothenburg Protocol**.
- The 1998 Protocol on Persistent Organic Pollutants (POPs); 23 ratifications parties. Entered into force on 23 October 2003.
- The 1998 Protocol on Heavy Metals; 27 ratifications parties. Entered into force on 29 December 2003.

- The 1994 Protocol on Further Reduction of Sulphur Emissions; 26 Parties. Entered into force 5 August 1998. **Oslo Protocol**.

- The 1991 Protocol concerning the Control of Emissions of Volatile Organic Compounds or their Transboundary Fluxes; 21 Parties. Entered into force 29 September 1997.

- The 1988 Protocol concerning the Control of Nitrogen Oxides or their Transboundary Fluxes; 29 Parties. Entered into force 14 February 1991.

- The 1985 Protocol on the Reduction of Sulphur Emissions or their Transboundary Fluxes by at least 30 per cent; 22 Parties. Entered into force 2 September 1987.

- The 1984 Protocol on Long-term Financing of the Cooperative Programme for Monitoring and Evaluation of the Long-range Transmission of Air Pollutants in Europe (EMEP); 41 Parties. Entered into force 28 January 1988.

The first international protocol to reduce pollutant emissions was held in 1984 and stated a target of 30% reduction in sulphur emission: sulphur was considered to have a major role in acid deposition at the time; in fact, the regulations imposed by the 30% protocol led to monitored decline in atmospheric SO_2 (and consequently SO_4^{2-} in rain), providing clear benefits, especially in Europe.

Later protocols involved further reduction of S emissions and extended controls to N compounds and VOC. The control measures greatly reduced the S emissions in the UK and Europe, as shown in Table 1.1, and as a consequence, ambient concentrations of SO_2 in Europe and North America have declined radically during the last decades.

As an example, some areas in the UK have experienced a reduction in mean annual concentration of a factor 10 from the 1950's-1960's to date. The main impact on the reduction was from the wide scale replacements of coal with natural gas as a fuel for power station uses, but also the domestic, commercial and industrial uses had an important role.

The S input to cropland has also been reduced, leading to fertilizer application of sulphur to sustain crop yield. In natural ecosystems, the sulphur related effects have declined.

The "natural" biogeochemical cycle of N, see [Soderlund and Svensson, 1976] has been disrupted during the last 100 years, as the atmospheric concentrations of

	1970	1980	1990	1991	1992	1993	1994	1995	1996	1997	1998	1999	%99
Comb. in energy prod.													
Public power	1457	1504	1362	1268	1217	1042	881	796	660	513	536	388	65%
Petroleum refining plants	121	131	77	81	73	74	68	71	72	67	49	47	8%
Other comb. & trans.	151	36	21	19	8	7	5	5	5	7	6	8	1%
Comb. in comm/inst/res													
Residential plant	261	113	54	58	52	57	46	34	36	32	27	27	4%
Comm/pub/agri Comb.	226	109	45	43	45	48	40	30	29	24	17	11	2%
Combustion in industry													
Iron & steel comb.	217	64	44	43	33	38	35	33	29	29	23	21	4%
Other ind. comb.	707	388	185	193	217	214	183	140	114	95	81	57	10%
Production processes	47	39	24	21	18	17	15	14	14	13	10	9	1%
Extr./distrib. of fossil fuels	3	3	8	3	4	3	3	3	4	3	3	1	0%
Solvent use	1	1	1	1	1	1	1	3	2	3	3	2	0%
Road transport	22	21	32	29	31	30	32	26	19	14	12	6	1%
Other trans/mach[2]	47	31	24	26	25	24	24	22	23	21	19	18	3%
Waste	2	3	3	3	3	2	2	2	1	1	1	2	0%
By fuel type													
Solid	1837	1571	1385	1337	1288	1085	922	821	679	577	591	437	74%
Petroleum	1273	774	406	374	373	423	361	303	280	194	148	112	19%
Gas	96	47	42	39	30	15	15	15	16	19	15	17	3%
Non-fuel	54	49	45	36	34	31	36	37	32	30	31	29	5%
Total	3259	2440	1877	1784	1724	1553	1333	1174	1005	819	784	594	100%

1 UK emissions reported in IPCC format (Salway, 2001) differ slightly due to the different source categories used.
2 Including railways, shipping, naval vessels, military aircraft and off-road sources

Figure 1.1: UK emission of sulphur by UNECE source category and fuel type, from [NEGTAP, 2001].

the various nitrogen compounds have changed according to changing anthropogenic activities: application of large amounts of fertilizers for intensive agricultural production, intensive farming practices, release of oxidised nitrogen from fossil fuels. During the period from 1870 to 1980, the emissions of ammonia have increased from 2.2 to 4.7 Tg of NH_3 per year, according to [Asman et al., 1988]. In Europe there is considerable concern over agricultural emissions of ammonia since they contribute significantly to total N deposition. In 1999 the UN Economic Commission for Europe (UNECE) developed the Gothenburg Protocol as a measure for reducing acidification, eutrophication and secondary aerosol production processes (see §1.2). For the first time in an international agreement, measures were included to reduce NH_3 emissions from agricultural activities, with possible economic impacts on the agricultural sector [Cowell and ApSimon, 1998]. For the UK, the target set for NH_3 emissions is to reduce by 11% the emissions values estimated in 1990 by year 2010.

The policies for reduction of harmful gases (such as ammonia and sulphur dioxide) are designed to maximise the environment benefit for the agreed extent of emission control: this process is achieved using the *Critical Loads* methodology. When it is not excessive, dry deposition of N compounds may be beneficial to some plant species as it provides nutrients, specially on poor soils with low nitrogen content. Studies across Europe, e.g. [Sutton et al., 1993c, Bobbink et al., 1992, Pitcairn et al., 1991] have shown that eutrophication can cause a shift in species population, promoting the presence of more N-tolerant species to the disadvantage of more N-sensitive species as is the case of heather being overtaken by grass, or the decline of moss population for example in the UK [Hornung et al., 2002].

The eutrophication and acidification damages caused by excessive N and S deposition onto sensitive ecosystems led to the introduction of the critical load concept, which is an estimate of ecosystem sensitivity to pollutant exposure. It was introduced to estimate thresholds for damage by acidification and nutrient loading based on ecosystem characteristics [Sutton et al., 1993e].

Critical loads are defined as *"a quantitative estimate of exposure to one or more pollutants below which significant harmful effects on sensitive elements of the environment do not occur according to present knowledge"*, [Nilsson and Grennfelt, 1988].

Critical loads currently offer the only quantitative methodology to assess environmental impacts of acidifying deposition at national or regional scales. Another indicator used for gaseous atmospheric pollutants is the critical level, which de-

fines the concentration in air of a pollutant experienced by a plant above ground. Critical loads and levels have been used with measured or modelled exposure and deposition data, and they represent the potential for damage of the environment by the pollutants. The gap between estimated deposition following the implementation of a protocol and the critical load or level is revealed as an exceedance and provides an indication of the areas in which pollutants have an effect on the ecosystem.

Assessment models are a useful tool in investigating the impact of long-range transport of the pollutants on natural ecosystems: they require as input inventories of emission, quantified by the magnitude and geographical distribution of sources, [Cowell and ApSimon, 1998][Buijsman et al., 1987].

In the case of NH_3, the modelled assessments present uncertainties due to spatial and temporal variation of ammonia fluxes, peak emissions events and factors controlling the volatilization of ammonia (such as meteorological conditions, soil factors, fertilizer type, management practices).

For SO_2, dry deposition can be simulated using a resistance analogy model, [Fowler and Unsworth, 1979], where empirical values can be used to parameterise the resistance terms (e.g. EMEP, 1998).

The concentration ratio $\frac{[NH_3]}{[SO_2]}$ is spatially very variable, in fact the sources of these two gases are very diverse, being large combustion (power stations, refineries) for SO_2 and mainly livestock farms for NH_3.

1.2 Ammonia as an atmospheric pollutant

Ammonia is a colourless substance, in the gaseous phase at room temperature having the boiling point at -33.4 °C. It is a very reactive gas and very soluble in water, therefore very difficult to measure at environmental concentrations, which are typically of a few ppbV. Because of its alkaline nature, NH_3 is an effective neutralising agent for acidic substances. Although atmospheric NH_3 concentrations are small, ammonia is the most abundant base in the atmosphere, and it is recognised as a major atmospheric pollutant for both its role in tropospheric chemistry and its detrimental effect on ecosystems, e.g.[Sutton et al., 1998].

Ammonia is emitted in the atmosphere primarily from agricultural sources, in particular livestock management, storage and land application of manure and fertiliser [Asman and van Jaarsveld, 1992] [Sutton et al., 1995b]. In the UK, 80% of

	1990	1991	1992	1993	1994	1995	1996	1997	1998	1999	%1999
Agriculture (cultivation with fertiliser)	41	44	34	30	29	25	20	23	22	25	9%
Agriculture (livestock)	223	214	212	214	215	211	211	213	217	215	75%
Combustion (stationary)	5	6	5	5	5	4	4	4	3	4	1%
Combustion (road transport)	1	1	1	3	5	7	10	12	14	16	6%
Fertiliser production	4	4	4	4	4	4	5	3	5	2	1%
Other industrial processes (coke, paper, sugar beet, chemicals)	2	2	2	2	2	2	2	2	2	2	1%
Landfill	4	4	4	4	4	4	4	4	4	4	1%
Other (waste burning, pets, market gardens)	16	16	15	14	14	14	14	14	14	14	5%
Sewage sludge disposal	5	5	5	6	6	6	7	6	6	6	2%
Total	301	296	283	283	284	278	276	281	288	287	

Figure 1.2: Estimates of UK emissions of ammonia in kT-N, from [NEGTAP, 2001].

the total NH_3 emissions derives from agricultural practices [Misselbrook et al., 2000] [Sutton et al., 2000]. Ammonia emissions increased considerably in the last few decades in Europe [ApSimon et al., 1987] [Asman et al., 1988].

In recent work, [Misselbrook et al., 2000] [Dragosits et al., 1998] estimates of UK ammonia emissions were made, starting from 1990, as is shown in Table 1.2.

1.2.1 Atmospheric processes involving ammonia

NH_3 is lost to the atmosphere by volatilization, that happens through the hydrolysis of urea and/or uric acid (eq.1.1), present in large quantities in animal wastes.

$$CO(NH_2)_2 + 3H_2O \longrightarrow 2NH_4^+ + HCO_3^- + OH^- \tag{1.1}$$

This process occurs for example during the spreading of fertilizers over crops, where a portion of 20% to 70% of total NH_x-N is lost, [RGAR, 1997]. The hydrolisis of urea and uric acid causes an increase of pH values and therefore the emissions from fertilizers based on such substances are greater than emissions from ammonium nitrate fertilizers.

Other processes that cause volatilization of ammonia are: treatment of sewage, land spreading of sewage sludge, biomass burning, incineration of wastes from landfill sites. These practices have a much smaller impact on the total budget in comparison to farming practices, being less than 10% [Sutton et al., 1995b].

After volatilization from mainly low-level agricultural sources, gaseous ammonia is dispersed and advected by the air flow until removal by chemical reactions and/or deposition to the surface. In the gas phase, NH_3 can reach a gas/particle equilibrium with the acidic species of $NH_3/HNO_3/NH_4NO_3$ and $NH_3/HCl/NH_4Cl$ [Allen et al., 1989]. NH_3 may be present in the atmosphere either as gaseous NH_3 or particulate NH_4^+ depending on environmental conditions, in particular temperature and relative humidity.

Other reactions include the absorption of ammonia into wet aerosols or cloud condensation nuclei: also, in clouds NH_3 can act as a catalyst for SO_2 oxidation as it controls the cloud water pH [Behra et al., 1989, Benner et al., 1992].

The main reactions of ammonia are connected to the neutralization of the acidity generated by the species H_2SO_4, HNO_3 (oxidation products of SO_2 and NO_x from urban emissions) and HCl, which lead to the formation of particulate ammonium (NH_4^+), ammonium sulphate ($(NH_4)SO_4$), nitrate (NH_4NO_3) and chloride (NH_4Cl).

The size range of NH_4^+ particles is in the sub-micron order of magnitude; therefore these particles have smaller dry deposition velocities in comparison to the reactive precursor gases and thus travel longer distances before dry or wet deposition [Fowler et al., 1991]. It is by the generation of these particulates that ammonia influences the atmospheric balance, taking part in the transboundary exchange of long-range transported air pollutants [RGAR, 1997]. Particulate NH_4^+ is then deposited on the surface via dry deposition of aerosols or wet deposition in rain, cloud droplets, snow and fog.

Once NH_3 is deposited on the surface, it can produce acidity through the nitrification of NH_4^+ by bacteria in soils (*Nitrobacter and Nitrosomonas*), as:

$$NH_4^+ + 2O_2 \longrightarrow 2H^+ + NO_3^- + H_2O \tag{1.2}$$

After the nitrification, the soil acidity increases, and may enhance the acidifying effects on other deposited acidic species such as SO_2.

The dry deposition of NH_3 onto terrestrial surfaces, the incorporation of NH_3 into acidic aerosols and cloud droplets and the scavenging by precipitation make up the bulk of removal processes for atmospheric NH_3. The combined efficiency of all these concurrent processes determines the atmospheric residence time of NH_3, that is of the order of a few hours.

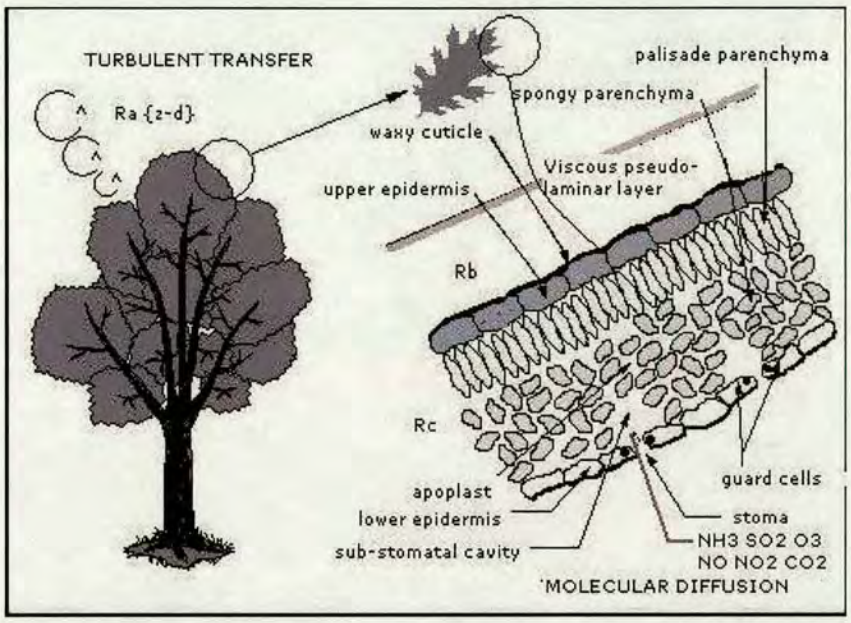

Figure 1.3: The transfer of NH_3 from air to plant: turbulent transport carries the gas from the air mass to the canopy, then molecular diffusion acts at the leaf surface level through stomatal exchange or cuticular absorption, from [Flechard, 1988].

1.2.2 NH_3 exchange between land and atmosphere

The interaction of vegetation with atmospheric NH_3 occurs at different levels: first, turbulent motion in the atmosphere transfers NH_3 to the canopy, then at the plant surface diffusion occurs through stomatal apertures into the sub-stomatal cavity and apoplast or deposition takes place on the wet surface and then transfer through the cuticle (see fig.1.3).

The rate of uptake of NH_3 by leaf cuticular surfaces has been shown to increase with atmospheric relative humidity [Sutton et al., 1995a], while dew or rain-wetted surfaces show substantially smaller canopy resistances, see [Flechard and Fowler, 1998]. In the atmosphere, the removal of NH_3 by gas-to-particle conversion is also a process more likely to occur at significant rates at large relative humidities and cool temperatures, and these conditions are generally associated with wet plant surfaces and reduced canopy resistances to NH_3 dry deposition. Conversely, the evaporation of NH_3 from aerosols is expected to occur mainly in warm weather at lower relative humidities when emission from ground level sources and surface resistance to dry deposition are both largest.

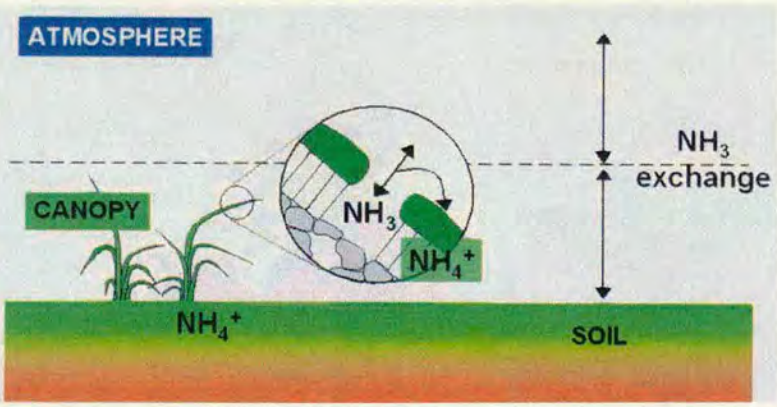

Figure 1.4: Diagram of bi-directional exchange of NH_3, from [NEGTAP, 2001].

The bi-directional exchange dynamics of NH_3 is mainly regulated by: nature of the ecosystem, management practices and atmospheric turbulence. In general, fertilized land acts as a source and due to their low N status, semi-natural ecosystems were generally believed to act as sinks for NH_3 [Duyzer et al., 1992, Sutton et al., 1993a]. However, different studies have proved the bi-directional behaviour of the fluxes for both ecosystems [Milford et al., 2001, Sutton et al., 1993d, Fowler et al., 1998a]. The application of micrometeorological techniques provides a measure of the exchange rate of ammonia between vegetation and the atmosphere; plant canopies can act both as a source or a sink for ammonia, [Fowler and Duyzer, 1989] [Monteith and Unsworth, 1990] [Sutton et al., 1993d].

Emission of NH_3 from semi-natural land occurs mainly in warm conditions and over arable crops with a larger N-content than semi-natural ecosystems. This has been interpreted as the consequence of the existence of a compensation point (χ_{cp}) for NH_3 [Farquhar et al., 1980], with emission from the surface occurring only when the ambient NH_3 concentration is smaller than χ_{cp}. The canopy compensation point represents an alternative way of expressing the existence of a residual concentration at the surface [Sutton and Fowler, 1993].

The direction of the NH_3 flux depends on the difference between the atmospheric and stomatal concentration of NH_3 (see fig. 1.4). The concentration at which absorption and loss processes are balanced, i.e. when the flux is zero, is commonly referred to as the stomatal compensation point, χ_{NH_3} [Farquhar et al., 1980].

Diurnal cycles of stomatal emissions from managed and semi-natural land were described in various studies, e.g. [Milford et al., 2001, Sutton et al., 1993d]. The

respiration activity of plant leaves governs the stomatal activity and therefore the stomatal exchange (stomatal resistance) of NH_3 between atmosphere and plant. During the daytime, stomata are open and if the concentration in the air is lower than the stomatal compensation point, emission of NH_3 occurs, viceversa absorption (deposition) when atmospheric ammonia is higher in concentration than the compensation point.

NH_3 measurement techniques

Detection of NH_3 has proved quite challenging in the past and only relatively recently have new technologies allowed the detection of gaseous ammonia at atmospheric conditions that are suitable for the application of micrometeorological methods to infer fluxes.

In Table 1.1 is shown a summary of the available instrumentation currently used for NH_3 concentration measurements.

Method	Source
Denuders	[Ferm, 1979, Andersen et al., 1993]
Passive Diffusion Samplers	[Svensson and Ferm, 1993][Tang et al., 2001]
Continuous-flow denuder: AMANDA	[Genfa et al., 1989]
(Ammonia Measurement by ANnular	[Wyers and Slanina, 1993]
Denuder sampling with on line Analysis)	[Wyers, 1998]
Thermo-denuder	[Keuken et al., 1988]
Photo fragmentation laser-induced fluorescence	[Schendel et al., 1990]
Differential Optical Absorption	[Sommer et al., 1995]
Spectroscopy (DOAS)	
Chemiluminescence	[Genermont et al., 1998]
NOx monitor with NH_3 converter	[Breitenbach and Shelef, 1973]
	[Van Hove et al., 1987]
Bubblers / Acid traps	[Genermont et al., 1998]
Fourier transform infra-red spectrometry (FTIR)	[Tuazon et al., 1978]
	[Griffith and Galle, 2000]
Tandem mass spectrometer (TMS)	[Shaw and Spicer, 1998]
Tunable diode laser	[Goretty, 1998] [Warland et al., 2001]
Photo acoustic monitor	[Rooth et al., 1990] [Pushkarsky et al., 2002]
Chemical ionization mass spectrometry (CIMS)	[Fehsenfeld et al., 2002] [Nowak et al., 2002]
GRAEGOR, ion chromatography	[Trebs et al., 2004]

Table 1.1: NH_3 concentration measurement techniques.

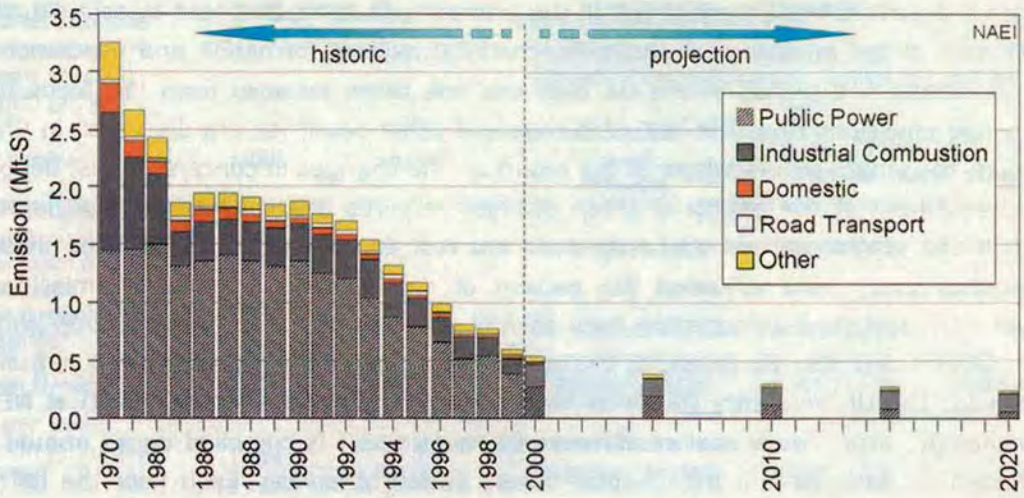

Figure 1.5: UK emission of sulphur from 1970 to 2020. Estimates from 2000-2020 are based on projections using: Department of Trade and Industry fuel demand and economic growth data, regulation of S content in fuel and expected S reduction in the power, refinery and cement industries. From [NEGTAP, 2001]

1.3 SO_2 as an atmospheric pollutant

Sulfur dioxide is a colorless gas with a pungent odor, about 2.5 times as heavy as air. It is a liquid when under pressure, and it dissolves in water very easily. Natural sources of sulphur dioxide include releases from volcanoes, oceans, biological decay and forest fires. The most important man-made sources of sulphur dioxide are fossil fuel combustion, smelting, manufacture of sulphuric acid, conversion of wood pulp to paper, incineration of refuse and production of elemental sulphur. Coal burning is the single largest man-made source of sulphur dioxide accounting for about 50% of annual global emissions, with oil burning accounting for a further 25 to 30%.

The SO_2 emissions profile in Fig. 1.3 shows a steady decline in SO_2 emission rate over the past thirty years [Goodwin et al., 2000].

1.3.1 SO_2 exchange between land and atmosphere

A number of studies on SO_2 deposition processes have shown with direct measurements of SO_2 fluxes the exchange dynamics between air and plants for different environments, such as grassland [Garland et al., 1973], forest [Erisman et al., 1994] and cereal crops [Fowler and Unsworth, 1979]. These studies show the variability

of deposition velocity over different types of vegetative surfaces, ranging from 1 mm s^{-1} to 20 mm s^{-1}.

The major sinks for SO_2 are stomata and external surface of vegetation (see fig.1.3). The stomatal uptake has been shown to behave consistently with the water stomatal exchange (allowing for the difference in molecular diffusivity), therefore the rate of stomatal uptake for SO_2 can be derived from atmospheric concentrations and stomatal conductance.

The external surface of vegetation includes epicuticular wax, surface debris and very often a layer of water. Water present on the leaf surface has a major influence over SO_2 uptake by foliar surfaces; the presence of a water layer does not necessarily need wet atmospheric conditions, as a thin layer of a few molecules depth is sufficient to regulate the reactions.

A very detailed work of simulation and comparison with the measured data of SO_2 deposition events has been reported by [Flechard et al., 1999] using a dynamic canopy compensation point model incorporating the major ion chemistry of the liquid film where the SO_2 is uptaken from the air (see fig.1.3.1).

The vegetation-atmosphere exchange of SO_2, unlike that for NH_3, is mainly deposition. However, from a study over moorland, [Fowler et al., 2001] it emerged that for some short periods SO_2 was released by the plants, and this happened in conditions where the air concentrations dropped from high values to below 0.6 μg m^{-3}.

1.4 Quantifying land-atmosphere exchange of NH_3 and SO_2

The removal from the atmosphere of pollutants occurs by wet and dry deposition. Wet deposition is the removal by precipitation that involves physical and chemical transformation, and dry deposition is the direct deposition as gases and aerosol to terrestrial or marine surfaces [Fowler, 2002].

Atmospheric pollutants are transported horizontallyto vegetation from their source through wind and turbulence. On average, the transport velocity in the planetary boundary layer ranges between 5 m/s and 10 m/s, thus horizontal daily transport is of the order of 500 km to 1000 km, [Fowler, 2002]. During the transport, the pollutants are subject to turbulent dispersion, and chemical reactions

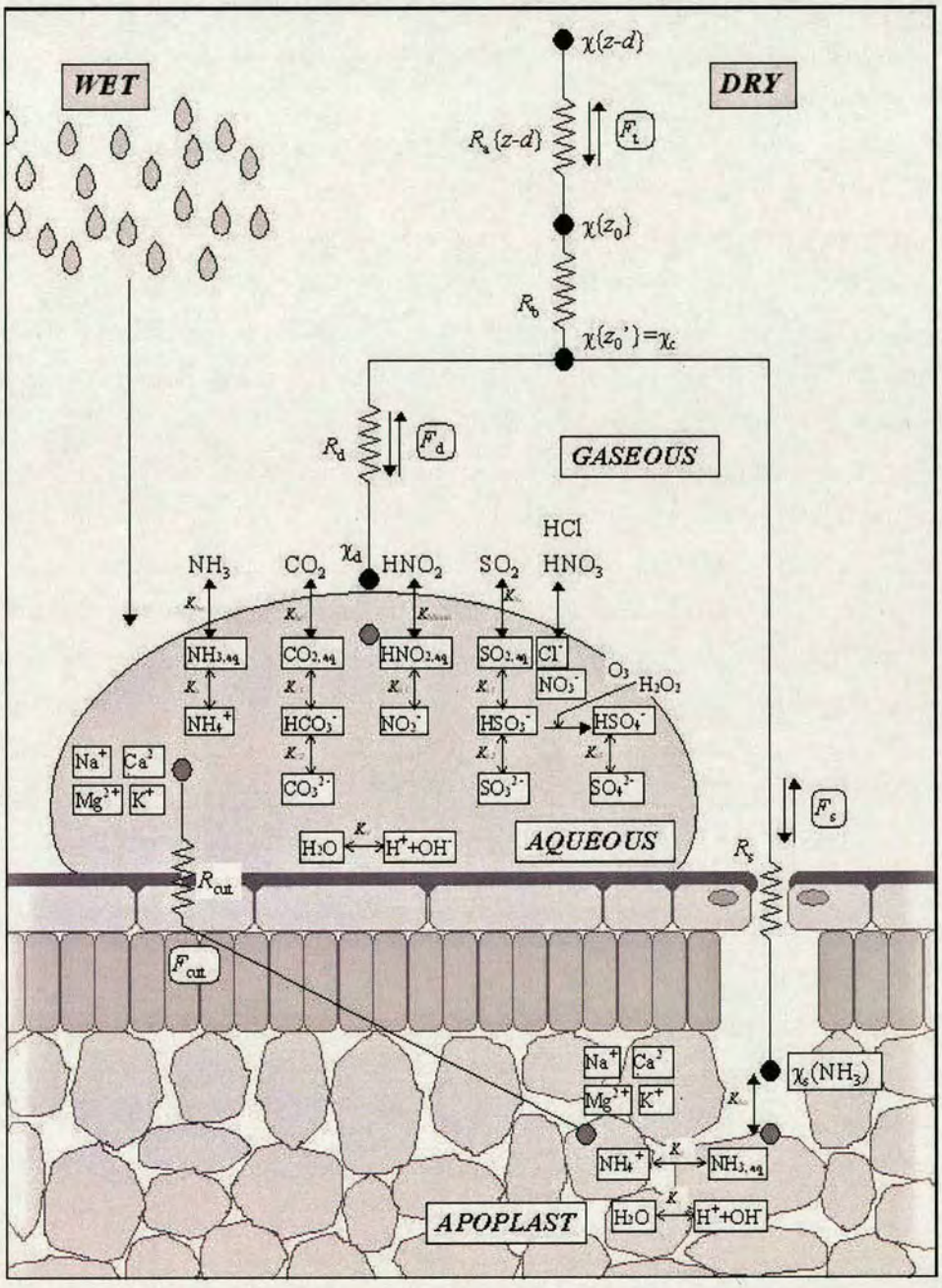

Figure 1.6: Schematic representation of the dynamic canopy compensation point model incorporating a leaf surface chemistry module, showing the exchange between the atmospheric gaseous phase, the aqueous phase of water droplets on leaf cuticles, and plant apoplast.

transform the primary gaseous pollutants into secondary pollutants and aerosols. Aerodynamically rough surfaces such as forests or urban areas induce much larger rates of turbulent diffusion than the ones occurring over short vegetation such as grass, or sea surface.

Transport of molecules through the viscous, quasi-laminar boundary layer close to the absorbing surfaces is by molecular diffusion and depends on the gas properties. The rates of molecular diffusion are several orders of magnitude smaller than the turbulent diffusion ones in proximity of the ground. Vegetation can react with the gas through the epicuticular waxes on leaf surfaces, or by diffusion through stomata and reaction with inter cellular fluids. Other surfaces have a rate of reaction that constitutes the major part of deposition.

Vegetative surfaces can act both as sources or sinks of ammonia, according to atmospheric and surface conditions and the plants N content [Sutton et al., 1993b] whereas for SO_2 vegetation is normally considered as a sink. In order to quantify the impact of total deposition of NH_3, it is necessary to understand the exchange dynamics between vegetation and atmosphere. While wet deposition episodes are widely monitored in Europe and North America, the dry deposition dynamics present more difficulties, as the instrumentation capable of measuring gaseous NH_3 requires higher contributions in terms of equipment and running costs, e.g. [Erisman et al., 1996]. The estimate of dry inputs to the various ecosystems are therefore evaluated by means of process-based exchange models, e.g. [Smith et al., 2000]. Large uncertainties are present in the estimates of fluxes, as the input provided by the measurements depends for example on the meteorology of the site, on the plant variety, on the ecosystem. Another problem connected to measurement data used for model input is the short-termed nature of the datasets. Development and validation of such models become a difficult task in the absence of long-term measurements of fluxes for a wider range of ecosystems and climates.

1.5 Objectives of this thesis

The state of the art in measuring surface-atmosphere exchange is closely connected to the quality of the instrumentation for detection of SO_2 and NH_3 in atmospheric conditions. While for SO_2 the exchange dynamics were studied since the early 1970's, for NH_3 the situation has largely improved relatively recently, with the introduction of new technologies that allow the fast measurement of ammonia

concentrations (see Table 1.1). The TDLAS technology allows to directly measure fast (up to 10Hz) mixing ratios of numerous chemical species (see Chapter 4): this technique is used for eddy covariance measurements as when coupled with the use of a sonic anemometer, it is able to measure the turbulent flux of a chemical compound. This technique can resolve the fine turbulent scale that dominates processes of exchange in the surface layer, and therefore is regarded as the most advanced and reliable micrometeorological method to infer fluxes in the surface layer. The TDLAS technology has been largely applied to a number of greenhouse gases (N2O, CH4, CO2) since the 80's, but for more reactive gas species such as NH3 or HNO3, the technique has been used very little; partially for the demand for measurements of more reactive species is more recent, and partially because these reactive species are present in very much lower concentrations in the atmosphere, and therefore require a better sensitivity from the sensors.
The recent improvements in these analysers have allowed the application of the TDLAS tachnique on the detection of NH3 concentrations at a fast rate (> 1 Hz). This aquisition rate, coupled to the sensitivity of the TDL instrument, should allow its usage for measurements of fluxes of NH_3 in field conditions by using eddy covariance. This hasn't been achieved as yet and constitutes a new step in the investigation of exchange processes for NH_3, that so far used gradient methods or relaxed eddy accumulation because of the time response limitations of the available instrumentation.
An objective of my thesis work has been to setup and test a TDL for NH3 eddy-covariance-flux measurements on a grassland field in Scotland. This contribution is crucial for a better understanding of the processes regulating the ammonia exchange between vegetation and air, as the high time-resolution of concentration measurements can describe in a better way fast processes occurring at the surface, that so far haven't been detected and therefore don't appear in the exchange budgets.

The data coverage and the information already present for SO_2 is due to the importance of sulphur deposition on environmental impacts started 30 years ago. Since then, the regional scale scenario for N and S has changed considerably: as a consequence to the reduction policies on sulphur, the proportions in the air of sulphur compounds have decreased, while the proportions of nitrogen compounds have increased. This caused the balance between N-compounds and S-compounds

to change, hence the need to further investigate a larger range of pollutant species to provide a bigger picture of the overall interactions.

In order to assess the balances for different countries for the main pollutants it is necessary to understand dry deposition dynamics as well as wet deposition ones. Dry deposition monitoring networks so far were conducted on short-based intensive field campaigns: these type of measurements are very labour-demanding and require a lot of infrastructure. Their outcome is very valuable for deeper understanding of the exchange dynamics, but the duration of these measurements is limited by these factors. Therefore, these field campaigns are not always the best solution when wanting to describe the seasonality of a chemical species on a certain environment, or when many different environments need to be characterised in terms of chemical climate. For this reason it is crucial to improve the surface-atmosphere exchange models for acidifying and eutrophying compounds such as NH_3 and SO_2.

This can be achieved by implementing dry deposition monitoring at selected sites for long term measurements, and by extracting from those measurements a better understanding of the surface-atmosphere exchange processes and model parameterizations.

Information about deposition, or emission of trace gases in the atmosphere are inherently very expensive in terms of equipment and labour involved in their operation on the field. Therefore, it is very difficult to produce long term datasets, but it would be equally useful in the development of the transport and process-based models currently providing deposition and concentration estimates on the regional scale.

At present, there are extensive measurement networks to define concentration fields for trace gases, including highly reactive ones such as NH3 and HNO3, but the flux to the surface is for many purposes a key for assessing the source/sink character of an environment. Especially for highly reactive gases, spatial and seasonal variability are very important factors for the assessment of a budget for the total exchange.

The research community has sought for a long time methods which average the flux over long time periods, reducing the costs and complexity of data analysis, and the development of a low-cost system able to provide long-term measurements of pollutants would allow the implementation of deposition monitoring networks, which would provide a very useful input in the parameterisation as well as in the

validation of models producing regional scale scenarios of air concentration and deposition of pollutants.

A second objective of my thesis is to setup and test a Time Averaged Gradient (TAG) system, in order to provide long period average fluxes with sufficient accuracy. The TAG system is applicable to a wide range of gases, and the cost of one monitoring station is considerably lower than an ordinary system for continuous flux monitoring. The TAG system objective is to provide: long term vertical profiles of concentration values for the chemical species of interest; long term measurement of fluxes (monthly, weekly or fortnightly values); meteorological variables every half hour, including turbulent fluxes of momentum and heat, in order to provide average values of total resistance.

In a second stage of this work, after the field work on the TAG instrument, an analysis of the uncertainties involved in the TAG protocol is required, by comparing the results from the TAG system to other established methods. Finally, the TAG data outcome will be applied for a comparison with a transport model, and will be used as parameters input for a process-based model.

Very little work has been done so far in the validation of the deposition models, and the datasets provoded by the TAG would constitute a very valuable tool for improving the models in the implementation phase.

Objectives of this work

- To obtain long-term surface-atmosphere NH_3 and SO_2 flux measurements using the aerodynamic flux gradient method by developing the TAG system and testing it over different ecosystems (semi-natural vegetation and intensively managed grassland).
- To measure NH_3 fluxes with eddy covariance using the TDLAS technique, on an intensively managed grassland in Southern Scotland.
- To compare the results of the long-term measurements with a process-based model of surface-atmosphere exchange.

Contents of the thesis

- Chapter 2: an introduction to micro meteorological methods, and in particular the flux-gradient and the eddy-covariance method,used throughout this

study.

- Chapter 3: a description of the TAG: low cost, long-Term Averaged Gradient system to measure exchange fluxes of NH_3 and SO_2. A presentation of the results of 5 years of continuous monitoring of SO_2 and 3 years of continuous monitoring of NH_3 fluxes at Auchencorth Moss by the TAG system, and a presentation of the results from the Easter Bush campaign where NH_3 fluxes were measured using the TAG system.

- Chapter 4: description of the TDLAS technique used to measure NH_3 fluxes described in chapter 5.

- Chapter 5: a presentation of the novel application of TDLAS to the measure of turbulent fluxes of NH_3; description and discussion over 3 months of continuous monitoring of NH_3 exchange fluxes at Easter Bush using eddy covariance technique.

- Chapter 6: a comparison of measurements versus the predictions of models currently used in the SO_2 and NH_3 deposition mapping in the UK.

- Chapter 7: a general synthesis and conclusions.

Chapter 2

Micrometeorology

2.1 Flow in the atmospheric boundary layer

The structure of the atmospheric boundary layer is regulated by thermal stratification, pressure gradients, Coriolis "force" and friction at the surface. These factors combine to different balance states which can roughly be divided in two, a daytime and a nocturnal structure of the boundary layer. When the boundary layer is maintained by heating from below it is called a *convective boundary layer*: a large surface heat flux results in a rapid growth of such a layer, which is limited by strong stable stratification of the overlying layer of atmosphere. The depth of the layer is defined by the height of this capping inversion. During the evening hours the solar heating decreases until net radiation changes sign, causing the cooling of the surface and of the layer of air in contact with it, until a surface-based inversion develops to a depth of a few tens of metres. One of the main sources of turbulence is lost and mixing decays; the mechanical mixing due to surface shear persists, but it is suppressed by the stability of the lower layers. This layer, defined as the *nocturnal boundary layer* is very different in character from its daytime equivalent.

The *surface layer* is the lowest portion of the atmospheric boundary layer in direct contact with the surface. When this layer develops over an extensive, flat area of uniform terrain, it is possible to assume that the momentum flux τ is constant with height, that wind direction doesn't change with height, and Coriolis turning can be neglected. For these reasons it was possible to develop dimensional arguments such as the Monin-Obukov similarity theory [Monin and Obukhov, 1954], to predict the structure of the surface layer. The height of the surface layer is variable according to the condition of the whole boundary layer, and it extends up to heights of a few hundreds of metres in well mixed conditions. In this layer there are strong vertical gradients controlling the transfer of momentum, mass and heat through it [Kaimal and Finnigan, 1994].

Simple laws, analogous to the ones that govern the molecular diffusion in laminar flows, are applied in this layer for describing the turbulent transport. Fluxes of momentum τ (also known as shear stress), fluxes of heat (H) and moisture (λE) can be expressed as:

$$\tau = K_m \rho \frac{\partial \overline{u}}{\partial z} \tag{2.1}$$

$$H = -K_h \rho c_p \frac{\partial \overline{\theta}}{\partial z} \tag{2.2}$$

$$E = -K_q \rho \frac{\partial \overline{q}}{\partial z} \tag{2.3}$$

where ρ is the air density, $\overline{u}, \overline{\theta}$ and $\overline{q}$ are the mean stream wise wind speed, mean potential temperature and mean specific humidity. K_m, K_h, K_ρ are the turbulent exchange coefficients for momentum, heat and moisture, that are the counterparts of viscosity, conductivity and diffusivity in laminar motion. The extension to turbulent motion of the laminar flow case is known as K-theory, e.g. [Stull, 1988]. It is common practice to express the shear stress τ in kinematic form, dividing it by the density of air ρ, and this has units of velocity squared ($m^2 s^{-2}$); from this follows the introduction of a reference velocity u_*, known as friction velocity, defined as:

$$u_* = (\tau_0/\rho)^{1/2} \tag{2.4}$$

It represents the effect of wind stress to the ground, τ_0 being the shear stress value at the ground surface. This velocity is a very important scaling quantity in surface layer studies, and it varies with the nature of the surface as well as the magnitude of the wind. The same scaling procedure can be applied to other variables such as temperature and concentration of a gas, resulting in friction temperature T_* and friction concentration χ_*. In neutral conditions, shear-generated eddies are roughly circular, and the friction velocity is the uniform tangential speed of the eddy. In unstable conditions, the eddies are distorted vertically, as vertical mixing and momentum transfer down wards is enhanced. In stable conditions the eddies are flattened as the friction that generates the eddy structure is inhibited [Monteith and Unsworth, 1990]. In Fig.2.1 the profile of wind speed in different atmospheric conditions are shown. K_M has dimension of height $\times$ velocity, so it can be represented by the product of the two corresponding scaling quantities, the length scale z and u_*.

$$K_M = k u_* z \tag{2.5}$$

k is the von Karman constant of proportionality whose value has been determined between 0.35 and 0.43; in the present work k= 0.41.

In a neutrally stratified atmosphere the wind profile can be therefore integrated from:

$$\frac{\partial \overline{u}}{\partial z} = \frac{u_*}{kz} \tag{2.6}$$

leading to

$$\overline{u}(z) = \frac{u_*}{k} ln \frac{(z-d)}{z_0} \tag{2.7}$$

where z_0 is the constant of integration known as roughness length: it is the height at which $\overline{u}$ is zero. This expression allows us to calculate the value of K_M from

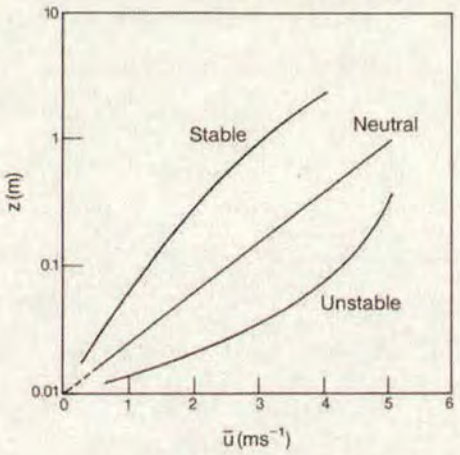

Figure 2.1: Wind profile in stable, neutral and unstable air (from [Kaimal and Finnigan, 1994]).

wind speed measured at two heights; assuming that the eddy diffusivities for momentum, heat and moisture have the same value close to the ground, see e.g. [Panofsky and Dutton, 1984], then by knowing the mean values of temperature and specific humidity measured at the same heights, it is possible to calculate their vertical fluxes.

The estimation of fluxes from profiles is subject to some restrictions: the fluxes have to be constant in height, which requires uniform and flat terrain, and the measuring heights to be in the surface layer. The logarithmic law applies only in neutral surface layers, and the estimates become less reliable in stable and unstable conditions [Kaimal and Finnigan, 1994].

2.2 The Aerodynamic flux gradient method

In steady state, in a regime of fully-forced convection and in a neutral atmosphere, wind speed increases with height in a purely logarithmic manner, and rates of turbulent diffusion for heat , water vapour and trace gases are the same as for momentum because those entities are transported vertically by eddies in the so-called constant flux layer [Thom, 1975]. According to the K-theory, in the surface layer the turbulent flux of a property χ is proportional to the product between its eddy diffusivity (K_χ) and its vertical gradient [Stull, 1988]. The aerodynamic flux gradi-

ent method estimates eddy diffusivities for trace gases from parallel measurements of turbulent diffusion rates for momentum, which are provided by measurements of wind speed and temperature at several heights. The turbulent flux F_χ of a trace gas concentration can be expressed in K-theory as:

$$F_\chi = -K_\chi \cdot \frac{\partial \chi}{\partial z} \tag{2.8}$$

where the eddy diffusivity for the trace gas K_χ is equivalent to the eddy diffusivity for momentum K_M and to the eddy diffusivity for sensible heat flux K_H. Diabatic profiles are generally not logarithmic and their analysis is consequently more complicated than 2.6: the form of the wind profile under stable or unstable conditions is:

$$\frac{\partial \overline{u}}{\partial z} = \frac{u_*}{kz} \cdot \Phi_m \tag{2.9}$$

and the eddy diffusivities follow from this,

$$K_\chi = K_M = K_H = \frac{k \cdot (z-d)}{\Phi_m} \cdot u_* \tag{2.10}$$

where d is the displacement distance (mean level of momentum absorption by the surface), z is the measuring sensor height, Φ_M is the dimensionless similarity function referring to momentum; it is height- and stability-dependent. Several alternative semi-empirical expressions for Φ_M, Φ_H and Φ_χ (calling Φ_H and Φ_χ the similarity functions referring to sensible heat and gas concentration respectively) can be found throughout the literature, e.g. [Panofsky, 1963]: under stable conditions, here the following relation [Webb, 1970] is used:

$$\phi_M = \phi_H = \phi_\chi = (1 - 5.2Ri)^{-1} \tag{2.11}$$

Under unstable conditions instead, the functions behave in different manners, as proposed by [Dyer and Hicks, 1970] and [Businger et al., 1971]:

$$\phi_M^2 = \phi_H = \phi_\chi = (1 - 16Ri)^{-0.5} \tag{2.12}$$

These functions are used to correct the flux for non-neutral profiles, to extend the logarithmic profile rules.

Ri represents the gradient Richardson number, which is a non dimensional parameter used to describe the stability conditions of the atmosphere, and can be expressed as:

$$Ri = \frac{g}{T} \cdot \frac{\frac{\partial \overline{T}}{\partial (z-d)}}{\frac{\partial \overline{u}}{\partial (z-d)}^2} \tag{2.13}$$

Ri is a very useful indicator, as it relies on gradient of mean quantities that are easy to measure; its physical meaning is the ratio of turbulent production between buoyancy and shear. It will have positive values for stable stratification, negative values for unstable stratification and it will be 0 for neutral stratification. The use of friction velocity u_* and friction concentration χ_* may be preferred to the eddy diffusivities: so, defining them as:

$$u_* = k \cdot \frac{\partial u}{\partial log(z-d)} \cdot \Phi_M^{-1} \tag{2.14}$$

$$\chi^* = k \cdot \frac{\partial \chi}{\partial log(z-d)} \cdot \Phi_\chi^{-1} \tag{2.15}$$

the turbulent trace gas flux can be seen as the product of the friction velocity and the friction concentration.

When the wind gradient in eq. 2.9 is integrated, having chosen a form for ϕ_m, the wind profile is:

$$\overline{u}(z) = \frac{u_*}{k}\left[ln\frac{(z-d)}{z_0} + \psi_m(\frac{z}{L})\right] \tag{2.16}$$

where the diabatic term ψ_m is the integral of $(1-\phi_m)/(z/L)$. As for ϕ, in stable conditions ψ_m and ψ_H assume the same value,

$$\psi_m = \psi_H = 4.7 \cdot \frac{z}{L} \tag{2.17}$$

whereas for unstable conditions

$$\psi_m = -2 \cdot ln\left[\frac{1+\phi_m^{-1}}{2}\right] - ln\left[\frac{1+\phi_m^{-2}}{2}\right] + 2arctan(\phi_m^{-1}) - \pi/2 \tag{2.18}$$

and

$$\psi_H = -2ln\left[\frac{1+\phi_H^{-1}}{2}\right] \tag{2.19}$$

The flux of concentration can then be written as:

$$F_\chi = -k^2 \cdot \frac{\partial \overline{u}}{\partial\left[log(z-d)+\psi_m\right]} \cdot \frac{\partial \chi}{\partial\left[log(z-d)+\psi_H\right]} \tag{2.20}$$

The same process can be applied to all turbulent fluxes, for example the sensible heat flux can be written as:

$$H = -k^2 \cdot \rho \cdot c_p \cdot \frac{\partial \overline{u}}{\partial\left[log(z-d)+\psi_m\right]} \cdot \frac{\partial \overline{T}}{\partial\left[log(z-d)+\psi_H\right]} \tag{2.21}$$

2.3 Turbulence and the "eddy flux"

The turbulent flow in the surface layer can be thought of as a superposition of eddies of a large range of sizes. These eddies interact continuously with the mean flow and they transmit the energy from bigger to smaller motion scales ("eddy cascade"), converting kinetic energy into turbulent kinetic energy, and eventually into internal energy through viscosity. The atmospheric boundary layer is continuously turbulent: in laminar flow, streamlines are smooth and essentially parallel to one another, while turbulent flow has an erratic appearance with seemingly random, chaotic motions of elements of fluid. A set of "symptoms" can be used to identify turbulence and to distinguish it from other atmospheric motions [Shaw and Finnigan, 2001]. Turbulence is rotational and three-dimensional, in fact it maintains itself through vortex stretching, which can only occur in three dimensional flow; it is *dissipative* and viscosity continually acts to convert the kinetic energy of the flow into internal energy raising the temperature of the fluid; it is *diffusive* in that mixing occurs much more rapidly in turbulent than in laminar flow; turbulent flow has a high Reynolds number. The Reynolds number expresses an estimate of the ratio of inertial forces to viscous forces; the flow will change to turbulent from laminar when viscosity is no longer able to suppress a disturbance introduced into the flow field. It is expressed as:

$$Re = \frac{ul}{\nu} \tag{2.22}$$

and it is a pure number, where u and l are characteristic velocity and length, and ν is the kinematic viscosity of the fluid. Because of the stochastic nature of turbulence, the governing equations of turbulent motion express the time rates of change of statistically averaged quantities rather than instantaneous values. A statistical description is assisted by adopting Reynolds notation, according to which a turbulent variable, for example the concentration of a gas χ, can be expressed as the sum of a mean component and a fluctuating one.

$$\chi = \overline{\chi} + \chi' \tag{2.23}$$

The mean value $\overline{\chi}$ is the average χ value of the portion of fluid observed: the measure of a spatial average is very difficult to achieve for instantaneous values. Taylor's frozen turbulence hypothesis enables us to convert temporal measurements at a point, as taken from a sonic anemometer, to spatial structures, through the transformation $x = \overline{u}t$. The assumption is that the turbulent field is frozen and

advects past the sensor with the speed $\overline{u}$, e.g. [Stull, 1988].

The time interval over which the average is formed must generally be long enough to include the largest significant scales of turbulence. Yet, this period should not be so long that conditions are influenced by larger scale atmospheric processes or diurnal changes. Near the surface, periods of 15 to 30 minutes are generally adopted, as over these time intervals the statistical properties of the flow are independent of time, and stationarity, or steady state, can be assumed.

2.3.1 Eddy covariance method

The *eddy covariance* method allows the definition of the fluxes in terms of the turbulent components of the properties being transferred; it is a very direct method, as the fluxes in the surface layer are a result of the exchange due to turbulent motion, but as seen in § 2.2, the fluxes of momentum, heat and scalars were defined in terms of mean vertical gradients of those quantities. The mean flux across a any plane implies correlation between the wind component normal to that plane and the variable in question. The covariance between the two gives exactly the measure of the flux across the plane. This requires no assumption about the mixing properties of the turbulent layer.

There are a few conventions used in the application of eddy covariance:

- by definition, the average of the fluctuations is 0
- if the x axis is defined in the direction of the mean flow only $\overline{u}$ is $\neq 0$, $\overline{v} = \overline{w} = 0$
- over a flat, level, homogeneous surface x and y are horizontal and z is vertical and positive up wards.

The fluxes of scalar concentration, heat and momentum (in terms of friction velocity) can then be expressed as:

$$F_\chi = \overline{w'\chi'} \tag{2.24}$$

$$H = \rho c_p \overline{w'T'} \tag{2.25}$$

$$u_* = \sqrt{-(\overline{w'u'})} \tag{2.26}$$

To measure the fluctuations in concentrations and wind speed, fast response sensors are required (5 to 20 Hz, depending on the height above the surface), that is much faster than needed for mean profile measurements. This is achieved using sonic anemometers for components of turbulence, and by chemical analysers that are able to sense an increasing variety of scalar concentrations at fast rates, such as LICOR for CO_2 and H_2O or TDLS for CH_4, N_2O, see e.g. [Grace et al., 1995] and [Fowler et al., 1995].

As the flux is determined as the product of the instantaneous fluctuations in both the concentration of the scalar being measured and in the vertical wind speed, a knowledge of the frequency response of a sensor is particularly important for eddy correlation measurements. If the frequency response of the chemical sensor is low, then the system won't be able to sense the fast changes in concentration due to transport by the small eddies, so the flux estimated with such a system won't be representative of the true flux.

2.3.2 Spectra and co spectra

The "eddy cascade" process of transfer of energy can be described by means of spectral analysis. A spectrum of turbulence provides a complementary information to the analysis of the central moments (mean, variance, etc.) of turbulent variables; a rapidly varying value of temperature for example could have the same mean value of a slowly varying one. In a spectrum of turbulence the importance of each eddy is taken into account, and the contribution of each frequency of motion is considered individually.

The power spectral density of wind speed for example, S_u, is defined as the total variance of u, expressed as the ensemble of the contribution to variance given by each unit interval of frequency ν.

$$\int_0^\infty S_u(\nu)d\nu = \overline{u'^2} \tag{2.27}$$

As turbulent motion covers a large range of scales of motion, to represent power spectral density it is common practice to use logarithmic scales of frequencies or wavenumbers; to represent the physical meaning of variance, the power spectral density is multiplied by the wavenumber. A spectrum can be divided in 3 regions: *energy production*, where the bulk of the turbulent energy is contained and where energy is produced by buoyancy and shear; *inertial*, where energy is not produced

nor dissipated but transmitted from larger to smaller eddies; *energy dissipation*, where kinetic energy is converted to internal energy [Kaimal and Finnigan, 1994]. [Kolmogorov, 1941] stated that in the inertial subrange the power spectral density should be a function only of the kinetic energy passing through this range towards the dissipation scales, and from dimensional considerations he argued that:

$$S_u(\kappa) = \alpha \epsilon^{2/3} \kappa^{-5/3} \tag{2.28}$$

When plotting on log-log scales $S_u(\kappa)$ versus κ, the slope of the curve in the inertial subrange is constant and equal to -5/3.

A cospectrum is defined by the covariance of 2 turbulent variables, for example w, u. It gives information on the frequency responses and averaging times needed for estimating fluxes. From experimental evidence, cospectral forms for the inertial subrange have been determined, e.g. [Kaimal et al., 1972], [Wyngaard and Cote', 1972], and a corresponding slope of the curve has been found to be -4/3.

Conversion of time data series for spectral analysis is achieved by Fourier analysis, and the fast Fourier Transform (FFT) is the most widely used method. The choice of record length T and sampling rate Δt affects the range and the resolution of the spectrum. To determine whether the record length is appropriate, the shape of spectra (and cospectra) should have a well-defined spectral peak in the power spectral (or co-spectral) density plot, and a roll-off feature towards the lower frequencies. For what concerns the sampling rate, according to Shannon's sampling theorem at least 2 samples per cycle are needed to to define a frequency component in the original signal (e.g. a wind speed trace). Therefore, for a fixed frequency f_N, the sampling interval Δt should be:

$$\Delta t \leq \frac{1}{2 f_N} \tag{2.29}$$

To ensure the instruments are able to resolve the smallest eddies contribution to the flux, the observation of cospectra gives a valuable tool.

A theoretical spectral output is shown in Fig.2.2: this outcome is verified when experimental conditions are suitable for eddy-covariance application. By observing the normalised cospectra of $\overline{u'w'}$ and $\overline{\theta'w'}$, as shown in Fig.2.2, it can be seen that the contribution of eddies with normalised frequency $\nu > 10$ are negligible: so, $\nu = 10$ can be taken as a measure of the frequency response required by the eddy flux measurements. translating to frequency in Hz,

$$f_{required} = \frac{10\overline{u}}{h} \tag{2.30}$$

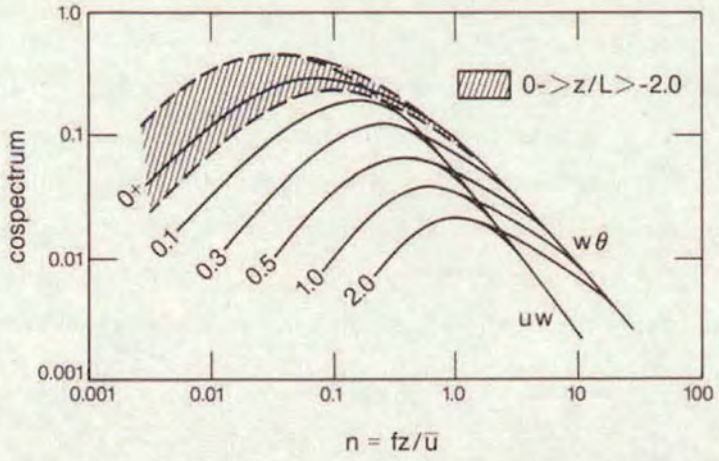

Figure 2.2: Normalised surface layer cospectra of uw and$w\theta$, shown varying with z/L, from [Kaimal and Finnigan, 1994]

where h is the measurement height. Typical values of sampling rate in flux measurement studies are 10-20 Hz, but this obviously depends on the instrument capability to resolve such high frequencies.

2.4 Fetch and Footprint

Over a homogeneous surface, the exact location of a sensor is not an issue, because the fluxes from all parts of the surface are by definition equal. However, if the surface is inhomogeneous, the measured signal depends on which part of the surface has the strongest influence on the sensor, and thus on the location and size of its footprint [Schmid., 2002]. In a micrometeorological context, the "footprint" may be defined as the upwind area most likely to affect a downwind flux measurement at a given height z [Schuepp et al., 1990], and it defines the spatial context of the measurement. When turbulent flux sensors are deployed, it is important to define precisely the surface over which the flux measurements integrate, and if possible the contributions to the flux for different areas.

The "fetch" is a homogeneous surface area between the measurement point and the change in surface roughness (e.g. changing land cover, slope of terrain, or

vegetation), see e.g. [Schmid., 2002]. However, the contribution to the measured fluxes are not constant over the available fetch.

Much recent work has focussed on methods to quantify the footprint within the fetch contributing to various fractions of the measured flux. The first analytical solution for an Eulerian footprint model was provided by [Schuepp et al., 1990] in the case of neutral stratification and constant wind speed atmospheric profile.

The Cumulative Normalized contribution to the Flux measurement (CNF) at height z, from an upwind area bounded by a distance x_L, may be regarded as the effective fetch and it is defined according to [Schuepp et al., 1990]:

$$\text{CNF} = \int_0^{x_L} \frac{U\Phi_M(\zeta)(z-d)}{u_* k x^2} \cdot e^{\frac{(-U\Phi_M(\zeta)(z-d)}{k u_* x}} = e^{\frac{(-U\Phi_M(\zeta)(z-d)}{k u_* x_L}} \tag{2.31}$$

where U is the average wind speed between the surface and observation height z, such that:

$$U = \int_{d+z_0}^{z} u(z)dz \Big/ \int_{d+z_0}^{z} dz = \frac{u_* \left[ln\frac{(z-d)}{z_0} - 1 + \frac{z_0}{(z-d)} \right]}{k\left(1 - \frac{z_0}{(z-d)}\right)} \tag{2.32}$$

This model is not entirely adequate to describe stable or unstable atmospheric stratification. Another analytical model has been proposed by Kormann and Meixner providing a solution to this question: it is a stationary gradient diffusion formulation with height independent crosswind dispersion, using a Gaussian crosswind distribution function.

The model uses arbitrary power laws for the wind speed and the eddy diffusivity, K_M, combined with K-theory in a second stage, and includes thermal stratification [Kormann and Meixner, 2001]. The authors define the *crosswind integrated flux footprint* at the downwind distance x and height z of a unit point source at the origin in the following way:

$$f = \frac{1}{x\Gamma(\frac{1+m}{r})} \cdot \left(\frac{Uz^r}{r^2 \kappa x}\right)^{\frac{1+m}{r}} \cdot exp\left(\frac{Uz^r}{r^2 \kappa x}\right) \tag{2.33}$$

where U is the mean plume velocity, m and r take into account the exponent of the wind speed and eddy diffusivity power law; κ is a constant used in the power law profile of eddy diffusivity; m, r and κ are used for relating the power laws to the Monin-Obukov theory. Γ is the so-called gamma function. This equation is an explicit algebraic relation in x and z, and thus, it constitutes the only truly analytical flux footprint model based on realistic profiles of K and $\overline{u}$ to date.

2.5 Sonic anemometry

The ultra sonic anemometer used during the field campaigns is a Metek Sonic USA-1, Metek GmbH, Elmshorn. It measures the wind vector and the air temperature at a frequency of 100 Hz; coupled with fast chemical analysers it is ideal for the application of eddy covariance techniques. Its principle of operation is the measure of ultra-sounds propagation time in the atmosphere: a pair of transducers frontally aligned act alternately as transmitters and receivers, sending pulses of high frequency ultrasound between themselves. There are therefore two signals travelling in opposite direction on the same path: the difference between the times of flight in each direction is due to the component of the wind vector lying on the same axis. The measure of t_1 and t_2 allows the determination of the speed of the air flow along the transducers line v.

$$t_1 = \frac{L}{(c+v)} \qquad t_2 = \frac{L}{(c-v)} \tag{2.34}$$

Calling c the speed of sound and L the distance between the transducers, that in the case of the USA-1 is 175 mm, v can be expressed as

$$v = \frac{L}{2} \cdot \left(\frac{1}{t_1} - \frac{1}{t_2}\right) \tag{2.35}$$

By arranging three pairs of transducers in different orientations, the direction and magnitude of the incident airflow may be unambiguously derived. The Metek Sonic USA-1 set up is shown in fig.2.3; the transducer pairs do not conform to Cartesian axes in order to minimise the systematic errors: by deriving every Cartesian component of the wind vector from every pair of transducers, and not from only one of them as would happen in an orthogonal set up. The transducers are connected to an analogue box, in which the signals are converted from analogue to digital, and sent to a PC by means of a serial cable. The output data give the values of the three components of the wind speed, and the air temperature T_s ("sonic temperature"). The speed of sound can be calculated from eq. 2.34 as a function of t_1 and t_2 in the following manner:

$$c = \frac{L}{2} \cdot \left(\frac{1}{t_1} + \frac{1}{t_2}\right) \tag{2.36}$$

The speed of sound is affected by environmental conditions such as the air composition, pressure, temperature and humidity. Its strong dependence on air temperature forms the basis for the method of measuring temperature [Kaimal and Gaynor, 1991].

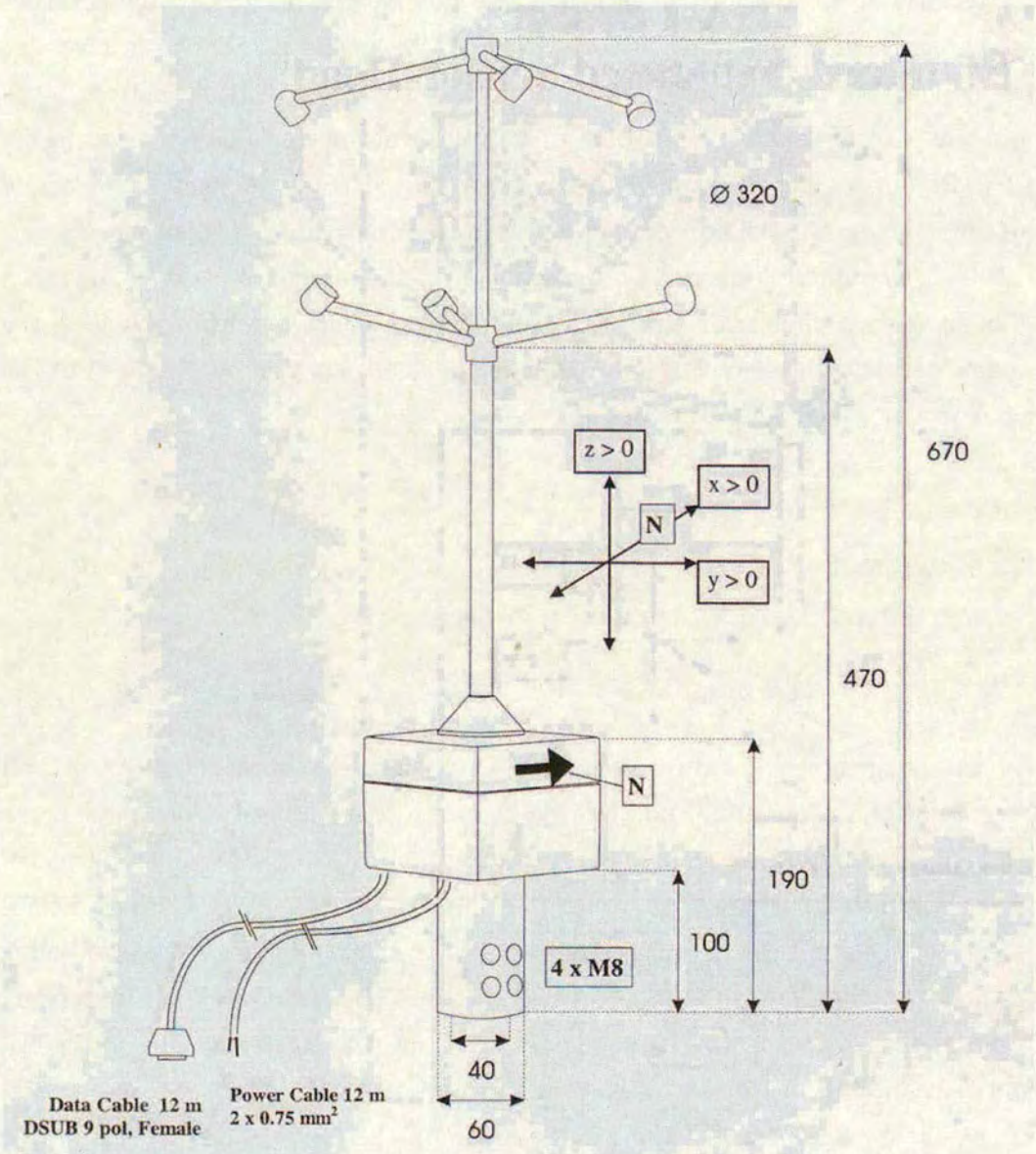

Figure 2.3: Diagram of the ultra sonic anemometer, from the user manual for the Metek Sonic USA-1.

The relationship commonly invoked [Kaimal and Businger, 1963] is:

$$c^2 = 403T_s(1 + 0.32\frac{e}{p}) \tag{2.37}$$

where e is the vapour pressure of water in air and p is the absolute pressure. Consequently, the sonic temperature T_s can be derived as [Kaimal and Gaynor, 1991]

$$T_s = \frac{L^2}{1612} \cdot \left[\frac{1}{t_1} + \frac{1}{t_2}\right]^2 + \frac{(v_n)^2}{403} \tag{2.38}$$

Where v_n is the component of wind speed normal to the transducers line. The temperature derived from speed of sound measurement in air very closely approximates the virtual temperature T_v, defined as the temperature at which dry air has the same density as moist air at the same pressure.

$$T_v = T\left(1 + 0.38\frac{e}{p}\right) \tag{2.39}$$

In fact, the sonic temperature can be also written as:

$$Ts = T\left(1 + 0.32\frac{e}{p}\right) \tag{2.40}$$

The difference of the coefficients of e/p in eq.2.39 and 2.40 is because in calculating T_s ratios of specific heats for water vapour and air are taken into account, whereas they are ignored for the calculation of T_v.
A typical data output from the sonic is shown in Fig.2.4: a time series of the instantaneous values of the 3 wind components and the sonic temperature.

2.5.1 Errors in sonic anemometer measurements

Errors in sonic anemometer measurements arise for two causes: *shadowing interference* and *physical limitations of the instrument for turbulence measurement*

Shadowing

The wake of the support frame and the other transducers of the sonic anemometer are likely to interfere with the air flow measured by the anemometer. If the wind flow strikes the sonic beam path at an angle $\theta < 75°$, the wake of the transducer will affect the velocity. The effect will depend on θ and on the ratio between transducer diameter a to path length L, see [Finnigan, 2001]. This is impossible to avoid, but corrections for minimising interference are provided by the manufacturer for the

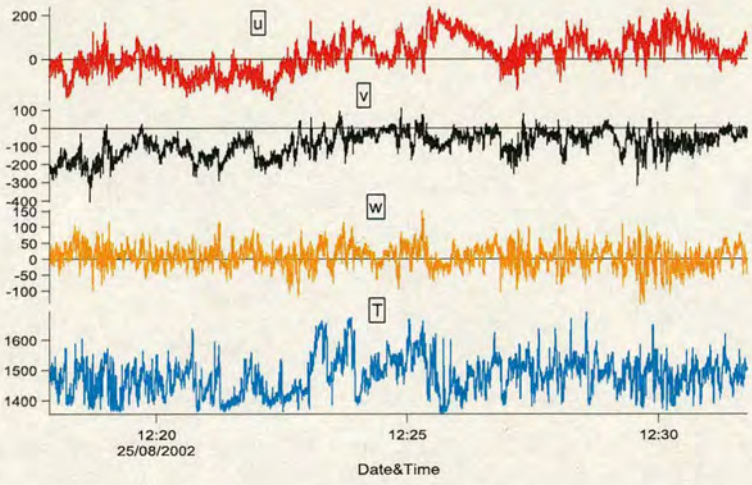

Figure 2.4: Values of the 3 components of the wind vector (expressed in m/s) and values of temperature (^oC) recorded at a frequency of 10Hz with the ultra sonic anemometer.

omnidirectional designed model (Metek, USA 1) used in the Easter Bush field campaign [Metek, 2001]. The presence of an inlet tube connected to the scalar analyser also influences the air flow measured by the anemometer: the position of the inlet tube arises from a compromise between minimising interference with the air flow and minimising the distance between inlet and sonic transducers, so that wind and scalar concentration are analysed on the same air parcel.

Spatial resolution

The main limitation to the frequency response of a sonic anemometer is imposed by line averaging along the sonic beam path L: the smallest eddy that can be resolved for example by the Metek USA-1 has a 30 cm scale, as the instrument path is 17.5 cm long. The problem of resolution of small eddies increases with beam path length, and this can be a problem over short plant canopies, as the sonic anemometers will not respond to fine scale turbulence from leaves, for example.

In practice, this limits the application at small heights (less than 1 m); conversely, the instrument is excellent for applications at heights of 2 m to tens of metres.

The configuration of a sonic anemometer is such that the distortion of the measured velocities is minimised. A transformation into the coordinate frame of the

analysis of the measured velocities is then required. This analysis has generally the main wind flow aligned with $\mathbf{u}$, the east-west direction along the x axis, z normal to the underlying surface and y parallel to the underlying surface. The method used for the Easter Bush field data aligns the analysis coordinate directions with the ensemble mean velocity vector of a set of N averaging periods T.

Chapter 3

Measurement of long-term average field-scale deposition fluxes by micrometeorology

3.1 Long-term deposition measurements

Micrometeorological methods have been shown to provide long-term semi-continuous flux measurements of trace gases: however, such methods generate large quantities of data output with the 30-60 min averaging necessary to satisfy the boundary conditions for flux-gradient analysis. For some time the research community has sought methods which average the flux over longer periods, reducing the cost and complexity of analysis.

The main goal of the Time Averaged Gradient system (from now on referred to as TAG) is to provide direct long-term average (1 to 4 weeks) flux measurements for a range of trace gas species, between atmosphere and terrestrial surfaces. This is necessary to understand the exchange dynamics and the different reactions between plants and air, which in turn are required for modelling at the local and regional scales. For certain (highly reactive) gases, the spatial distribution is strongly linked to the presence of local sources, and therefore it can be very spatially variable. For this reason the input data used in the models must contain the necessary information for the range of environments simulated, and monitoring at a wide range of locations allows for a more realistic model to be developed.

According to the specific environment and to the seasonal and climatic conditions, vegetation can act as a source or a sink for the different chemical compounds. The system therefore needs to be able to provide the long-term net flux and to characterise the specific environment over a wider range of conditions throughout the year.

The measurement of long-term fluxes of trace gases between atmosphere and vegetation has historically been difficult because of the costs of instruments capable of continuous monitoring of atmospheric concentrations and the excessive work required for their maintenance.

The overall idea of the TAG instrument follows from the consideration that in principle, a long-term averaged vertical gradient of concentrations measured with simple methods would substitute for such expensive continuous monitoring.

Over daily periods, atmospheric conditions can range from high stability, where the vertical gradients of ambient concentration are enhanced due to very small diffusivity, to highly unstable conditions, in which concentration gradients are small due to the intense turbulent activity of the surface layer. By sampling continuously over a long-term period, the large vertical gradients generated by high stability

would lead to an over-estimate of the actual flux.

It is necessary, in developing the TAG system, to develop techniques which avoid the bias due to these processes. To overcome this problem, the TAG system operates conditionally, sampling the micrometeorological variables within a carefully defined range of stability.

Despite the early work, there has to date been no rigorous analysis of the potential of TAG systems for long-term fluxes measurements. The work reported here therefore provides the necessary analysis.

This chapter describes the evolution of TAG methods beginning with the prototype of the TAG instrument (TAG1) as it was first developed during the LIFE project [Flechard, LIFE REPORT 1998].

My work started from the analysis of the data collected after the LIFE project conclusion (1998) with the second version of the instrument (TAG2) described in §3.3. The data were collected on two sites, Auchencorth Moss, and they are discussed in §3.4, and Plynlimon (results to be reported elsewhere), in this work used only for model comparison in Chapter 6).
An analysys of the uncertainties concerning the TAG method is shown in §3.5, by using a continuous series of data recorded in parallel to the TAG placed at the Auchencorth Moss field site, simulating the protocol of the TAG instrument.
These first results led to further development of the instrument, shown in a new (TAG3) system which has been tested on a different field site, and the results are discussed in §3.6.

3.2 Approach and Method

The TAG instrument is based on the application of the aerodynamic flux gradient method, and the conditional sampling criteria are chosen to fulfill the requirements of such a method (see §2.2).

Over a period of more than twelve hours, continuous averaged gradients can lead to biased fluxes because the averaging period may include conditions unsuitable for the application of the aerodynamic gradient method. The procedure followed with the TAG instrument requires stationary atmospheric conditions to avoid advection and storage errors. Micrometeorological information, such as wind speed and temperature, are therefore averaged over short periods, typically of 30 minutes; this period is long enough to sample the full spectrum of turbulent eddies

contributing to the flux, but short enough to provide reasonably constant surface and atmosphere conditions.

The measurements system is programmed to sample only when the fetch (see §2.4 for explanation) is unaffected by obstacles, as defined by inspection of the surface topography and land use within the distance of interest (500 m circa) at the measurements site. The system samples concentrations of the pollutant in the air when atmospheric neutrality conditions are met.

The gradient Richardson number, defined in the following equation, is the chosen parameter to assess the stability condition of the atmosphere.

$$\mathrm{Ri} = \frac{(z-d)g}{T} \frac{\overline{\frac{\partial T}{\partial log(z-d)}}}{\left[\frac{\partial u}{\partial log(z-d)}\right]^2} \tag{3.1}$$

where: z is the measurement height, d is the displacement height, T the absolute temperature, u the horizontal wind speed, g the gravity acceleration.

The gradient Richardson number has been chosen as the indicator of atmospheric neutrality because it may be calculated directly from gradients of mean wind speed and temperature, and expresses immediately the importance of buoyancy in the surface layer relatively to mechanical production. The sign of Ri is determined entirely by the sign of the potential temperature gradient, therefore positive values will mean stable conditions and negative values will mean unstable conditions. As both mechanical and buoyant production depend on the height in the layer, also Ri will be height dependent, and the chosen reference height is 1 m. It is calculated on a half-hourly basis, and whenever it indicates neutral conditions, the system will be sampling. The "window of neutrality" chosen for the experiments on conditional sampling was set for values of Richardson number between -0.02 and +0.02. This choice is not dictated by a rule, it follows from empirical observations. In fig. 3.1, a *stability factor* F is plotted logarithmically against the Richardson number (Ri). F is defined as (Thom, 1975):

$$\mathrm{F} = \frac{1}{\phi_M \phi_H} \tag{3.2}$$

where ϕ_m and ϕ_h are the stability functions for momentum and heat flux (see § 2.2).

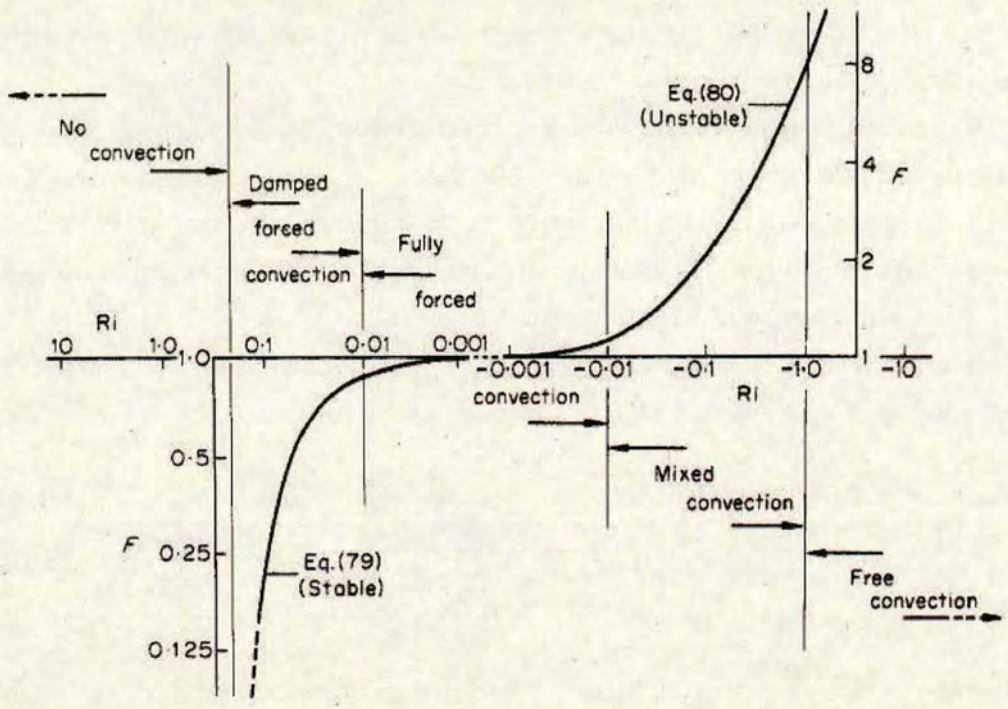

Figure 3.1: Stability factor F plotted against Ri number values (Thom, 1975)

The fluxes calculated in non-neutral conditions, using profile-gradient equations valid for neutral conditions are multiplied by F. According to the Thom, the fully forced convection window lies between values of Ri of -0.01 and +0.01. The various convection regimes are shown in the chart, where the absolute value of F increases more rapidly as the atmospheric conditions move towards free convection or lack of convection. It is therefore necessary to set the Ri values for the conditional sampling window "fairly close" to the fully forced convection region; the question of how close stays open, and up to the operator. The observation of the measuring site atmospheric features can help in this decision.

During the field campaign at Auchencorth Moss (see § 3.4) continuous measurements with a sonic anemometer showed that for most (60% circa) of the time Ri spans between -0.02 and +0.02: fig.3.1 shows that in this interval F equals 1 $\pm$ 0.2. This window represents a compromise to maximise the time acquisition of data and being acceptably close to atmospheric neutrality.

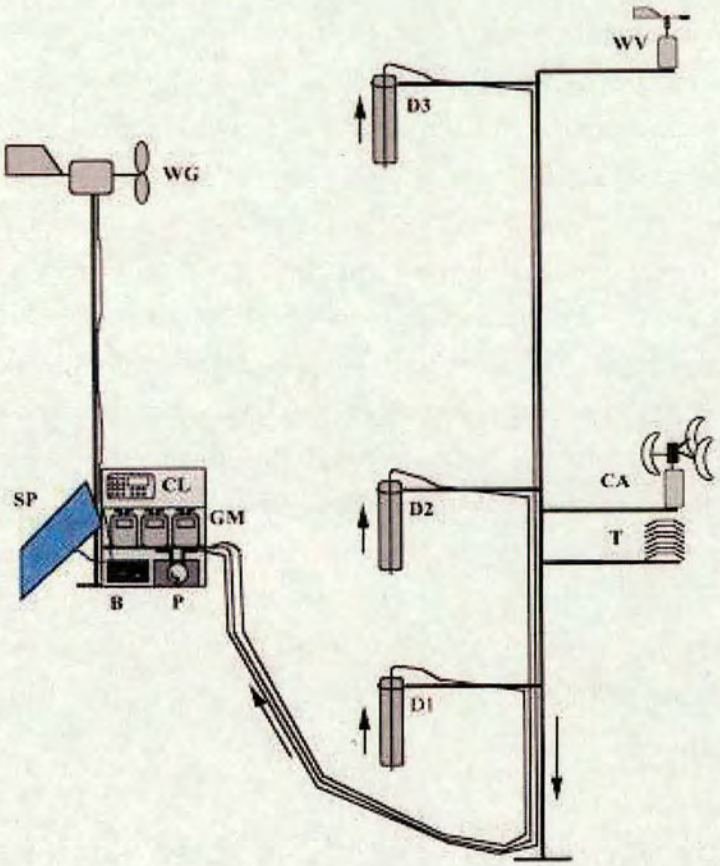

Figure 3.2: First prototype of the instrument TAG 1. CA: cup anemometer T: temperature sensor WV: wind vane GM: gas flow meters WG: wind power generator SP: solar panels B: battery P: air pump CL: Campbell 21X logger D1,2,3: denuders

3.3 Description of the TAG system

The prototype of the TAG instrument was developed in 1998 at CEH Edinburgh. The system is shown in fig. 3.2 and it consists of a cup anemometer and a wind vane to measure the wind speed and direction, a temperature sensor and a set of three denuders, which work on the principle of chemical capture of a substance to measure a gas concentration [Flechard, C. R. and Fowler, D., 1998]. The denuders are placed on a mast at three different heights arranged logarithmically, and are connected by means of plastic tubes to three gas flow meters and eventually to an air pump (fig.3.3). All these components are connected to a programmable

Campbell 21X data logger which is programmed to store and average the data, as well as to control the pump connected to the denuders, according to the wind speed and direction values, making the gas capture possible only in the desired conditions, i.e. excluding bad fetch conditions (low wind speed and wind direction from flow-disturbed areas).

The denuders are coated on their inner walls with a solution to capture the trace gas of interest whenever the air is flushed through them, i.e. every time the pump is activated. The chemical analysis of the exposed solution is done at arbitrary time intervals (typically of 1, 2 or 4 weeks). The power supply is provided by a solar panel and a wind power generator, both connected to a battery in case of low wind and/or low solar radiation conditions, to allow use at remote locations.

During the usage of the first TAG model, the instrument was placed at a field site together with a full flux gradient measurement system consisting of 3-point profile of gas concentrations (SO_2, O_3, NO, NO_2), temperature and wind speed measurements from a sonic anemometer. This provided the necessary information to measure fluxes and the micrometeorological data to compare with the prototype TAG system.

3.4 The Auchencorth Moss data series

The TAG instrument prototype was operated for a 178 days-period, from May to November 1998 measuring NH_3 fluxes over a moorland site, see [Flechard and Fowler, 1998]. As this prototype had only one wind speed sensor and one temperature sensor, the conditions for sampling were set according to wind speed and direction values: low wind speed (< 2 m s^{-1}) and poor fetch conditions were not sampled. The first TAG has been modified following the first test: a second temperature sensor and a second cup anemometer were added in order to provide independent estimates of vertical gradients of wind speed and temperature. A series of five years data (1999-present day) have been recorded for SO_2 fluxes. In both the experiments, results obtained from TAG were compared with continuous (half-hourly) monitoring systems for concentrations of SO_2 and NH_3 coupled with a sonic anemometer, which provided the necessary micrometeorological information to calculate fluxes using the aerodynamic flux-gradient method.

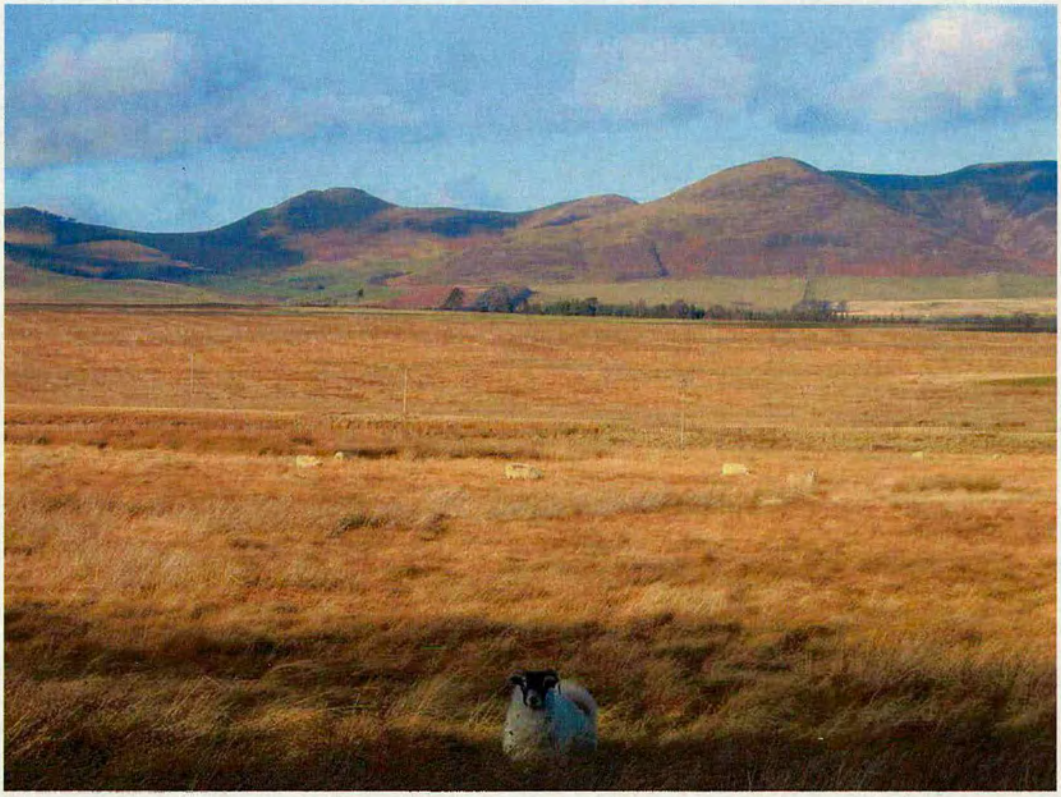

Figure 3.3: View of Auchencorth Moss.

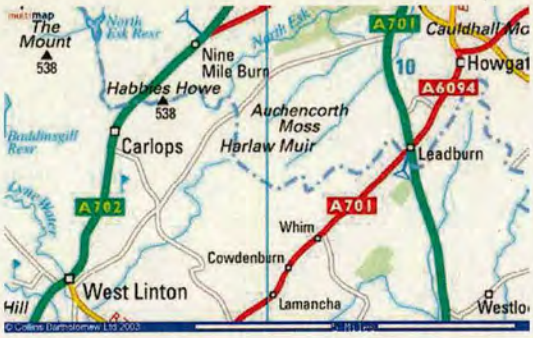

Figure 3.4: Auchencorth Moss topography. Green areas are woodland (often coniferous), otherwise area within the red outline is peat bog (from Collins-Bartholomew Map, Scale 1:100000).

3.4.1 The field site characterisation

Auchencorth Moss is a blanket bog covering a flat area of approximately 1000 ha located in the Scottish Borders (NT221562, lat. 55°47'30", long. 3°14'20"). The peat is on average 60 cm deep and is water-logged most of the time during the year, except for the summer season, when the moss becomes generally drier.

Vegetation

The moorland vegetation comprises a succession of hummocks and hollows (vertical range: 50 cm) that can be divided into sub-zones, see [Lindsay, 1995]: the low ridge and hollows (the lowest 30 cm) are the wetter parts and possess an almost continuous mixed carpet of *Sphagnum* species that are adapted to water-logged and acidic conditions. Within this carpet, other bryophyte species such as *Polytrichum comune*, and also a large community of sedges e.g. *Carex nigra* and *C. ovalis*, and monocotyledons such as *Eriophorum angustifolium* are present. The hummocks (the top 20 cm) are naturally drier, often *Polytrichum*-formed mound-like tussocks about 10-30 cm above the bog moss carpet; they contain a lower density of *Sphagnum* species and more vascular plants than the hollows. Hummock tops and the high ridge are dominated by grasses and sedges including *Deschampsia flexuosa, Molinia caerulea, Eriophorum vaginatum, Eriophorum angustifolium* and *Festuca ovina.* Ericaceous dwarf-shrubs such as *Erica tetralix, Calluna vulgaris* and *Vaccinium myrtillus* are scarce and patchy in their occurrence at this site.

The site is used for sheep grazing at a very low density of about 0.1 to 1 sheep

Figure 3.5: Auchencorth Moss. Red lines are arbitrary boundaries of the peat bog. The red rectangle marks the measurement point (from Collins-Bartholomew Map, Scale 1:1000).

per hectare all year round; very often no animals are visible from the site. It is generally greener and drier in the brief summer than in winter, and the weather is typical of British Upland environments, being generally wet, windy and cool. The agricultural activities in the vicinity of the site are fairly low intensity, the nearest farm with intensive livestock production (poultry) is located at 2.7 km south of the site and 6 farms are located at distances of 0.5 km to 3 km.

A photograph taken at the site (Fig.3.6) shows the characteristic vegetation in Auchencorth Moss.

Site climate

The series of data collected with the TAG system at Auchencorth Moss show daily temperatures averaging between 0 ^{o}C and 15 ^{o}C, with some exceptions recorded during winter and summer, where the half-hourly temperatures range between -5 ^{o}C and 28 ^{o}C respectively; averaged values including night and day times show very regular seasonal variations (Fig. 3.7): during winter time the average temperature is around 4 ^{o}C and in summertime around 14 ^{o}C, with an overall annual average temperature of 8.8 ^{o}C. The cup anemometer placed at 2.5 m on the TAG mast measured an overall mean wind speed of 4.75 m s^{-1}, with a median value of 4.76

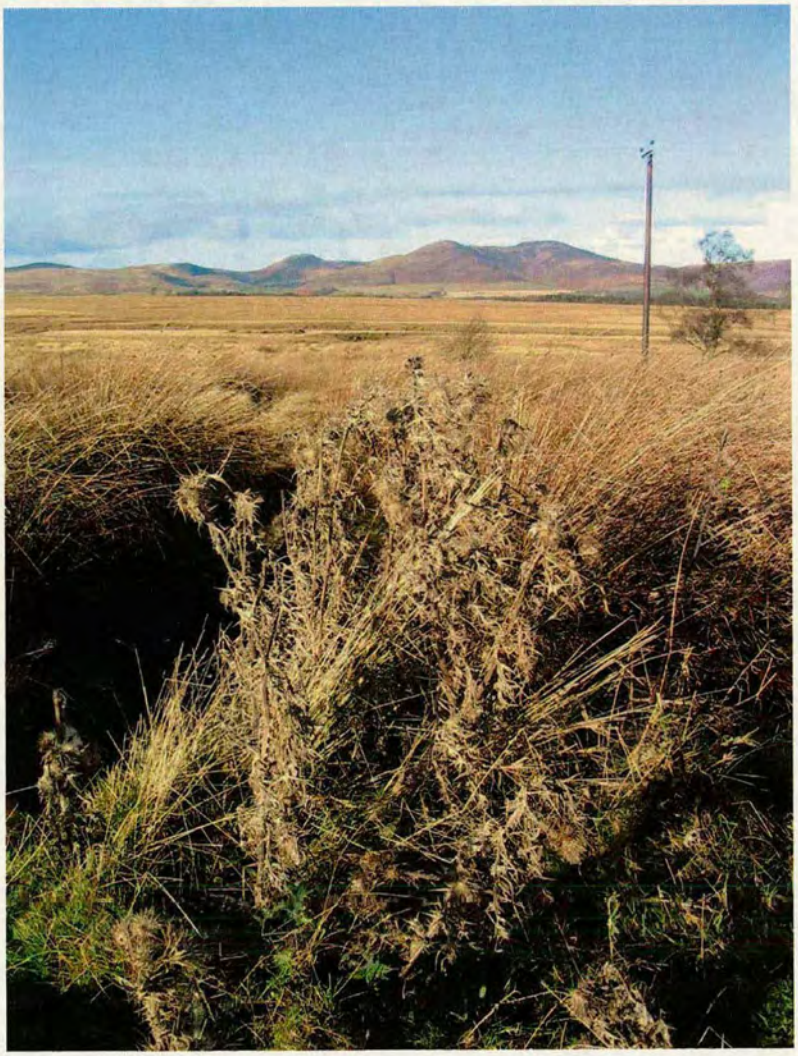

Figure 3.6: Example of hummocks at the Auchencorth Moss field site; a close-up to the canopy shows the irregularity of the surface.

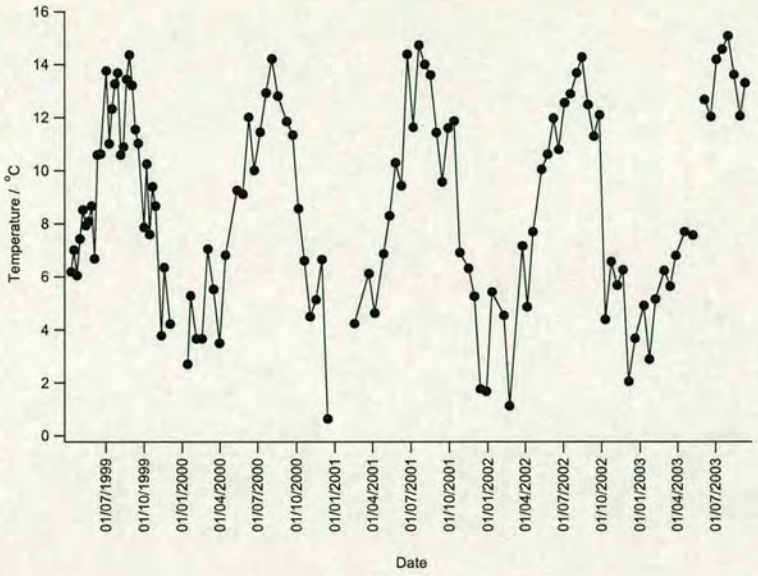

Figure 3.7: Time series of air temperature recorded at Auchencorth Moss

m s^{-1}. Wind speeds range between 0 m s^{-1} and 14 m s^{-1}, with maximum values recorded generally during autumn and winter, when precipitation is also largest as can be seen in Fig. 3.8 and 3.10. A diagram of the frequency distribution of wind direction measured at Auchencorth Moss in the years between 1999 ans 2003 is shown in Fig. 3.9. The prevailing wind sector is SW, with a NE weaker contribution: the SW-NE dominant direction and the constriction of the air flow over the field are the effects of the two ranges of 600 m high hills, the Pentlands, which lie in a SW-NE direction to the N and S of the site. The locations of the farms surrounding the site are out of the prevailing wind sector.

A Bowen-ratio monitoring instrument was placed nearby the TAG system to provide sensible (convective) heat (H), latent heat (λE), soil heat (G), total solar (S_t) and net radiation (R_n) fluxes and rainfall. The annual rainfall (see Fig. 3.10 showing monthly averaged values for the years between 1999 and 2003) is of the order of 800 mm, of which two thirds to three quarters fall between September and March, while summers (April to August) are generally slightly drier, although summer rainfall may vary from year to year.

During a previous study, wind profile measurements were made simultaneously at Auchencorth Moss for a period of 5 months for a comparison between different micrometeorological methods [Flechard, C. R. and Fowler, D., 1998]. 5 sensitive

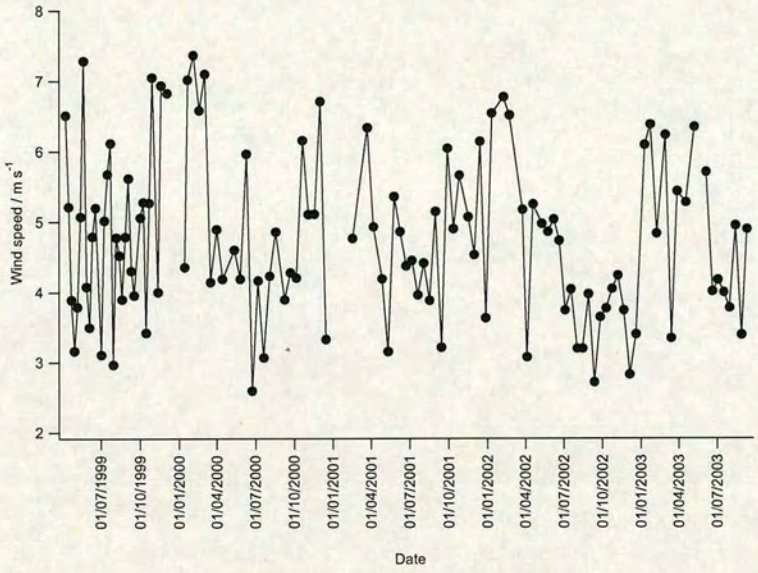

Figure 3.8: Time series of horizontal wind speed recorded at Auchencorth Moss

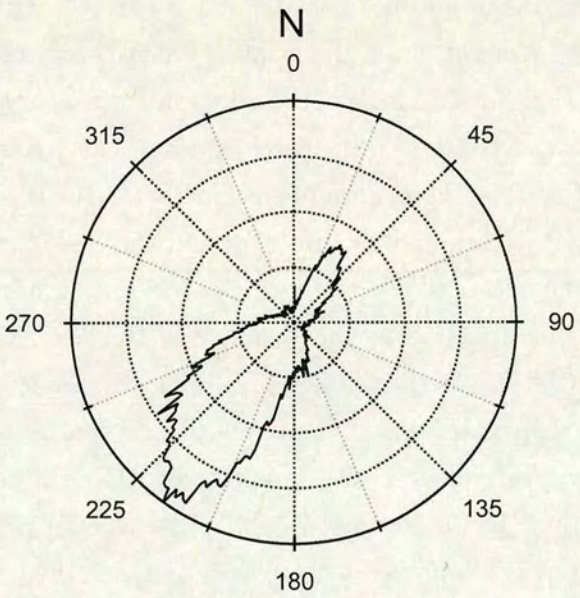

Figure 3.9: Wind direction frequency recorded at Auchencorth Moss for the period from 1999 to 2003.

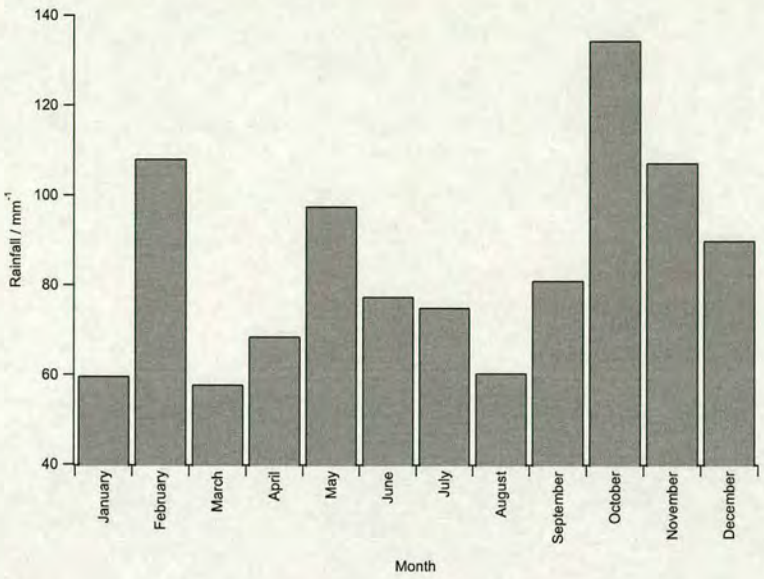

Figure 3.10: Monthly averaged rainfall recorded at Auchencorth Moss for the period from 1999 to 2003.

cup anemometers (Vector Instruments, Rhyl, Clywd, UK) were mounted on a mast at heights of 3.1, 1.9, 1.3, 0.8 and 0.6 m in the surface layer. These measurements provided estimates of displacement height (d) and roughness length (z_0) (see§ 2.4 for their definition): an evaluation of d was found by plotting ln(z-δ) against u, where δ is an estimate of d varying between 0 and canopy height. The best estimate for d is the value of δ providing a straight line of ln(z-δ) against u in neutral conditions for the atmosphere [Thom, 1975]. Similar procedures applied to a large number of neutral runs revealed that d varied between about 0.2 m in summer with a fully-grown 0.5 m-high canopy, down to about 0.1 m in winter subsequent to canopy senescence and partial decay. An average annual cycle of d has been extrapolated by these measurements, and it is shown in Fig. 3.11. Values of roughness lengths were estimated typically between 10 and 20 mm, and a sample of them is plotted in Fig. 3.12.

Energy partitioning

Seasonal temperature variations in the local climate at Auchencorth Moss are clearly coupled with variations in total solar and net radiation (Fig. 3.18); solar total radiation, S_t, may reach 900 W m^{-2} on clear-sky summer days, allowing solar

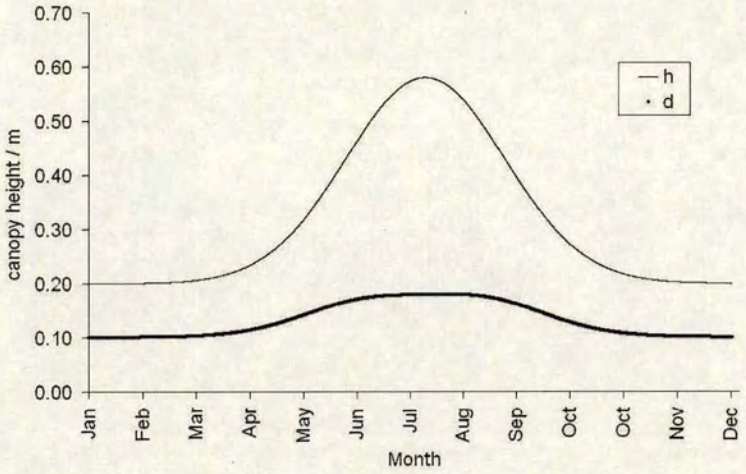

Figure 3.11: Seasonal variation in displacement height (d) at Auchencorth Moss (thick line). Values of the canopy height throughout the year have been recorded and are shown as a thin line.

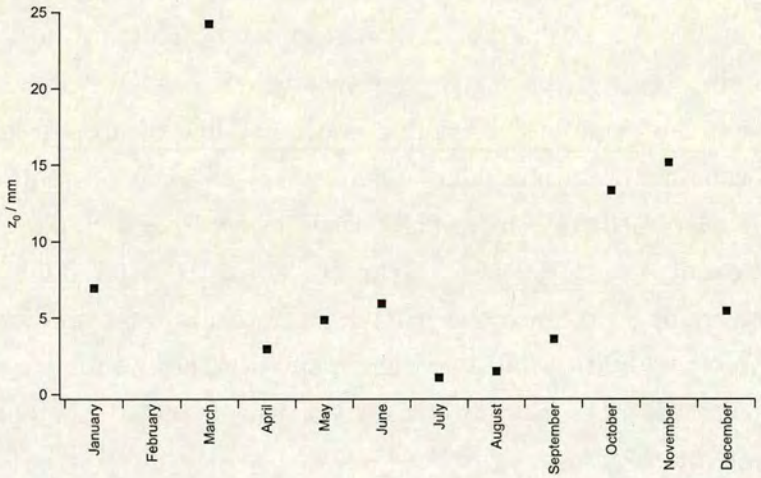

Figure 3.12: Seasonal variation in roughness length (z_0) at Auchencorth Moss. Values are monthly geometric means.

net radiation values, R_n, up to 600 W m^{-2}. Nighttime maximum radiative losses (R_n <0) are between -10 W m^{-2} and -60 W m^{-2}, showing no clear systematic seasonal trend.

The partitioning of net radiation into sensible (convective) heat (H), latent heat (λE) and soil heat (G) fluxes was found to depend on canopy wetness. Latent heat fluxes dominate the heat loss for the site, and it is relatively larger when the moorland canopy is wet, while in dry conditions the majority of the available energy (R_n-G) is lost as convective sensible heat. Soil heat fluxes averaged 0.4 W m^{-2} overall (not significantly different from 0), with maximum values up to 65 W m^{-2} on sunny windy days, and minimum values down to 46.8 W m^{-2}. The convective loss of sensible heat was typically about 100 W m^{-2}, reaching values of 292 W m^{-2} on dry sunny days. The latent heat flux was of the same order as the sensible heat flux on warm summer days, and two to five times larger than H on wet days. Energy budgets for Auchencorth Moss typical for summertime and wintertime are presented in Fig. 3.13 and 3.14 respectively; the latent heat flux is calculated using the energy conservation equation ($\lambda E = Rn - H - G$).

The partitioning of the available energy into sensible and latent heat has often been interpreted in terms of the Bowen ratio $\beta = H/\lambda E$ [Miranda et al., 1984]. In summer, β often exceeds 1, implying that more short-wave radiative energy is converted and lost as sensible heat than is used to evaporate water from the surface. By contrast, in winter, wet and cool conditions, latent heat is generally larger than sensible heat by a factor of 2 to 5 (see e.g. Fig. 3.15). These findings are consistent with those of [Miranda et al., 1984] who found β values of 2.0 and 0.6 for dry and wet heather canopies, respectively.

Fetch and footprint study

The method by Schuepp described in § 2.4 can provide an estimate of the area within the upwind fetch contributing to the sink for the deposition of the trace gas; it is quantified by the Cumulative Normalised contribution to the Flux measurement (CNF) in relation to the upwind distance x_L from the wind sensor. By using the meteorological data output from the TAG, it was possible to assess the contribution to the flux of the footprint area in Auchencorth Moss, as shown in Fig. 3.16; the CNF is plotted versus the upwind distance x_L for two half-hourly measurements made with the TAG, considering the top height for wind speed measurements, at 2.5 m above the ground. In neutral conditions (continuous lines),

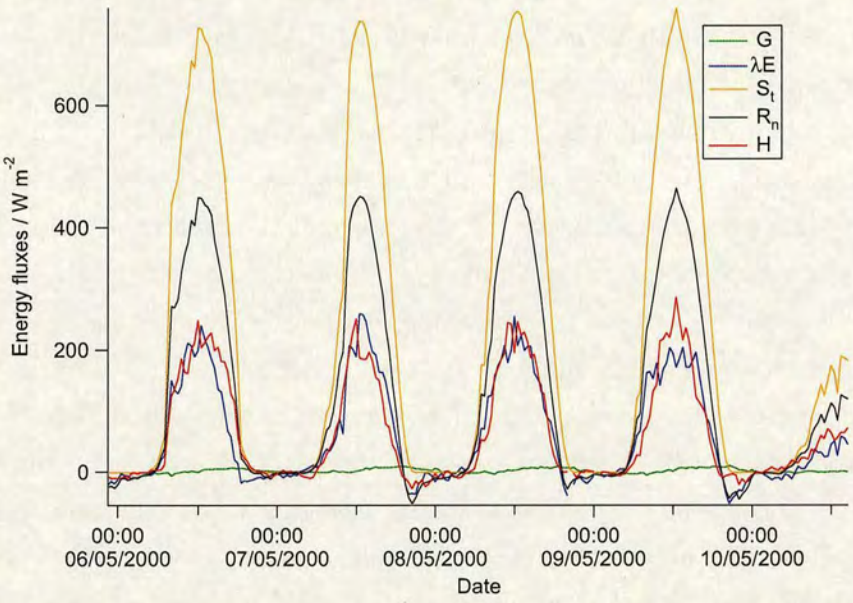

Figure 3.13: Energy balance recorded at Auchencorth Moss showing a typical behaviour of energy fluxes in dry, sunny conditions during the summertime.

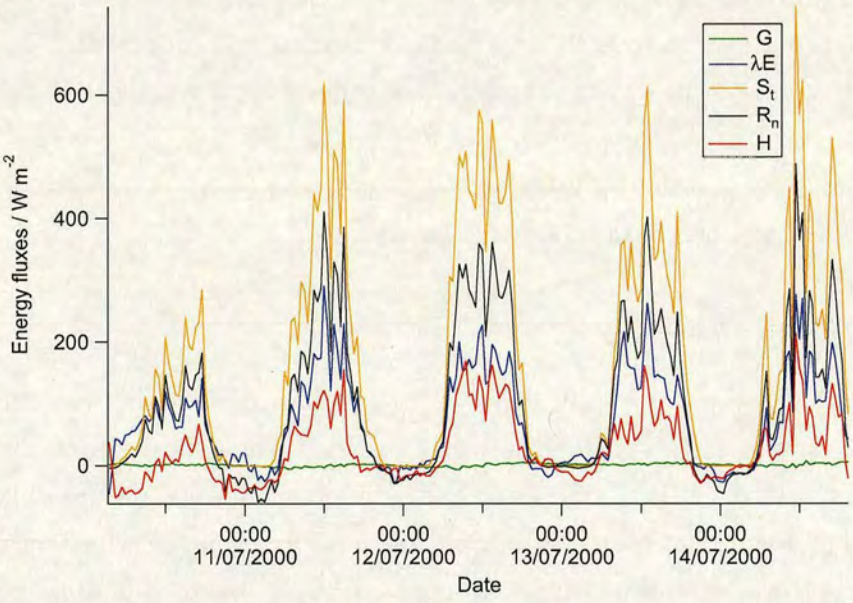

Figure 3.14: Energy balance recorded at Auchencorth Moss showing a typical behaviour of energy fluxes in wet conditions during the summertime.

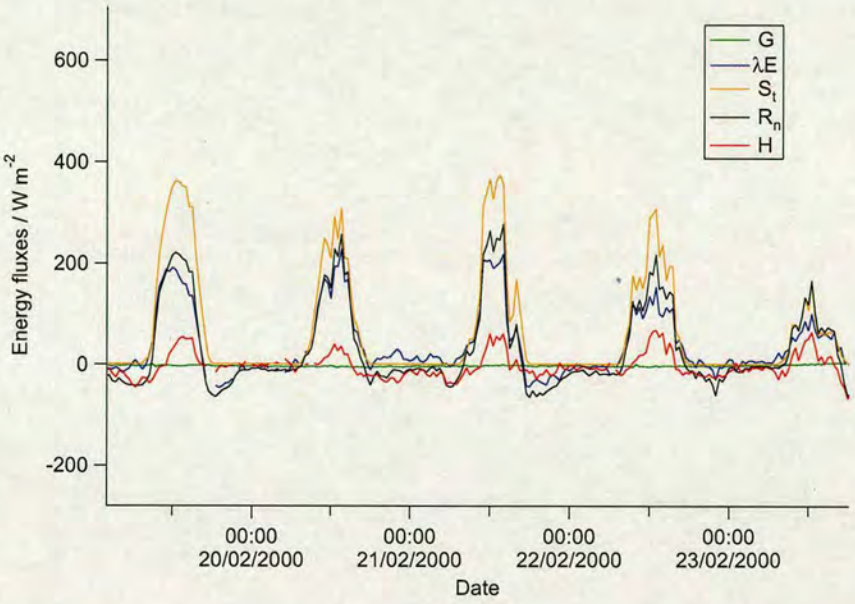

Figure 3.15: Energy balance recorded at Auchencorth Moss showing a typical behaviour of energy fluxes in wet conditions during the wintertime.

between 70% and 80% of the flux would be contributed by the nearest 400 m upwind. However, the runs presented are stable (14/05/00 20:00) and unstable (14/05/00 15:00); the stability corrections ϕ_M applied as in Eq.2.31 to both runs induce a shift of the curve upwards downwards, in unstable or stable conditions, respectively. This implies for instance that 60% of the flux is contributed by the nearest 100 m in the unstable case (dotted line), or by the nearest 1100 m in the stable case (dot-and-dashed line). When applying the same method to the data from the sonic anemometer placed at 3.6 m height, a differential in flux footprints calculated by both techniques is observed, as can be seen in the example in Fig. 3.17.

This is because the measurement height z for the sonic anemometer (3.6 m) is higher than that of the TAG system (2.5 m), and the vegetation height and thus roughness was larger in the nearest 50 m upwind of the instruments masts inside an enclosure where sheep were not allowed to graze. The contribution of the area outside the enclosure (lower z_0) to the CNF was larger for the measurements made by the sonic anemometer than for the measurements by the TAG wind profile, yielding e.g. u_* values estimated with the sonic anemometer smaller than u_* values measured by the wind profile of the TAG.

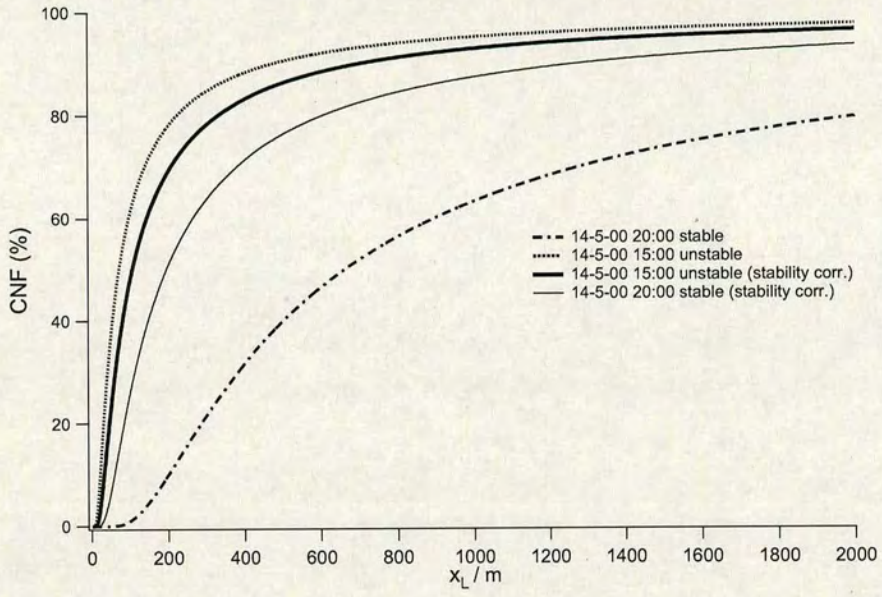

Figure 3.16: Contribution to the measured flux (CNF) by an upwind area bounded by the upwind distance x_L from the measurement point. The dotted lines refer to the runs not corrected for stability.

This difference in flux footprints may to some extent be related to discrepancies between friction velocity or sensible heat fluxes as measured by eddy covariance and flux-gradient methods.

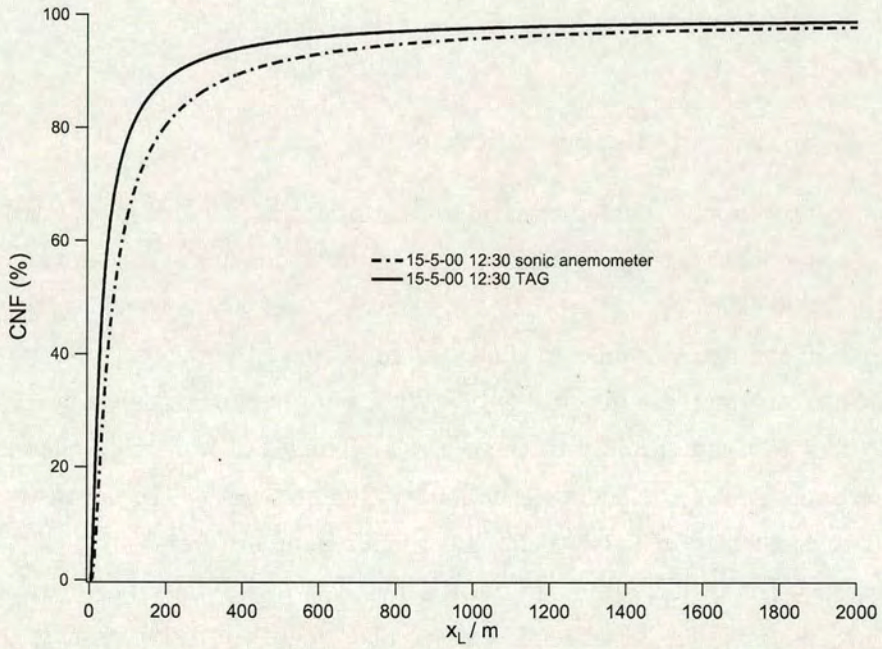

Figure 3.17: An example of CNF calculated for neutral atmospheric conditions using the sonic anemometer data (dotted line) and TAG data (continuous line).

Variable	Average	Median	Min	Max
H (W m^{-2})	0.38	2.16	-180	300
u_* (m s^{-1})	0.35	0.34	0	1.4
k_m	0.15	0.14	0.004	0.33
V_d (mm s^{-1}) SO_2	0.41	0.18	-25.58	39.91
V_d (mm s^{-1}) NH_3	17.6	14.47	-2.78	43.74

Table 3.1: Basic statistics on the sensible heat fluxes (H) and friction velocity (u_*), deposition velocities for SO_2 and NH_3, and eddy diffusivity recorded at Auchencorth Moss from 1999 to 2003.

Turbulent fluxes and chemical climate

In Fig. 3.18 the sensible heat fluxes values are plotted, averaged over fortnightly periods. Seasonal changes are noticeable in this chart; the fluxes vary between -180 W m^{-2} and 300 W m^{-2}; temperatures are plotted once again to show the agreement between the two variables in time: the increase of temperature is delayed in comparison to the increase in sensible heat flux, but they follow the same pattern. The heat flux responds rapidly to the seasonal changes in radiation, whereas the air temperature shows the effect of the longer time it takes to the oceans to store heat and consequently increase theirs and the air temperature.

Turbulence conditions are characterised by the friction velocity, or u_*, shown in Fig. 3.19 as fortnightly averaged values. The long-term mean value is 0.35 m s^{-1}, with a very close median value of 0.34 m s^{-1}; friction velocities range between 0 m s^{-1} in very stable situations and 1.4 m s^{-1} in convective ones. In Table 3.1 are summarised the main statistics for some turbulent variables of interest.

The chemical climate of Auchencorth Moss is here reported from the data collected by the TAG instrument. To measure SO_2 concentration, glass denuders have been coated with a solution of sodium carbonate in glycerol; likewise for NH_3 concentration a solution of citric acid in methanol was used to coat the denuders walls. The samples were extracted after the fortnightly exposure of the denuders, and the concentrations were determined by Ion Chromatography for SO_2 and by conductivity analysis for NH_3 using an AMFIA (Ammonia Flow Injection Analyzer, ECN, Petten, NL). The precision on the concentration value is of the order of 10% for both cases, whereas the detection limit (calculated as three times

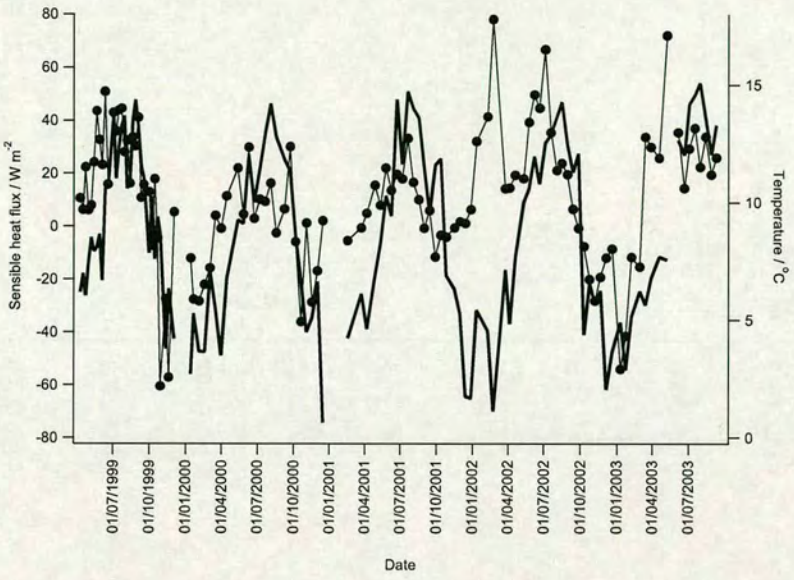

Figure 3.18: Time series of sensible heat fluxes recorded at Auchencorth Moss (markers and thin line) and temperature values (thick line).

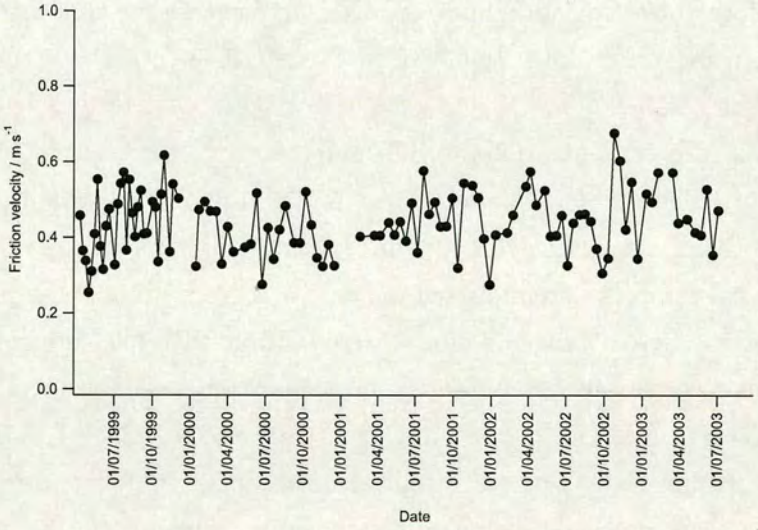

Figure 3.19: Time series of friction velocity recorded at Auchencorth Moss.

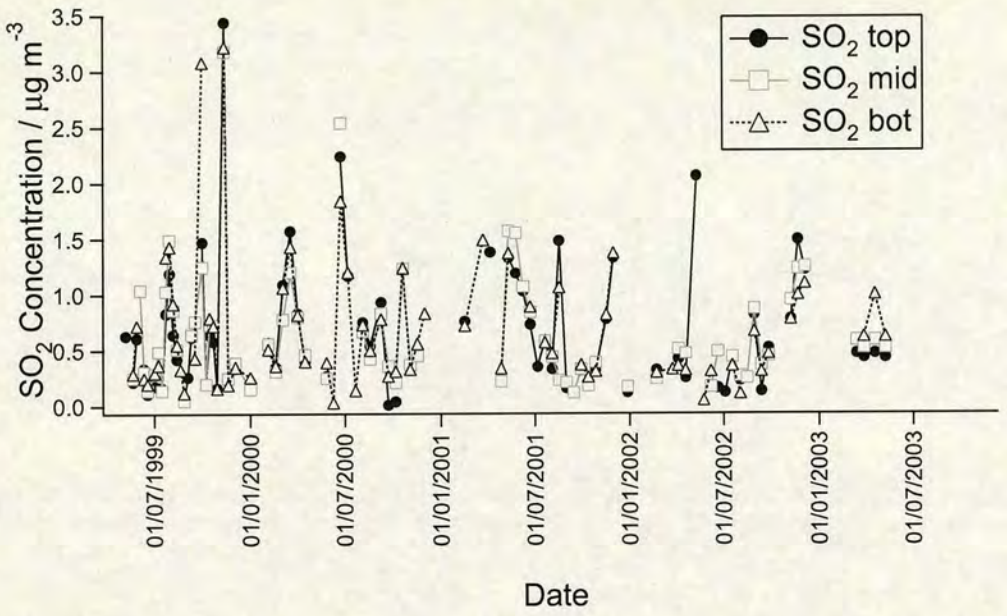

Figure 3.20: Time series of concentration values for SO_2 recorded at Auchencorth Moss.

the standard deviation around a blank value) of the denuder applied technique is 0.036 $\mu g/m^3$ for SO2 and 0.003 $\mu g/m^3$ for NH_3. The value of the difference in concentration between the single heights is for SO2 included between 0.15 to 0.22 $\mu g/m^3$, therefore above detection limit. For NH_3 in one case the concentration step was lower than detection limit, but was on average 0.18 $\mu g/m^3$, therefore above detection limit as well.

In Fig. 3.20 the concentrations of SO_2 show a range between detection limit and 3.4 $\mu g/m^3$. The different markers refer to the different heights at which the samples were taken, respectively at 2.52 m, 1.16 m, 0.51 m.

The chemical samples were analysed weekly for the first six months period, and then fortnightly. These averaged values are compatible with measurements of SO_2 concentrations recorded at the site during previous years, see [Fowler et al., 1996], ranging between 0 and 3.44 g m^{-3}, having a total mean value of 0.67 μg m^{-3}. These concentration levels are quite typical of a background site, and their low value makes the chemical detection often difficult: values of the blank samples sometimes are similar to the exposed samples, increasing the uncertainty on the concentration gradient.

In Fig. 3.21 the time data series of NH_3 concentration recorded at Auchencorth

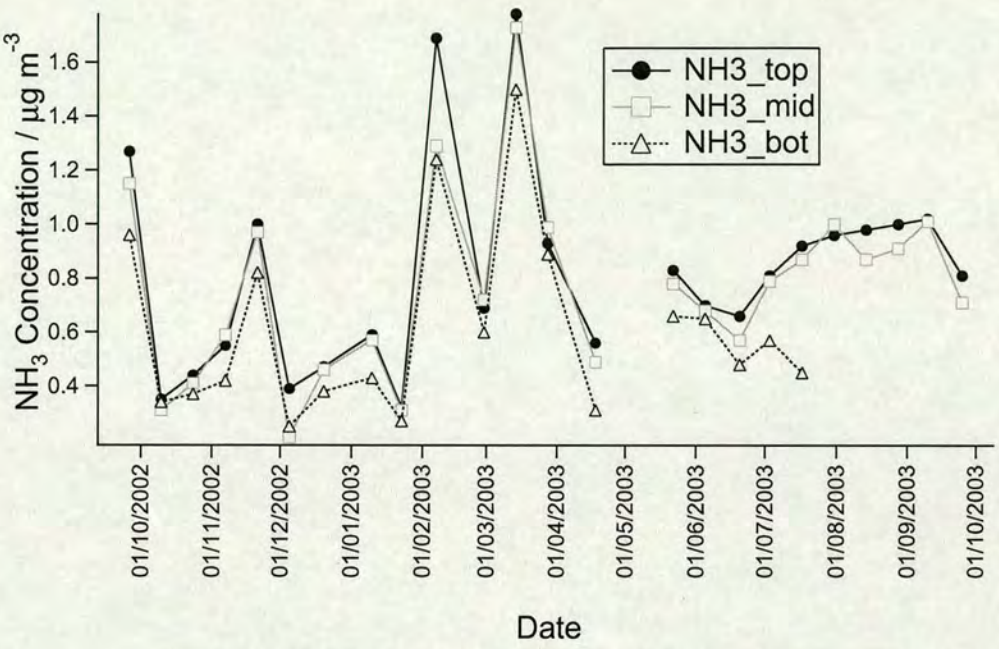

Figure 3.21: Time series of concentration values for NH_3 recorded at Auchencorth Moss.

Moss with the same TAG system is shown; the denuders used for NH_3 are placed in series with the SO_2, therefore the heights of measurement are the same as above. It can be seen from Fig. 3.21 that most of the measurements periods were characterised by a deposition gradient, in fact the bottom sensor (triangles) measured the lowest value on average, followed by the middle one (squares) and then by the top sensor (dots). Only in one occasion the gradient indicates emission (August 2003) of ammonia from the ground, and for some cases the order top-middle-bottom (or vice versa) didn't form a monotonic gradient. The chemical analysis of the samples plays an important role in the evaluation of these gradients, and poor capture or contamination in one of the samples affects the quality of the gradient after the rejection by the chemical analysis. Table 3.2 below reports some statistics regarding the concentrations of the chemicals monitored by the TAG system.

Sample location	Average	Median	Min	Max
NH_3 ($\mu g\ m^{-3}$) top	0.821	0.810	0.320	1.778
NH_3 ($\mu g\ m^{-3}$) mid	0.766	0.751	0.209	1.729
NH_3 ($\mu g\ m^{-3}$) bot	0.612	0.483	0.251	1.504
SO_2 ($\mu g\ m^{-3}$) top	0.662	0.470	LOD	3.444
SO_2 ($\mu g\ m^{-3}$) mid	0.634	0.480	0.049	3.178
SO_2 ($\mu g\ m^{-3}$) bot	0.623	0.472	LOD	3.216

Table 3.2: Statistics on the concentrations of SO_2 and NH_3 recorded at Auchencorth Moss.

3.4.2 Gradient calculation and data rejection

Following from Eq.2.20, the gradients used to compute the fluxes are calculated as:

$$\text{grad}\chi = \frac{\partial\chi}{\left[\partial log(z-d) + \psi_H\right]} \tag{3.3}$$

$$\text{gradu} = \frac{\partial u}{\left[\partial log(z-d) + \psi_M\right]} \tag{3.4}$$

for chemical concentration profiles and wind speed profiles, respectively.
ψ_M and ψ_H are the integrated stability correction functions for momentum and heat at all the heights in the surface layer where measurements of wind speed, temperature and trace gases are made (see §2.2).

The TAG system used at Auchencorth Moss had two measurement points for wind and temperature profiles, and three chemical sensors located at three heights. The uncertainty on the vertical profiles of wind speed and temperature is therefore limited to the error that is associated with the precision and accuracy of the cup anemometers and the thermocouples. The situations of low wind speed were therefore excluded from the dataset, choosing a threshold of 0.4 m/s (the threshold of the cup anemometers being 0.2 m/s, the accuracy 1% at wind speeds in the range of 10 to 55 m/s). The copper-constantan thermocouples used in the TAG system are able to provide readings with an error of 0.5% for the temperature measured at the field site, corresponding on average to 0.02^{o}C: the average temperature difference between the two sensors was of 0.1^{o}C. Overall, the data rejection on the meteorological data was of 3.6% : in fact Auchencorth Moss is a very windy site (see Fig.3.8) and low wind conditions are very rare events. The height displacement between the sensors allowed a temperature difference that was in more than 96% of the cases above the sensitivity of the thermocouples.
As for the minimal number of wind speed and air temperature sensors, very little can be said about uncertainty of the TAG meteorological gradients without comparingthe outcome ofthe system to an established method. For this purpose, in section 3.4.3 is shown a comparison of the TAG performance in assessing momentum and heat fluxes by using the vertical profile approach with the data collected from a sonic anemometer.

For what concerns the chemical profile, the gradient was calculated using the least square method as the slope of a line determined by three points.

SO_2	top-mid	mid-bot	top-bot
Slope	0.56	0.51	0.92
Intercept	-0.028	-0.011	-0.021
r^2	0.43	0.62	0.66
NH_3			
Slope	0.98	0.90	0.99
Intercept	0.11	0.037	0.003
r^2	0.38	0.42	0.99

Table 3.3: Summary of regression parameters for NH_3 and SO_2 gradients.

To qualitatively assess the reliability of these three-points-gradients, the gradient values from two points in all possible combinations (i.e. top-middle, middle-bottom, top-bottom) were calculated for each of the measuring periods, and by observing the difference between these three gradient estimates and the least squares gradient it was possible to identify a poor gradient estimate from a good one.

When neutral conditions are met, or when stability corrections are applied, the vertical profile should be logarithmic for concentration, wind speed and temperature: therefore every estimate of a vertical gradient done in the same conditions should lead to the same result. A big difference between the different estimates indicates a fault in the data, and even though this procedure doesn't quantify the error on the flux estimate, it is useful in the phase of rejection of data.

Examples of gradient estimates for NH_3 and SO_2 are shown in Fig. 3.22 and 3.23, and linear regressions between gradients calculated with the least square method (reference values) and the two-points gradients for NH_3 and SO_2 respectively are plotted in Fig. 3.24 and 3.25. In Table 3.3 are summarised the regression parameters relative to these charts, respectively for NH_3 and SO_2 gradients.

The minimum value of the gradient calculated with the 2-point-approach is subtracted from the 3-points gradient, giving the biggest negative deviation on the gradient value. Analogously the 3-points gradient is subtracted from the maximum of the 2-points gradient values, returning the biggest positive deviation on the gradient value. These deviations are plotted in Fig. 3.26 and 3.27 as error bars along the gradient lines.

The deviations between the differently calculated gradients are not errors on the expected value of the gradient; the bigger the absolute value of the gradients,

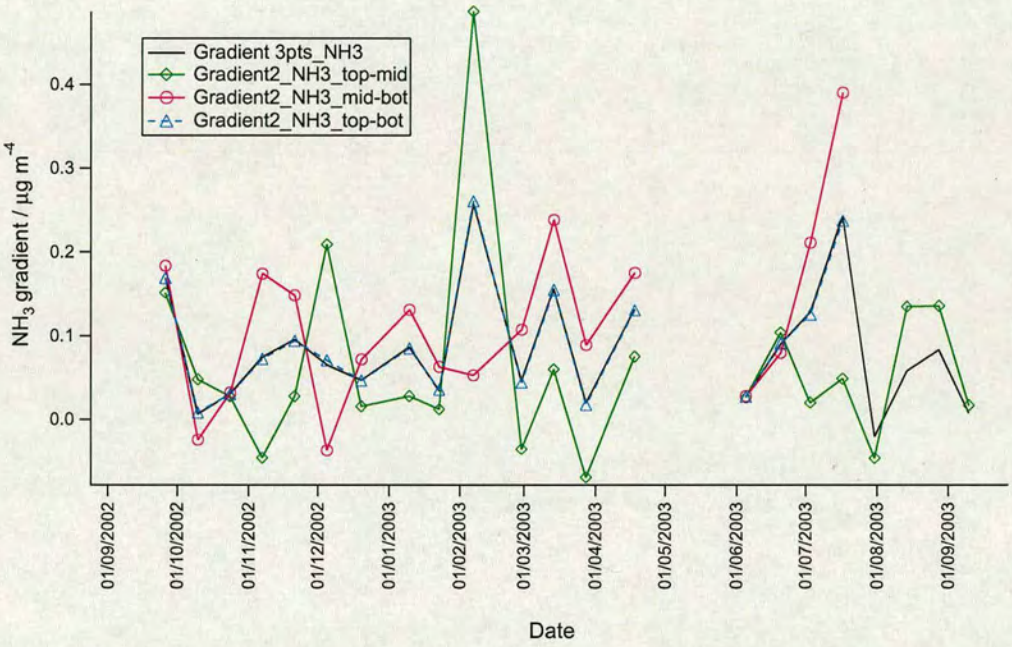

Figure 3.22: NH_3 gradients measured during year 2003. Each set of data correspond to different combination of the sensors considered in the calculation of the gradient: diamonds refer to top and middle heights, circles to middle and bottom, triangles to top and bottom.

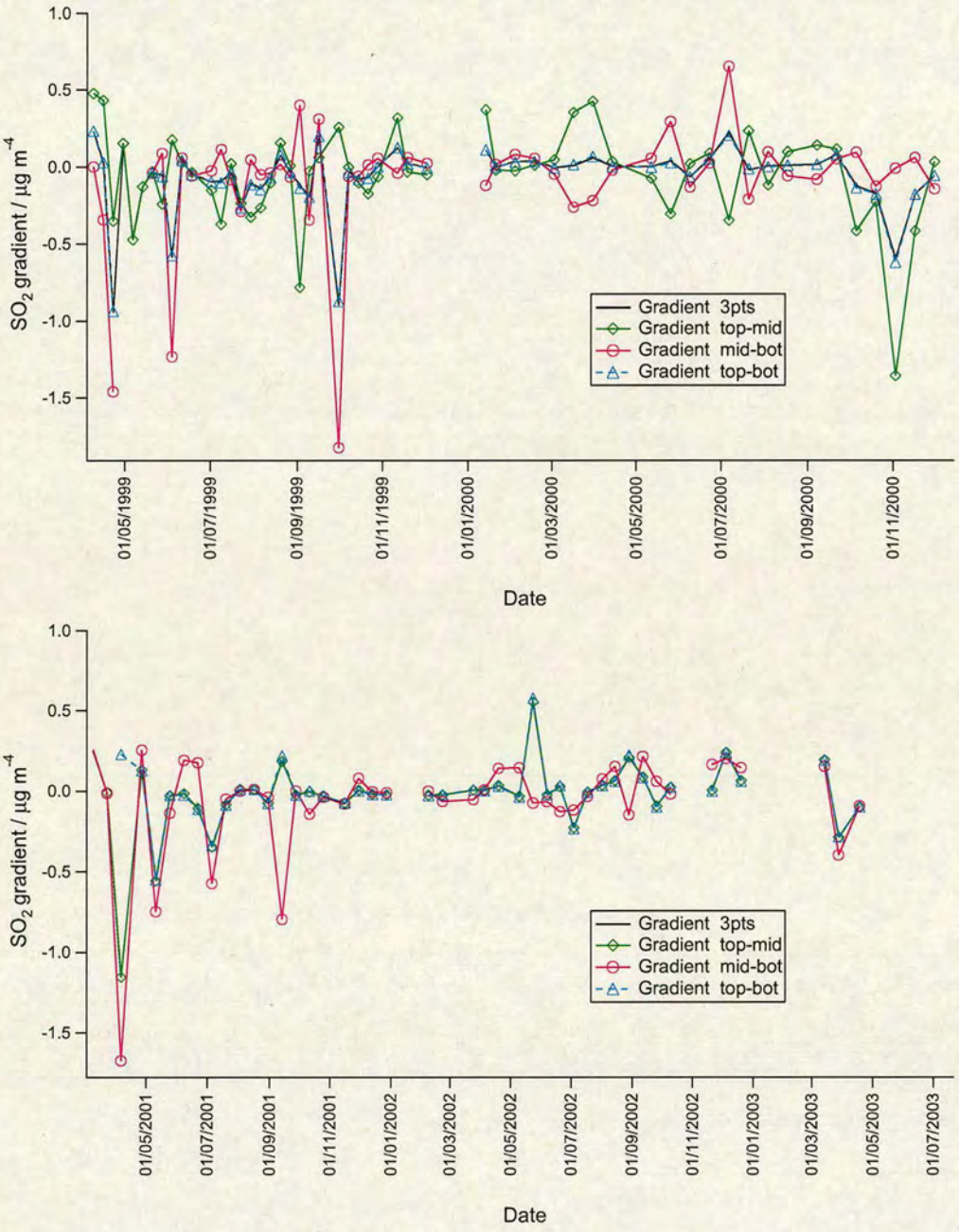

Figure 3.23: SO_2 gradients measured from year 1999 to 2003. Each set of data correspond to different combination of the sensors considered in the calculation of the gradient: diamonds refer to top and middle heights, circles to middle and bottom, triangles to top and bottom.

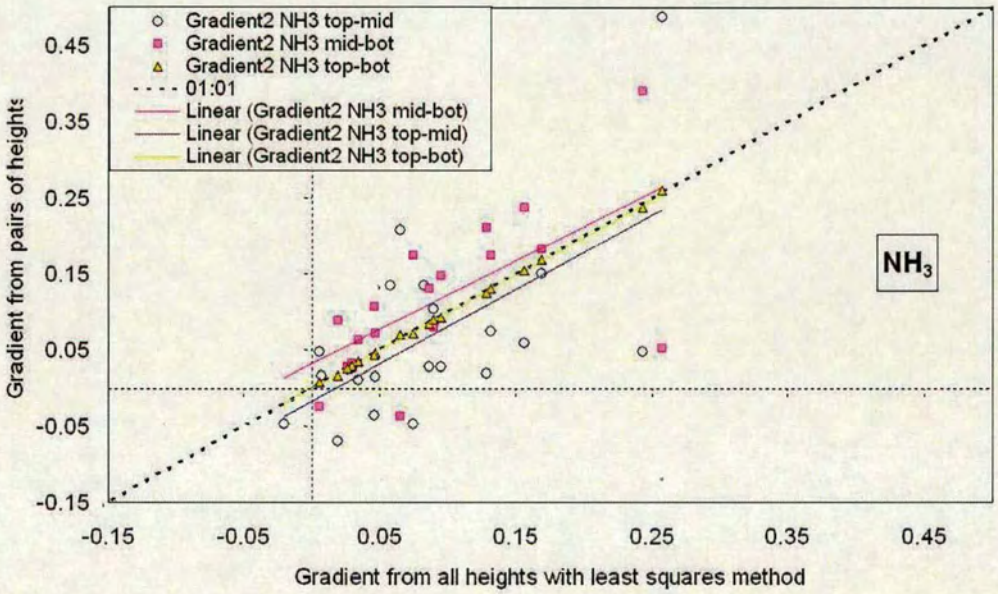

Figure 3.24: Correlation between the NH_3 gradients calculated using the least squares method between the three heights (x values) and the pairs of heights (y values).

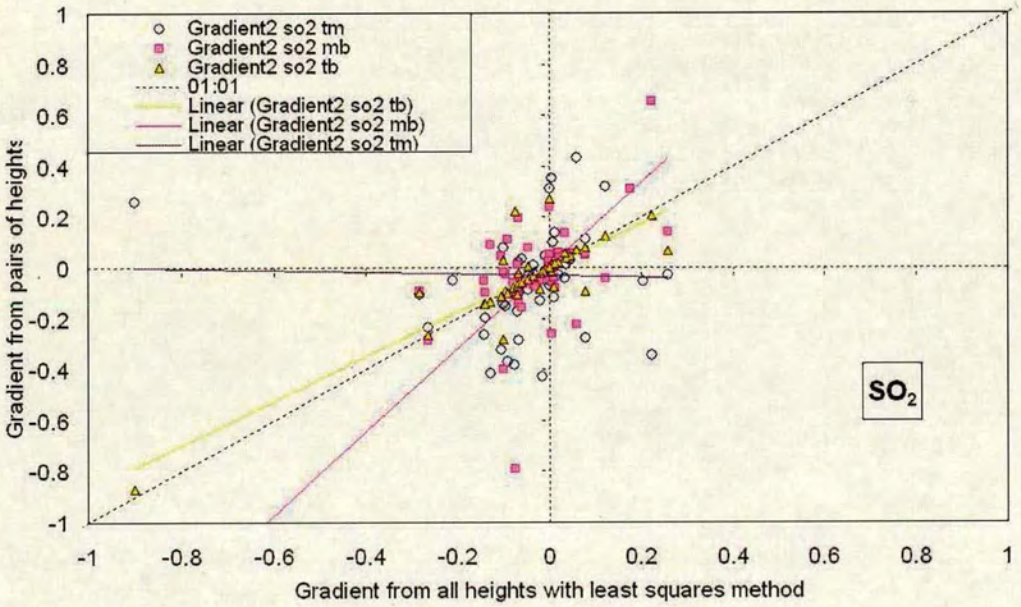

Figure 3.25: Correlation between the SO_2 gradients calculated using the least squares method between the three heights (x values) and the pairs of heights (y values).

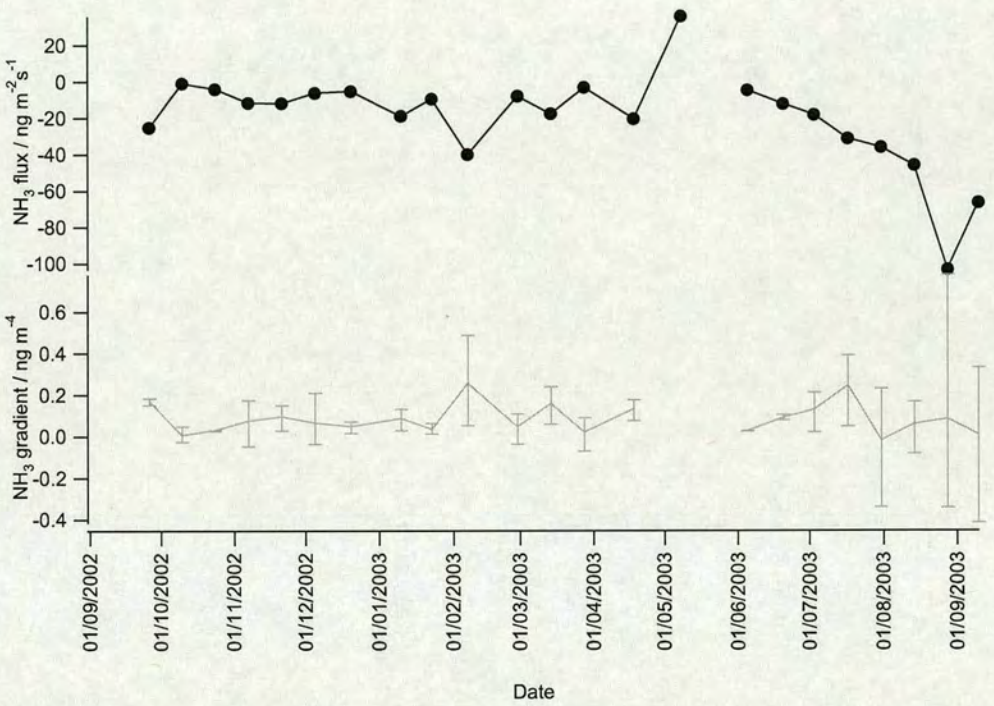

Figure 3.26: Bottom: NH_3 gradient values calculated using least squares method from the three heights. Error bars refer to the distances between the gradients calculated from the alternate pairs of heights. Top: NH_3 fluxes recorded at Auchencorth Moss during 2002-2003.

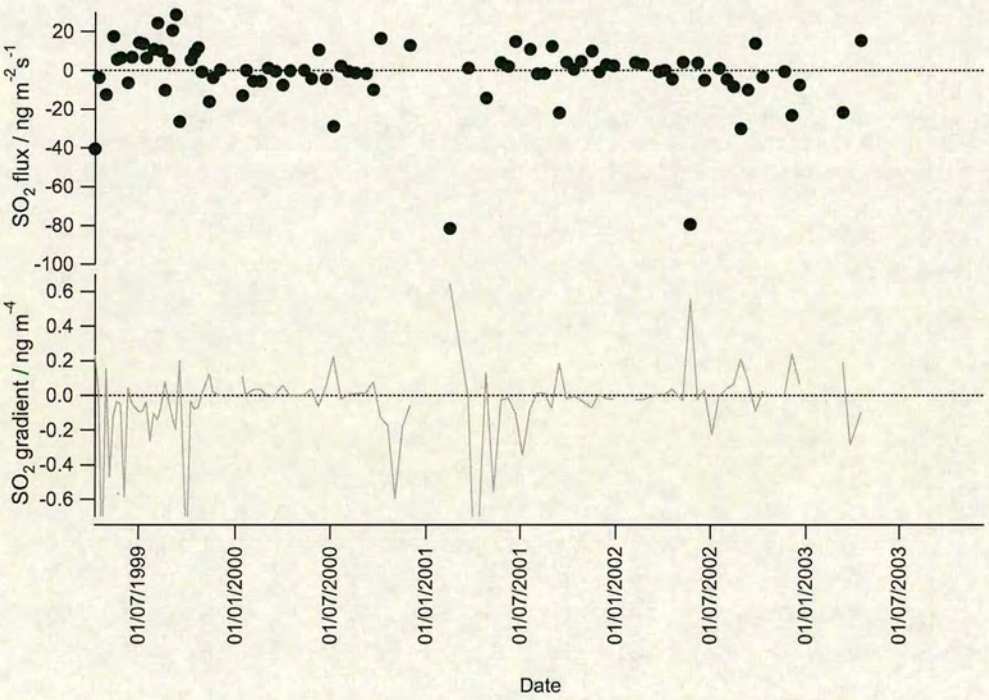

Figure 3.27: Bottom: SO_2 gradient values calculated using least squares method from the three heights. Error bars refer to the distances between the gradients calculated from the alternate pairs of heights. Top: SO_2 fluxes recorded at Auchencorth Moss during 1999-2003.

the bigger the deviation. A percentage standard error provides a measure of the reliability of the gradient estimate, but at the same time the information on the deviations sign would be lost, along with the qualitative information about the emissive or depositing character of the phenomena.

In order to retain as much as the possible information, the chosen data rejection criteria were a compromise between the following. A first rejection criterion for the gradient data is to exclude all gradient values that, with different methods, lead to both emission and deposition fluxes for the same case; a second criterion is given by the magnitude of the relative standard error. A third factor to be taken into account is the chemical analysis uncertainty; concentration values that showed low capture, or possible contamination of the system, or poor zero reference values were rejected.

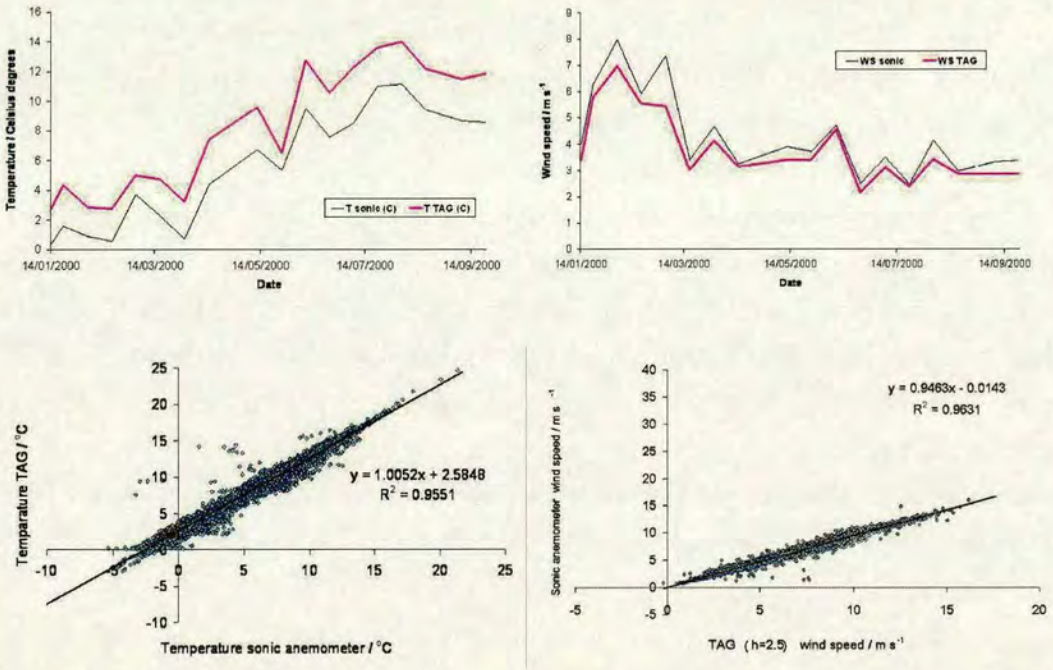

Figure 3.28: *Top*: temperatures and wind speeds measured by the TAG profiler (bold line) and by sonic anemometer (thin line). *Bottom*: comparison between temperature and wind speed values recorded by the TAG system and the sonic anemometer at Auchencorth Moss.

3.4.3 Comparison with sonic anemometer

A comparison between the wind speed and temperature measurements from the vertical profiler of the TAG and the sonic anemometer measurements (Fig.3.28) shows that the wind speed values have a good agreement and the TAG profiler is slightly underestimating the wind speed; this is probably due to the effect of very low wind conditions, where the cups of the propeller anemometers stop. The temperatures measured by the TAG profiler show an offset of 2 m s^{-1} when plotted against the sonic temperatures: this difference is probably due to the error that characterises sonic temperature measurements, see e.g. [Kaimal and Gaynor, 1991] on sonic thermometry.

Linear regression plots are shown in Fig.3.28: for both wind speed and temperature the agreement between the TAG profiler and the sonic anemometer is good, with correlation coefficients values r above 0.97 for both cases.

An example of diurnal trends for friction velocity and sensible heat fluxes mea-

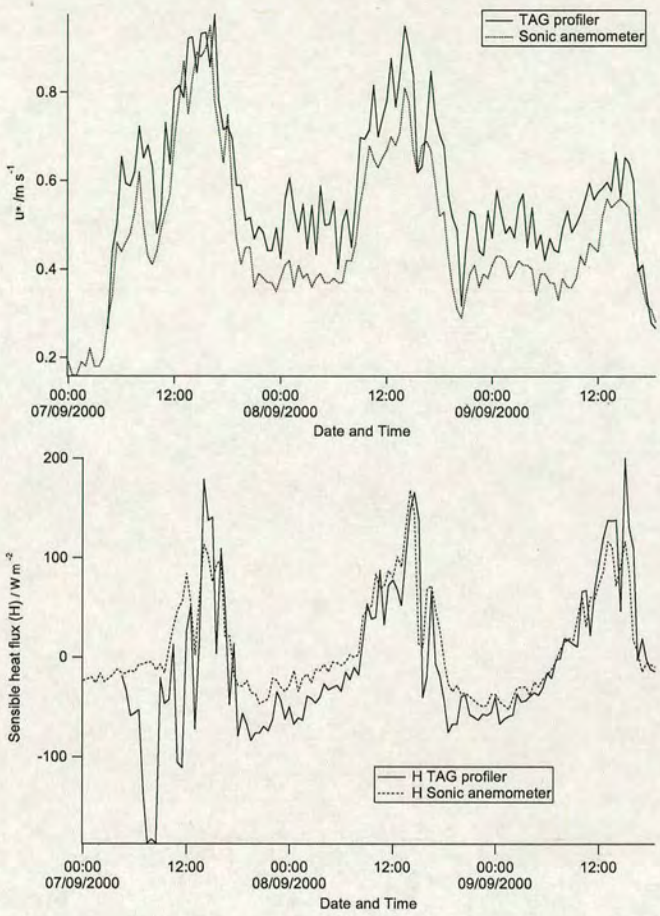

Figure 3.29: Diurnal cycles of friction velocity (*top*) and sensible heat flux (*bottom*): the dotted lines are the values measured with the sonic anemometer, the bold lines refer to the TAG profiler data.

sured with the TAG profiler and with sonic anemometer is shown in Fig. 3.29; turbulent fluxes measured by the TAG profiler are well correlated with eddy covariance fluxes (r>0.8 in both cases). u_* values seem slightly overestimated, with an offset of 0.14 m s^{-1}, whereas sensible heat fluxes seem to be underestimated by the TAG profiler, as shown in Fig.3.30.

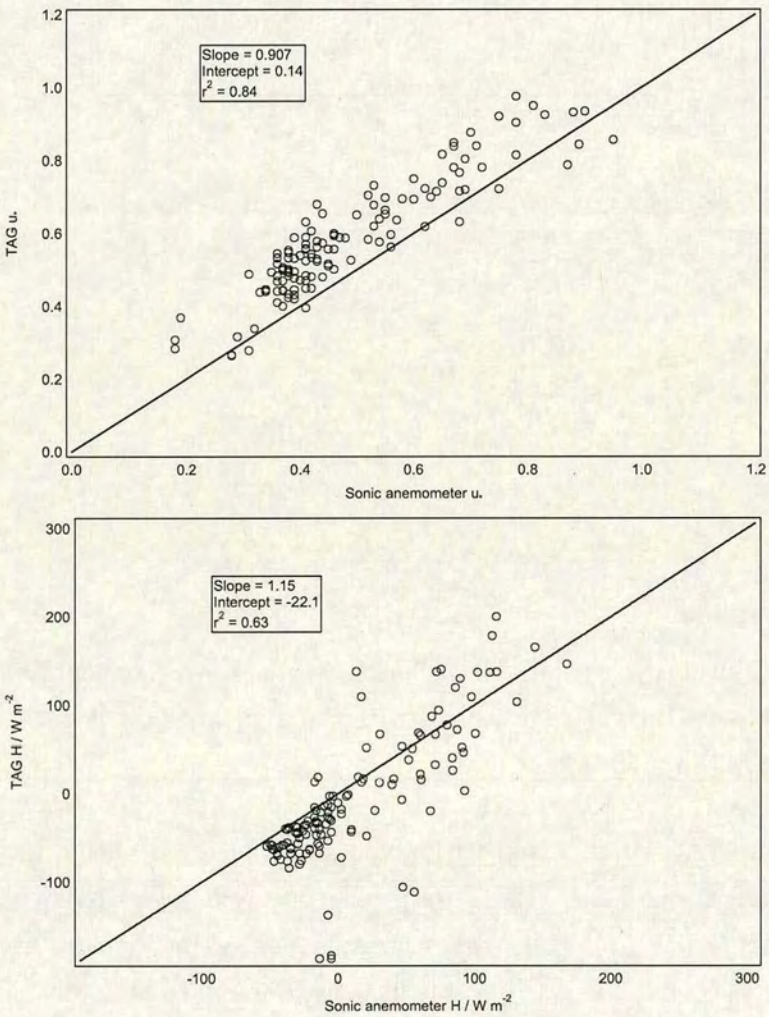

Figure 3.30: Regression plots for u_* (*top*) and H (*bottom charts*)

3.5 Evaluation of uncertainties in the TAG method: a simulation of TAG using continuous gradient data

In order to assess the validity of the TAG system it is necessary to discuss the protocol of the instrument. The main issue to be raised is the effect that is caused by omitting the stable and the highly unstable conditions from the measurements. A simulation of the TAG behaviour has been done by using the data collected in Auchencorth Moss with a continuous analyser of SO_2 coupled with a sonic anemometer. The results of this simulation have been compared to the experimental data collected from the TAG and to the continuous data provided by the flux-gradient system. The data used for the simulations have been collected at Auchencorth Moss during the year 2000. An ultrasonic anemometer (Gill Instruments Ltd, USA) has been operating continuously, giving half-hourly output data for wind speed and air temperature. An SO_2 analyser (Thermoelectron 43CTL) was operating continuously switching between 3 inlet heights and outputting half-hourly data that were coupled with the wind data from the ultrasonic anemometer. The SO_2 analyser works on pulsed ultra violet fluorescence (UVF). The response time of the instrument can be set by the operator and ranges between 1 s and 100 s; the sampling time for each inlet was set to 2 min with an additional purging time of 1 min.

This system uses a hybrid method. It uses eddy covariance to infer the friction velocity and the meteorological parameters necessary to the calculation of the flux, coupling them to the chemical concentration profiles from the SO_2 analyser: eventually, the flux is calculated by the aerodynamic flux gradient method, following Eq.2.8. The flux is calculated on-line and logged every half-hour period by means of a Campbell Scientific datalogger.

The simulation consists of three steps:

- Assessing the impact due to the exclusions of non-neutral conditions from the sampling.

- Assessing the impact of the TAG protocol, taking into account the averaging procedure applied to the meteorological variables and the stability parameters.

- Assessing the impact of different analytical techniques used to measure the SO_2 concentrations.

3.5.1 Effect of non-neutral conditions removal

The first step was to assess what portion of the fluxes was lost by omitting stable and highly unstable conditions from the TAG sampling.
To achieve this, the fluxes from the continuous flux-gradient system were averaged over the periods in which the TAG system was measuring, by excluding the half-hourly periods where the TAG was not sampling.

The method used to calculate the stability parameters and the fluxes for the continuous flux-gradient system was a hybrid method, using eddy covariance to estimate the parameters and the main meteorological variables, and the aerodynamic flux gradient method to calculate the fluxes. This first study doesn't consider the difference between experimental methods, but it is useful to provide in principle what could be the outcome of the TAG instrument.
In Fig. 3.31 are shown the linear correlations between these two sets of data, i.e. all values from continuous flux gradient system and averaged values from continuous flux gradient system over TAG sampling periods. A linear regression has been done for: u_*, H, SO_2 flux, SO_2 concentrations.

For what concerns the friction velocity (Fig. 3.31 top left), the exclusion of the stable conditions seems to cause a slight overestimate of the friction velocity values. The linear fit shows an offset of 0.08 m s^{-1} between TAG-time sampling and continuous sampling, and a slope of 0.93: this can possibly be explained by the fact that in stable conditions the momentum transfer due to friction is very low, leading to a lower average value of u_*.

The correlation plot for sensible heat flux (top right) shows that the TAG sampling protocol under-estimates the flux in comparison to the sonic anemometer, providing a value that is the 74% of the flux measured by the sonic. The correlation coefficients for both sets of data regarding u_* and H show a very good agreement (above 90% in both cases) between TAG sampling time and continuous system suggesting the removal of stable conditions from the sampling period doesn't modify the evaluation of the turbulent fluxes, although it introduces a bias.

The SO_2 fluxes calculated omitting stable conditions under-estimate the fluxes of SO_2 measured by the continuous system by providing fluxes that are the 77% of the values estimated with the continuous system. The correlation coefficient shows

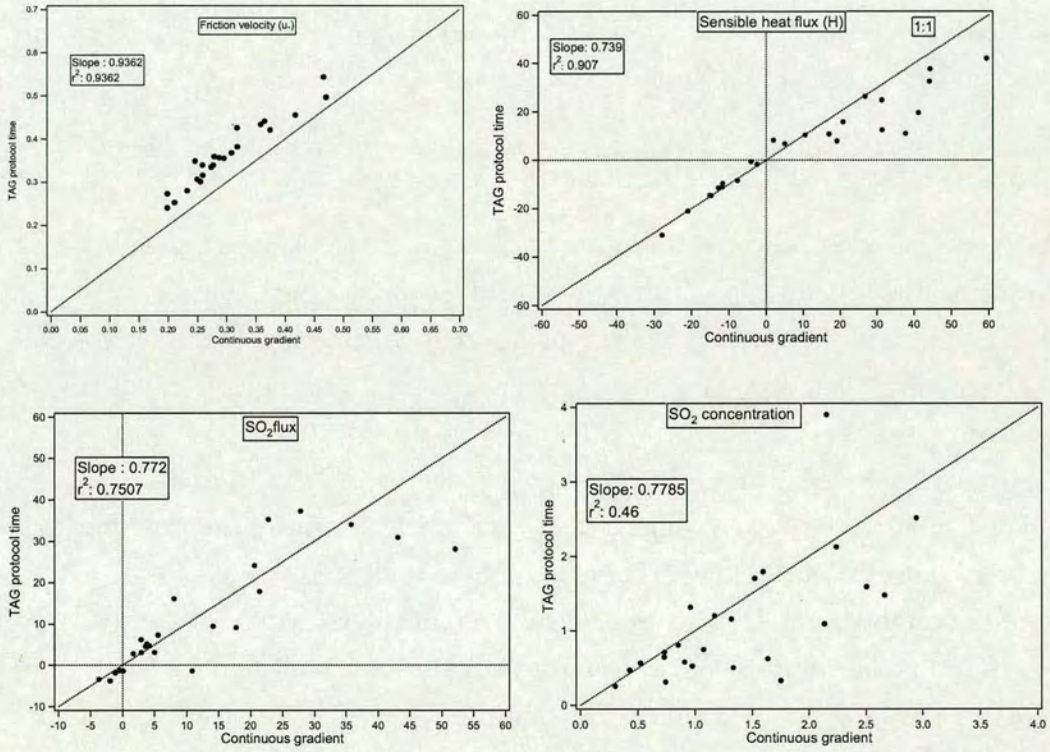

Figure 3.31: Linear regression between values of u_*, H, SO_2 flux and SO_2 concentration from the continuous gradient system: on the y axis the values averaged over the same time as the TAG system (excluding stable conditions); on the x axis the values averaged over all conditions.

that for the 75% of the cases the 2 protocols (TAG and continuous flux gradient) agree.

The SO_2 concentration values are shown in Fig. 3.31 at the bottom right: concentration values averaged over times omitting stable conditions give lower (77%) values in comparison to the continuous monitoring, and this is because of stable atmospheric conditions present typically a lack of mixing in the surface layer. The correlation coefficient for this set of data is considerably lower than the ones found for the fluxes: this doesn't mean that the TAG instrument wouldn't be suited to measure the conditions but rather that stable conditions strongly affect the concentration values in the surface layer, as already well known.

3.5.2 Effect of TAG protocol

A second question concerns the protocol itself, i.e. the choice of sampling just during neutral conditions of the atmosphere, in fully forced convection and in the steady state. To do this, the continuous data of concentration from the SO_2 analyser were used, averaging them only over neutral atmospheric conditions to simulate the TAG behaviour.

To assess the neutrality, the stability parameters such as Ri and L were calculated from the sonic anemometer data, and used to identify the time intervals to be included in the averages. These results are compared (see Fig. 3.32 to 3.35) with the total dataset of the continuous flux-gradient system.

The outcome of this second step of simulation is actually similar to the outcome of the first step, excluding the times in which tha TAG system was not sampling.

The friction velocity calculated following the TAG protocol is larger than u_* measured with continuous sampling: this time the offset is negligible (-0.012 m/s) but the slope is > 1, leading again to an overestimate of u_* as final result. The sensible heat fluxes are under-estimated by the TAG protocol, specially for higher values of H.

The SO_2 fluxes and concentrations estimated with the TAG protocol show an under-estimate when compared to the continuous sampling protocol; by observing the linear regression of H, SO_2 fluxes and concentrations it appears that the same bias is characterising the TAG protocol estimates, in fact the slope values all lie between 0.76 and 0.79, suggesting the exclusion of non-neutral conditions leads to an underestimate of 78% of the actual values, when the continuous sampling

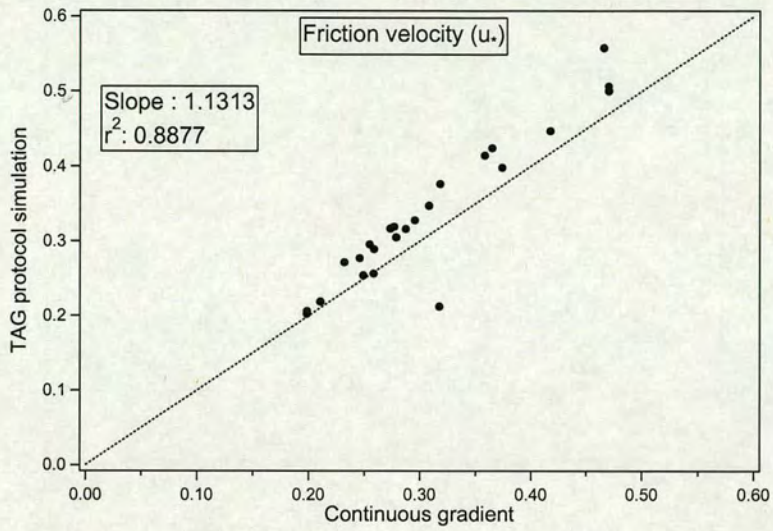

Figure 3.32: Linear regression between values of friction velocity: TAG protocol simulated data versus continuous gradient data.

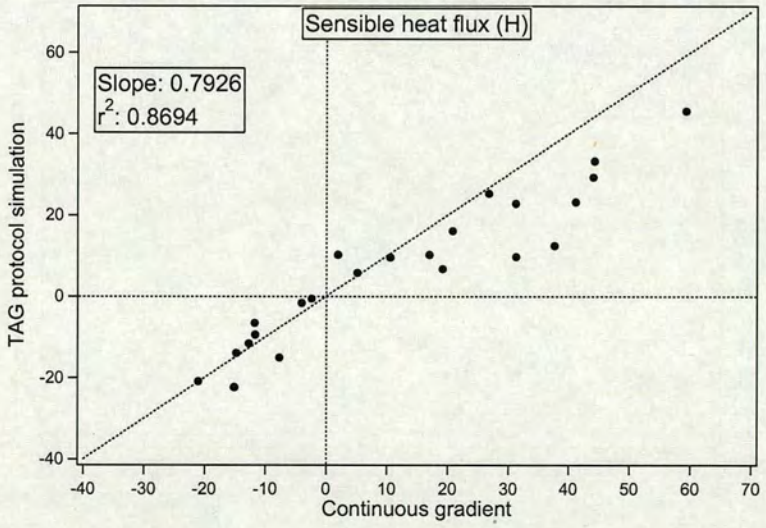

Figure 3.33: Linear regression between values of sensible heat flux: TAG protocol simulated data versus continuous gradient data.

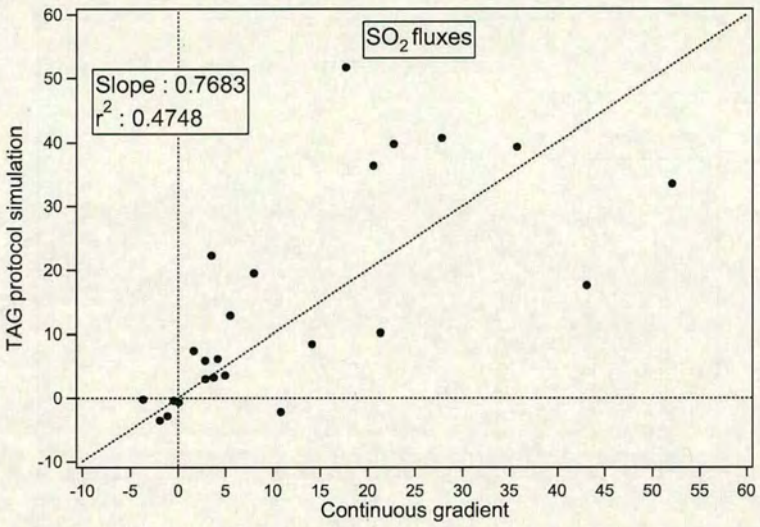

Figure 3.34: Linear regression between values of SO_2 flux: TAG protocol simulated data versus continuous gradient data.

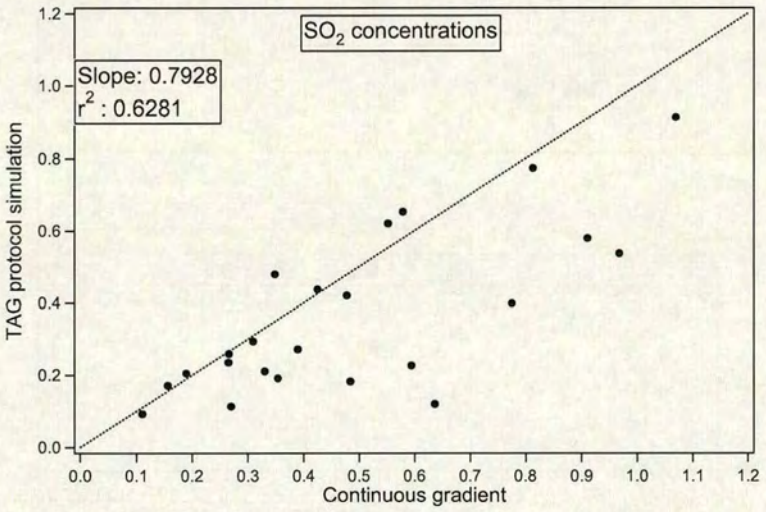

Figure 3.35: Linear regression between values of SO_2 concentrations: TAG protocol simulated data versus continuous gradient data.

system is taken as a reference.

The differences between the outcomes of step 1 and step 2 of this simulation are due to the different principle used to calculate the stability parameters. In the first case, the stability classes were assessed by the TAG instrument (using aerodynamic flux gradient method) , in the second case by the sonic anemometer (using a hybrid method between eddy covariance and flux gradient).

3.5.3 Effects of different analytical techniques

Finally, the third step was to inspect the effect of the different analytical techniques: UVF for the continuous SO_2 analyser, ion chromatography for the denuders used with the TAG. Again, the TAG simulated data (according to simulation in step 2) were compared to the experimental results from the TAG system.

Concentration values for the three heights (2.52 m top, 1.35 m middle, 0.65 m bottom) are compared in Fig. 3.36. The concentration data have been filtered according to different rejection criteria from the chemical analysis, related to the chemical capture percentage (data rajected if chemical capture $< 75\%$). The correlation between the denuders and the UVF measurements is rather satisfactory (r^2=0.69), but there is a bias factor of 0.87 on the TAG measurements that remains unexplained and needs further investigation.

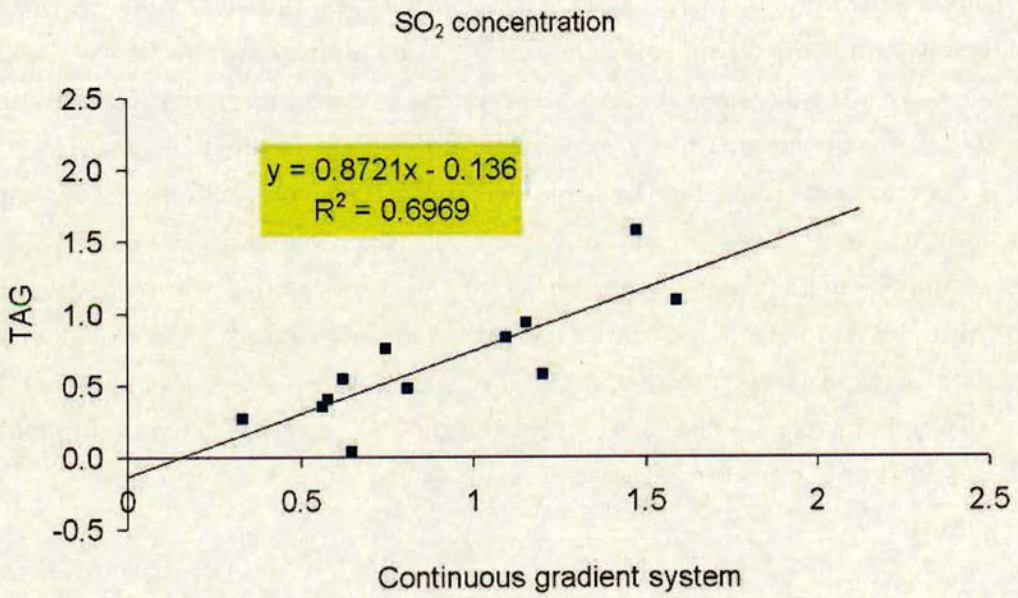

Figure 3.36: SO_2 average concentrations recorded with the TAG instrument are plotted against concentration values outcome from the simulation of the TAG protocol using continuous gradient data.

3.6 Further developments: the Easter Bush field campaign

The comparison with more accurate micrometeorological methods shown in the previous section highlights some scatter in the turbulent fluxes measured with the TAG system. A lack of precision in the observation of fluxes by this kind of instrument is certainly attributable to the limited quality of the vertical gradients of wind speed and temperature: these two gradients are determined using only two values taken at two different heigths. The malfunctioning of only one of the sensors leads to wrong estimates of vertical gradients that strongly affect the evaluation of fluxes as well as of stability parameters, therefore increased rejection of the data.

The quality of the stability parameters estimate plays an important role in the amount of data collected in nearly neutral conditions (i.e., inside the window of neutrality). A better estimate of the stability parameters would lead to more significant information, as the sampling of the TAG system depends on that. In order to meet these requirements, a new model of TAG (TAG3) has been developed during a second stage, and will be described in the following section.

The *TAG3* model developed during the Easter Bush field campaign is basically the same as its predecessors *TAG1* and *TAG2*, with an addition of two chemical sensors to provide a total of five, a third cup anemometer, and a total of five thermocouples which provide better quality vertical profiles and more reliable gas concentration gradients, reducing the fraction of data rejected.

Easter Bush is located south of Edinburgh (southern Scotland), close to the Pentland Hills. The field site is an intensively managed grassland, covered by more than 90% with *Lolium Perenne*: it is used for silage production and cattle and sheep grazing. The site has a good fetch, it is flat and has got a uniform landcover, with presence of regular wind; a more thorough description of the field site is given in § 5.4. TAG3 has been measuring NH_3 concentrations gradient and deposition from September 2001 until the May 2003.

3.6.1 Effect of improved gradients on stability parameters

In fig. 3.38 are shown the values of the Ri number, estimated from a 2-points vertical gradient (*TAG 2*) and from a 3 (wind speed) - 5 (temperature) point vertical gradient (*TAG 3*). This was achieved calculating the 2 points gradient

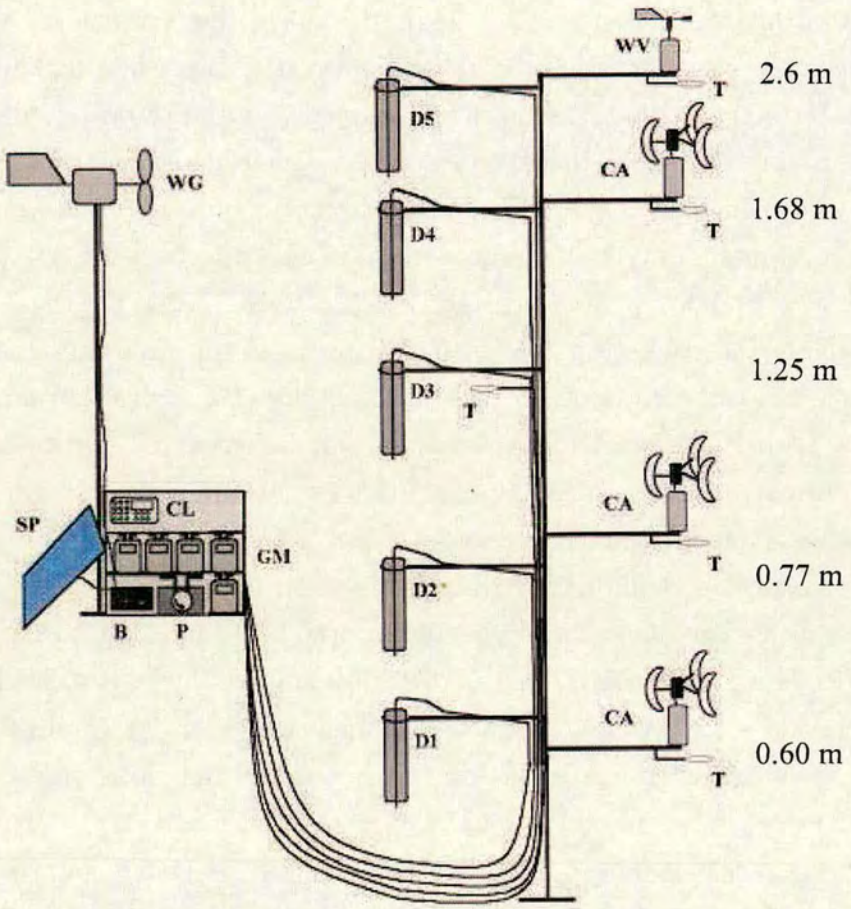

Figure 3.37: Second version of the instrument *TAG3*. CA: cup anemometer T: temperature sensor WV: wind vane GM: gas flow meters WG: wind power generator SP: solar panels B: battery P: air pump CL: Campbell 21X logger D1,2,3,4,5: denuders

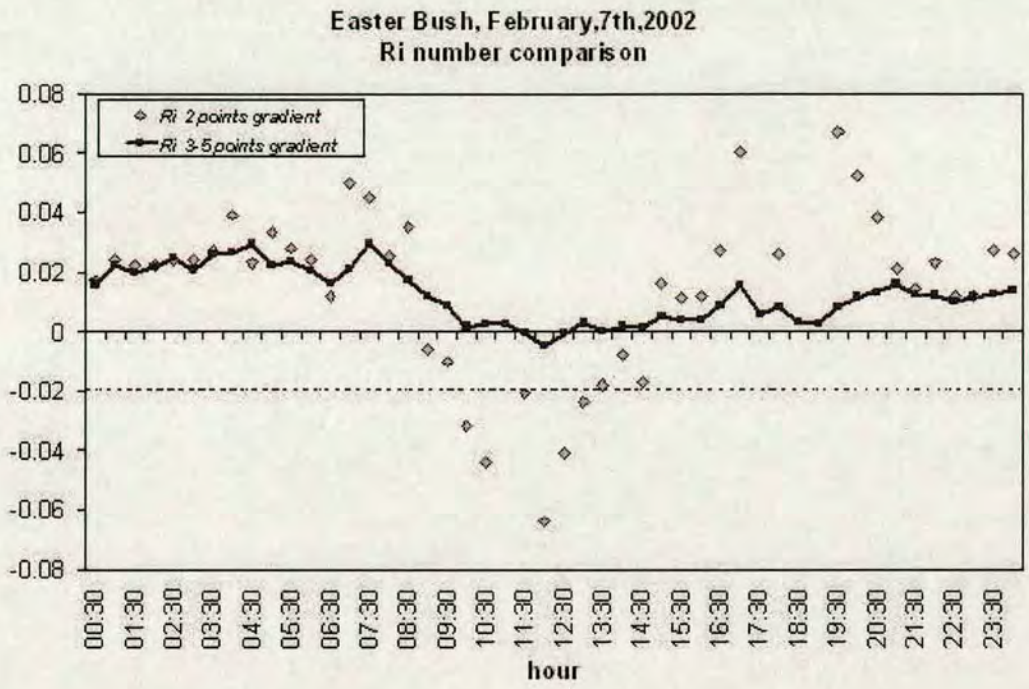

Figure 3.38: The Richardson number calculated by the two vertical gradient profiles.

values from the same data set, but choosing the data acquired by the two sensors set in the same heights as the old TAG model.

The two horizontal dashed lines enclose the chosen range of neutrality, and the 2-points gradient data set shows a smaller number of detected "neutral cases". This suggests that the same condition is detected to be, for example, stable by TAG2 system and neutral by TAG3. The portions of sampling time therefore change, increasing or decreasing, according to the system used, as shown in fig. 3.39.

This implies a different flux estimate from the same measuring conditions. It would be expected that the more accurate gradient would provide the most reliable estimate of the Richardson number. This is actually confirmed by a comparison between the TAG system and a sonic anemometer (which is considered here as a reference, given its higher accuracy, resolution and precision) concerning the Ri number, fig. 3.6.1.

During the field campaign at Easter Bush continuous measurements with a sonic anemometer show that a significant portion (60% of the time circa) of the

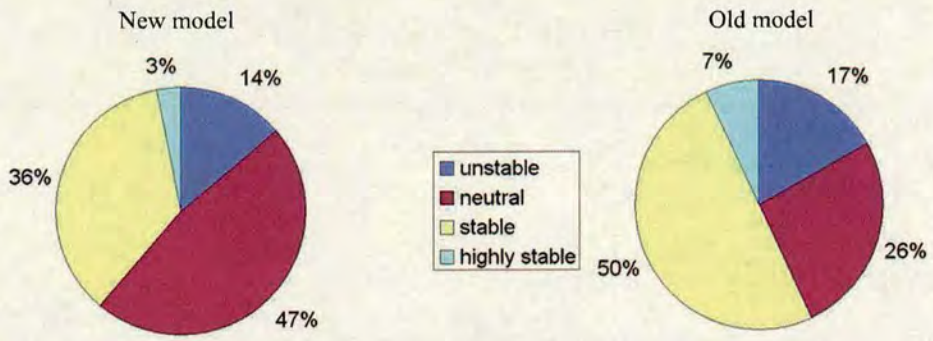

Figure 3.39: Atmospheric conditions frequencies detected by the two vertical gradient profiles in Easter Bush, during autumn 2001.

time is characterised by values of Ri between -0.02 and +0.02 (see fig.3.6.1): Fig.3.1 shows that in this interval F equals 1 $\pm$ 0.2. As discussed in § 3.1, this window provides a compromise between having a significant amount of sampling time and being acceptably close to atmospheric neutrality.

The "window of neutrality" chosen for Auchencorth Moss allowed a sampling time coverage of nearly 70%. During a first trial period during the autumn 2001, the TAG at Easter Bush was running according to the same window. The percentage of time coverage was of 47%, as shown in Fig. 3.39. In order to increase the time covered by the sampling, the condition on the Ri number was extended to a window between -0.03 and +0.03, and this caused the data coverage to increase from 47% to 68%.

Percentages of the different atmospheric conditions deduced from the sonic data appear more similar to the ones deduced from TAG3 than to the ones deduced from TAG2.

By passing from a 3 points profile to a 5 points one, the estimate of gradients improves. To quantify this, a test of significance of the regression can be done calculating the standard error on the regressions for the temperature and wind speed profiles, as well as for the chemical profiles. The coefficient of determination ($r\_^2$) and the standard error of the regression coefficient give an immediate idea for the quality of the gradient, and they can be used in the quality control stage;

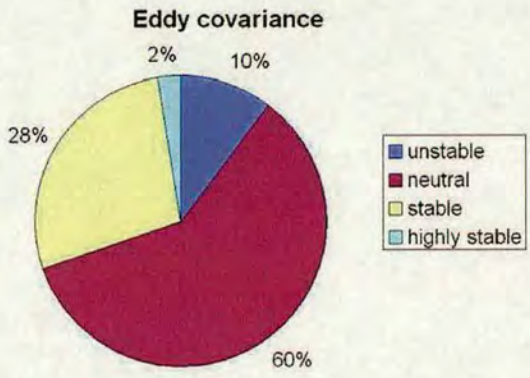

Figure 3.40: Atmospheric conditions frequencies detected by the sonic anemometer in Easter Bush, during autumn 2001.

an example is shown in Fig.3.41.

This approach is more rigorous and direct than the one used in §3.4, and provides a useful tool in the assessment of the fluxes reliability. It has been applied to the vertical profiles of both temperature and wind speed, and it proved very useful in the identification of periods where the data were not reliable. Its main application is on the chemical vertical profiles, as they are the main source of uncertainty in the whole TAG protocol.

In Fig.3.42 is shown an example of sensible heat flux values measured with the sonic anemometer and TAG3 on 19th May 2002; a good agreement between the two methods is confirmed by a linear regression on the whole dataset, which returns a slope of 0.89, with a value of $r^2 = 0.86$. For u^*, the correlation coefficient over the whole dataset is $r^2 = 0.89$, and the slope is 1.08. These results are consistent with the outcome of the Auchencorth Moss data series.

3.6.2 Results

The values of u_* range from 0 to 0.9 m s^{-1}, having a quite high average value of 0.24 m s^{-1}, due to the windy nature of the site (see Chapter 5), which recorded over the whole measurement period for the TAG3 an average wind speed of 3.8 m s-1. The sensible heat fluxes ranged between -117 W m-2 and 183 W m-2, with a total average annual value od 1.02 W m-2. The annual average temperature was of 9.3 ^{o}C, ranging from -2.5 to 27 ^{o}C.

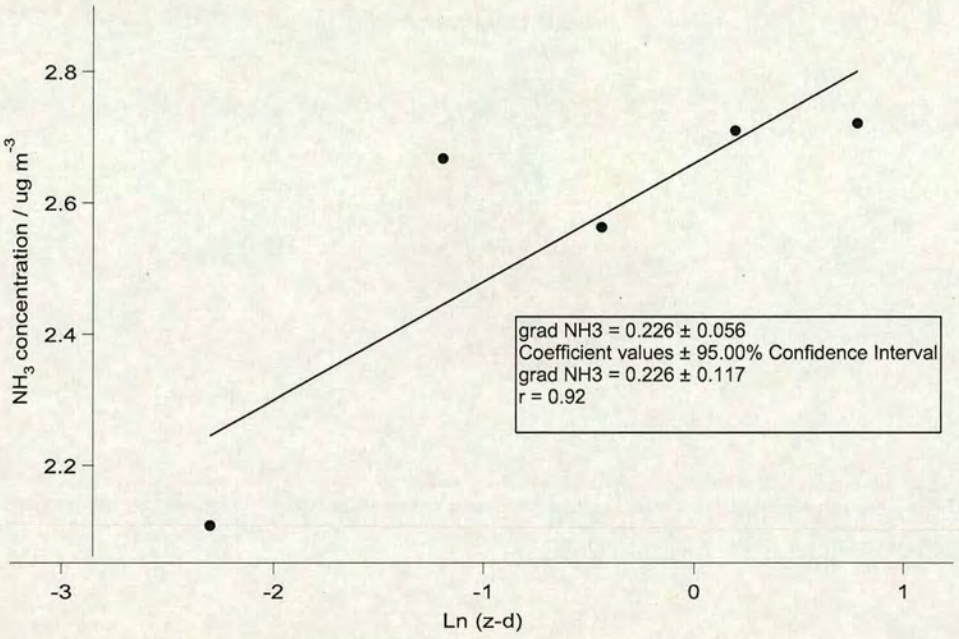

Figure 3.41: NH_3 concentration values measured at 5 heights versus the logarithm of (z-d).

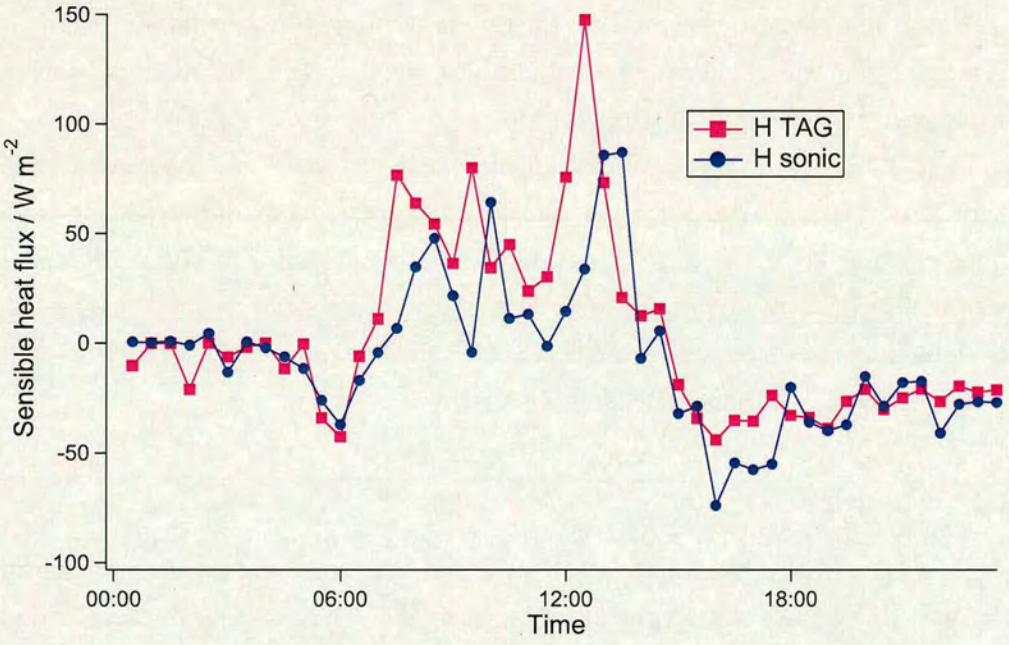

Figure 3.42: Sensible heat fluxes measured at Easter Bush on 19^{th} May 2002, with the TAG3 system and the sonic anemometer.

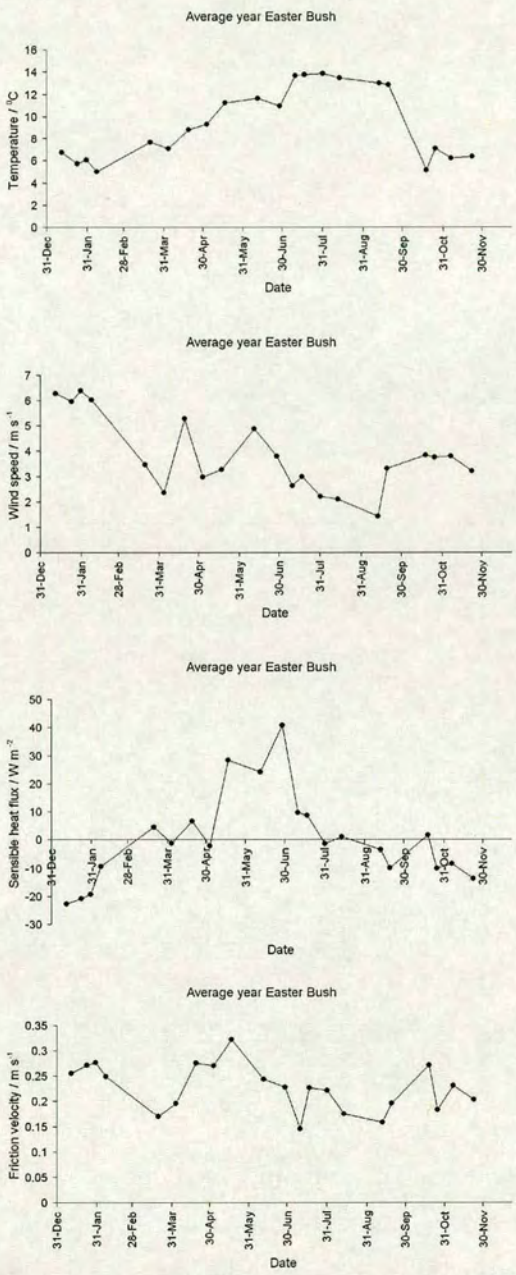

Figure 3.43: Values of temperature (top left), wind speed (top right), sensible heat flux (bottom left) and friction velocity (bottom right). The values are fortnightly averages considering an average year recorded at Easter Bush between 2001 and 2003.

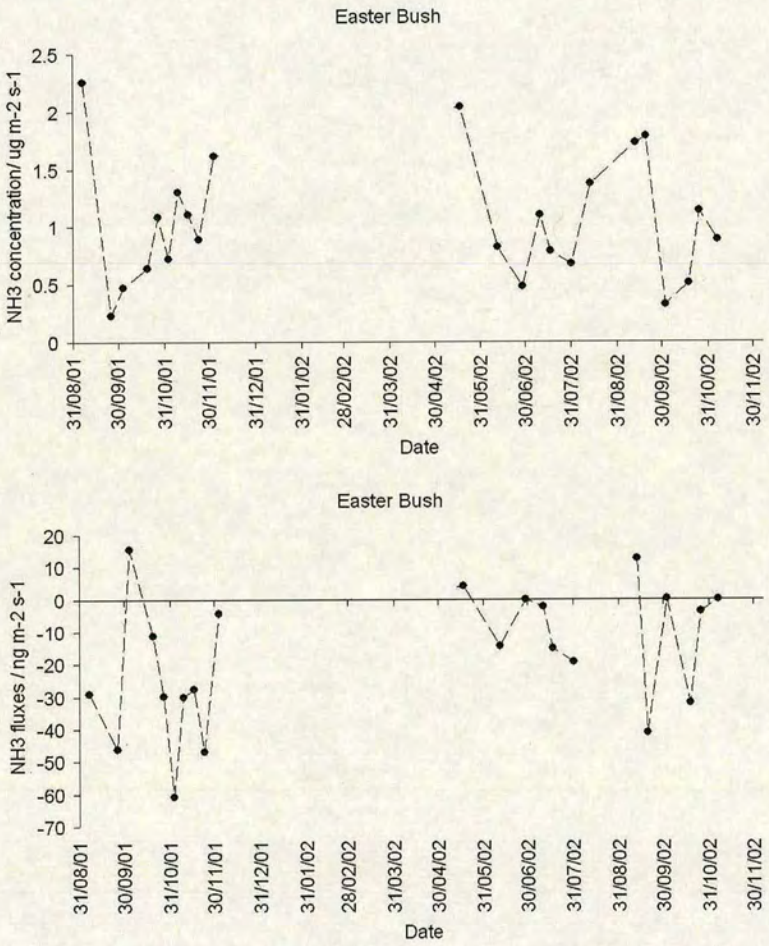

Figure 3.44: Concentrations of ammonia recorded at Easter Bush (top). The values are fortnightly mean values recorded at 1 m height. Values of the NH_3 fortnightly fluxes recorded at Easter Bush between 2001 and 2002.

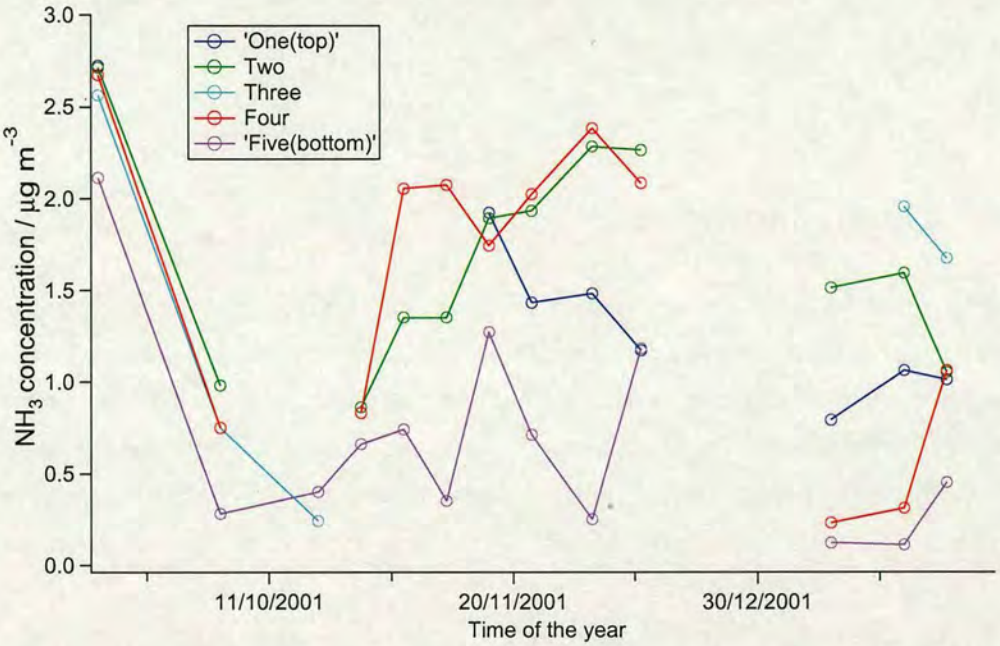

Figure 3.45: NH_3 concentrations measured during the period from September to December 2001 by the TAG3.

The fluxes of ammonia measured with TAG3 show a general deposition phenomenon. The overall average value is -12.2 ng m-2 s-1: this result is due to a lack of intense vegetation-atmosphere exchange episodes, during the autumn-winter times, due to the almost dormant vegetative activity, and the occurrence of a particularly wet season during 2002 that reduced the impact of emission events, such as fertilisation or grass cutting.

In Fig. 3.45 is shown an example of the NH_3 concentration values recorded by the five measuring heights of TAG3. The concentrations present some scatter, at times not generating very regular gradients; actually, the levels of atmospheric ammonia during the autumn-winter period are quite low, and the error on the measures is therefore more critical. There is however a pattern, revealed by the calculations of the gradients, that indicates generally deposition, as expected in absence of events like grass cutting or fertilisation. A marked irregularity in the concentrations was found for denuder 3, and this was due to a fault between the pumping capacity regulator and the gas flow meter connected to that denuder; it was leading a larger amount of air through the denuder, without measuring it properly, and it caused a higher concentration measure. In the period from

25/10/01 to 1/11/01, denuder 1 became contaminated; therefore the values have been rejected.

3.7 Discussion

Long-term net fluxes of reactive gases such as SO_2 and NH_3 are shown to be measured with adequate accuracy and precision by a TAG system. The series of data collected in Auchencorth Moss showed that the application of the TAG system allows us to characterise the climate and the chemical climate of a field site as well as to describe the seasonality of that particular environment. It can also provide the net contribution of the specific field site to the emission or deposition of the investigated chemical compound.

When choosing the "window of neutrality", it is necessary to look for a compromise between amount of data recorded and degree of neutrality; this compromise is not the only controversial issue arising from the conditionality criteria. If the application of the aerodynamic gradient technique necessitates atmospheric neutrality, on the other hand the fluxes are not occurring only in such conditions, or at least this can't be excluded a priori. A possible solution to this problem would be to collect the concentration samples for different classes of stability, and then infer the fluxes for each of these categories: unstable, neutral and stable. At this point the correction factor F values would have a large range, and it seems sensible to raise the question whether a correction derived from a parameterisation in the neutral conditions would still provide the same reliability for inferred fluxes in stable or unstable conditions. Nevertheless, sampling the different stability classes, the information about the emission/deposition contribution would be clearer; in fact, without this information, it could only be stated which portion of the time is characterised by stable, unstable or neutral atmosphere, but no information on the air-vegetation gas exchange dynamics is given whenever the atmospheric conditions aren't neutral. The implementation of such a system would strongly affect the costs of the TAG linked to the chemical routine analysis.

The study conducted over the Auchencorth Moss data series simulating the TAG protocol demonstrates the ability of the TAG system to provide deposition fluxes over the long term; a correction factor can be applied to neutralise the bias introduced by excluding the stable conditions during sampling. The time-averaged

micrometeorological instrument is shown to estimate u_* and sensible heat fluxes within 15% of a standard eddy covariance system, and it also provides average values of R_c, and concentrations which prove very useful in model inputs.

In practice, the measures are limited by the detection of the gradient in concentration for both NH_3 and SO_2, which can prove challenging in the case of SO_2 in particular, due to the low atmospheric concentration at background sites.

Fluxes of NH_3 measured by the TAG system at Auchencorth Moss have an average value of -7.6 ng $m^{-2}s^{-1}$ showing good agreement with a previous study made at the same site with continuous annular denuders (AMANDA system), that gave -5.3 ng $m^{-2}s^{-1}$ as an average value, [Flechard, 1988].

The SO_2 concentrations ranged from 0.1 to 2.5 μg m^{-3}, and the fluxes show a predominant deposition, even though occasionally emissions can occur from the vegetation, that re-emits the deposited SO_2. The impact of these emissions is very small compared to the depositions'. Fluxes of SO_2 measured by the TAG system at Auchencorth Moss for an average year have an average value of - 3.4 ng $m^{-2}s^{-1}$ showing good agreement with a continuous UVF gradient system, that gave -2.8 ng $m^{-2}s^{-1}$ as an average value.

The data series collected at Easter Bush with an improved vertical profiler (more sampling heights) allowed a better error analysis on the gradients, and showed consistency with the studies conducted before on the same site about NH_3 fluxes from grassland by [Milford et al., 2001].

In order to reduce the data rejection on chemical gradients especially at background sites, a new TAG model has been deployed at the Auchencorth Moss field site. This new model has the same number of sensors as TAG3 deployed at Easter Bush, but it is setup on a different verical range, having the top sensor at a height of 5.7m, and the other four sensors equally spaced on a logarithmic scale between the top height and the bottom height (0.5 m). The increased distance between the sensors allow greater differences in gas concentration, wind speed and temperature, therefore reducing the error on the estimate of the vertical gradients. A picture of this new system, including 4 wind speed sensors, one wind vane, 5 thermocouples and 5 chemical sensors is shown in Fig.3.46.

The new model includes filter packs as well as denuder tubes for particles measurements, by following the protocols adopted by the national monitoring network for reactive gases and particles, and applying that to the same method of the original TAG.

Figure 3.46: New TAG version implemented at Auchencorth Moss to measure fluxes of gases and particles.

Chapter 4

Measurements of ambient NH_3 concentration using Tuneable Diode Laser Absorption Spectroscopy

4.1 TDLAS

The first TDL (Tuneable Diode Laser) systems were developed around the mid 1960s, and immediately found application as tuneable sources for absorption spectroscopy at high resolution, referred to as TDLAS (Tuneable Diode Laser Absorption Spectroscopy). Nevertheless, it was only in the 1980s that this technique started to be widely used to measure trace gases in the atmosphere, as faster acquisition times were made available, maintaining the precision, selectivity and sensitivity that distinguished TDL systems from the beginning [Werle, 1999].

In atmospheric trace gas monitoring, very high spectral resolution is required to avoid interferences between species, particularly from the ubiquitous water and carbon dioxide. Spectrometers capable of resolving individual rotational-vibrational features, with line widths typically 2×10^3 cm^{-1}, are required to provide reliable identification of constituents of polluted air samples or even of clean air samples where high sensitivities are required. Tuneable diode laser spectrometers have a spectral resolution between 2×10^5 cm^{-1} and 1.7×10^2 cm^{-1}; they can therefore distinguish the fine rotational structure of various atmospheric species at pressure conditions in the Voigt regime (see §4.1.1).

The TDLAS, coupled with turbulence measurements, allows fluxes of matter between vegetation and the atmosphere to be quantified directly for the majority of trace gases.

In particular, when coupled with a sonic anemometer (see § 2.5), a TDL spectrometer can be used for eddy covariance measurements, as the frequency response of these instruments is large enough (up to 10 Hz) to detect turbulent eddies at the small scale (0.2-2 m). Eddy covariance measurements are routinely made for many trace gases, CO_2, H_2O, CH_4, N_2O. However, the application of a TDL to ammonia flux measurements is novel, as its background concentration in the atmosphere is very small and only the newer versions of the TDL systems have sufficient sensitivity and response times to enable this application.

The new model of TDL implemented at Aerodyne Research is a dual path instrument (see fig. 4.1); in which it is possible to measure absorption spectra in two different spectral regions (one for each diode laser operating).

Figure 4.1: Dual TDL system, Aerodyne Research Inc.

4.1.1 Theory of operation for a Tunable Diode Laser Absorption Spectrometer

The principle of a TDL instrument is rather simple: several monochromatic light streams emitted by a laser diode pass through a gaseous sample and the transmitted light intensity is revealed for each wavelength, producing an absorption spectrum. The intensity of light transmitted through a gas sample is given by the Lambert-Beer law:

$$I = I_0 e^{-\sigma(\nu)Cl} \tag{4.1}$$

where I = intensity of light transmitted through the sample gas
I_0 = intensity of incident light
$\sigma(\nu)$ = molecular absorption cross section of the absorbing species, depending on radiation frequency (n) C = absorbing species concentration l = path length through the absorption cell

The absorbance (A) of the gas sample is defined as the logarithmic ratio between incident (I_0) and transmitted (I) intensity of the radiation;

$$A = log\left(\frac{I_0}{I}\right) \tag{4.2}$$

it can also be written as:

$$A = \sigma(\nu)Cl \tag{4.3}$$

From equation 4.3, it can be seen that the absorbance A is proportional to the concentration C of a gas sample, when considering a beam of frequency ν with a fixed path length l. Also, it can be seen that the best sensitivity conditions are obtained for the largest values of σ and l.
Other important features for atmospheric measurements are the shape and width of the spectral line: these, as the absorption cross section, depend on temperature and pressure conditions for each gaseous species.
For pressure values in excess of 133 hPa in the mid-infrared region, the collisions between molecules cause a broadening of the spectral line, which can be fitted by a Lorentzian function. This condition enhances the measurement sensitivity as it maximises the line centre absorption cross section, but involves the risk of superposition of different lines in the spectrum.
By reducing the sampling pressure to less than 133 hPa, the predominant phenomenon is the molecular thermal motion which causes the so called Doppler enlargement of the spectral line, which can be described in shape and width by a

Gaussian function. In this case, the selectivity of the line is enhanced as interferences from other species are minimised, but the low intensity of absorbed radiation leads to a poor measurement sensitivity ([Schiff et al., 1994]).
The optimal pressure condition for absorption spectroscopy is the result of a compromise between sensitivity and selectivity. Since lower pressures and narrower line widths result in fewer interferences from other absorbing species and sharper contrast between absorption line and base line, the optimum sampling pressure is a trade-off between decreasing the line centre absorbance and narrowing the line width. When reducing the pressure, the sensitivity does not decrease significantly with respect to atmospheric pressure conditions, as long as the ratio between Lorentzian and Gaussian line widths is between 0.5 and 1, i.e. for pressure values between 13.30 and 66.60 hPa as shown in fig.4.2.

4.1.2 Description of the TDLAS system

The layout of a TDL system setup for atmospheric measurements requires the following elements:

- Diode laser with tuneable frequency of emission
- Cooling and temperature control system of the diode
- TDL current control and modulation system to increase sensitivity
- Optical bench to direct the radiation through the air sample
- An optical path length long enough to guarantee a high sensitivity of the measurement
- A detector and associated optics to detect the transmitted radiation
- Computer hardware and software to control the system and for collection, manipulation, display, and storage of data.

Diode lasers

Diode lasers used for monitoring trace gases in the atmosphere usually operate in the mid-infrared spectral region (2.5 to 25 μm). In particular, the region between

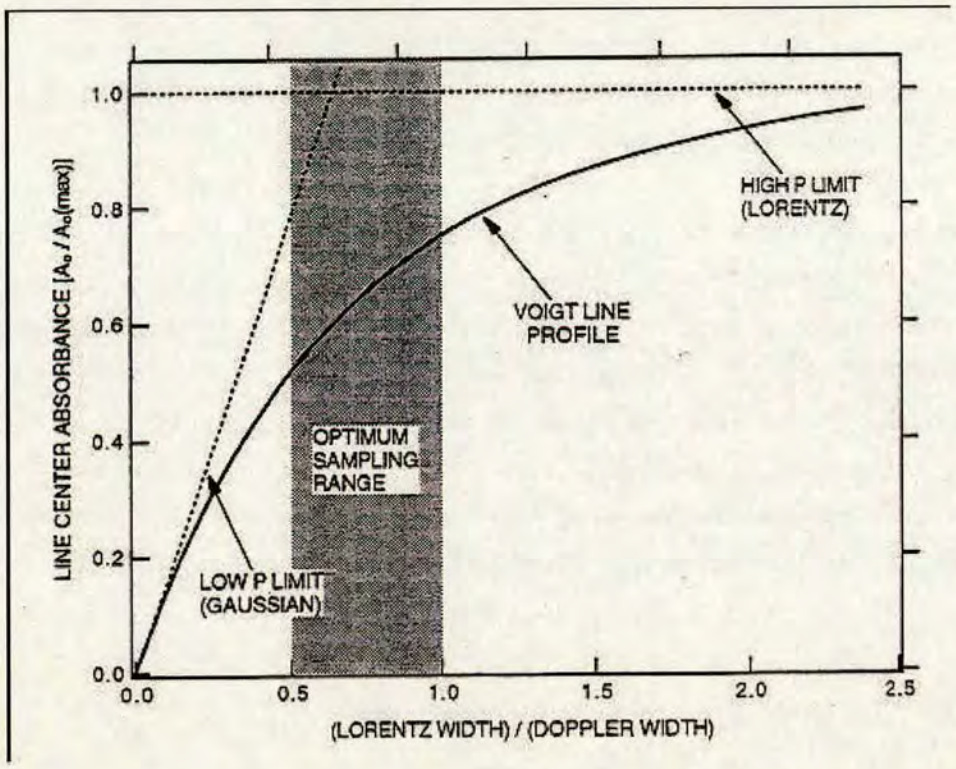

Figure 4.2: Line centre absorption as a function of line width ratio (from [Zahniser et al., 1997]). The Voigt profile function is the convolution of a Gaussian and a Lorentzian function; it is used to fit the shape and width of the absorption line when operating in such pressure conditions, which are ideal for TDL system operation and are also known as Voigt regime, e.g. [Werle, 1998].

3 and 15 μm appears to be the most suitable, as most chemical species of environmental interest have here strong fundamental and roto-vibrational absorption bands. Moreover, the major constituents of the atmosphere, such as O_2 and N_2, have a symmetrical structure and their dipole moment is null; thus they do not have absorption bands in the infrared, and the specificity of the measurement is not compromised by interference with very high intensity absorption lines. Commonly used tuneable diode lasers are made of lead-salt compounds such as $Pb_{1-x}Se_x$, $Pb_{1-x}Sn_xTe$, $Pb_{1-x}Ge_xTe$, $Pb_{1-x}Sn_xSe$, $Pb_{1-x}Cd_xS$. The wavelengths of lead salt lasers range between 3.3 and 29 μm, corresponding to a gap between conduction and valence bands of less than an electron-Volt, typical of this kind of laser. This gap depends on the chemical composition of the laser and hence different wavelengths can be produced by altering the diode chemical composition.

A p-n junction is formed in the crystal which is then cut into pieces typically smaller than 1 mm in length and 0.3 mm x 0.2 mm in depth and height. Electrical contacts are attached, and the diode is mounted onto a support such as copper which serves as a temperature controller during operation. The application of a bias current to the p-n junction produces a population inversion between the nearly empty conduction band and the nearly full valence band, providing the gain mechanism through which stimulated emission occurs via electron-hole recombination [Schiff et al., 1994]. Like other semiconductor lasers, the wavelength of lead salt lasers changes with temperature. While such shifts could be seen as a nuisance at shorter wavelengths, they can be valuable at the mid infrared wavelengths: molecular spectra are particularly complex in this region, and the ability to generate a narrow laser line and tune its wavelength can be useful. Thus lead salt lasers are designed to render their wavelengths temperature-sensitive and are packaged so that their output can be temperature-tuned [Finlayson and Pitts, 1986].

Cooling and temperature control

The population inversion in proximity of the junction is achieved for currents higher than the threshold value: at room temperature such current value is very high; therefore the diodes are operated in cryogenic conditions [Hinkley et al., 1976]. The laser diode used for the measurements of NH_3 at Easter Bush was operated at temperatures in the range of 98 to 107 K, with injection currents lower than 700 mA. To maintain such operational conditions, the diode is located inside a Dewar vessel: liquid nitrogen (T = 80 K circa) is periodically poured in the vessel by means of a timer-triggered cryogenic solenoid valve, in order to keep the system in cryogenic conditions. The system used approximately 2 to 3 ℓ of liquid N per day, depending on diode operating temperatures and currents.
The temperature tuning rate of most diodes is greater than 1 cm^{-1} K^{-1}, requiring temperature stability in the order of 10^{-3} K. Up to eight diodes can be held on a cold-finger in a cryocooler, and up to two diodes can be operated at the same time. Temperature control and tuning is provided by a heating element used in combination with a semiconductor temperature sensor attached to the diode inside the Dewar.

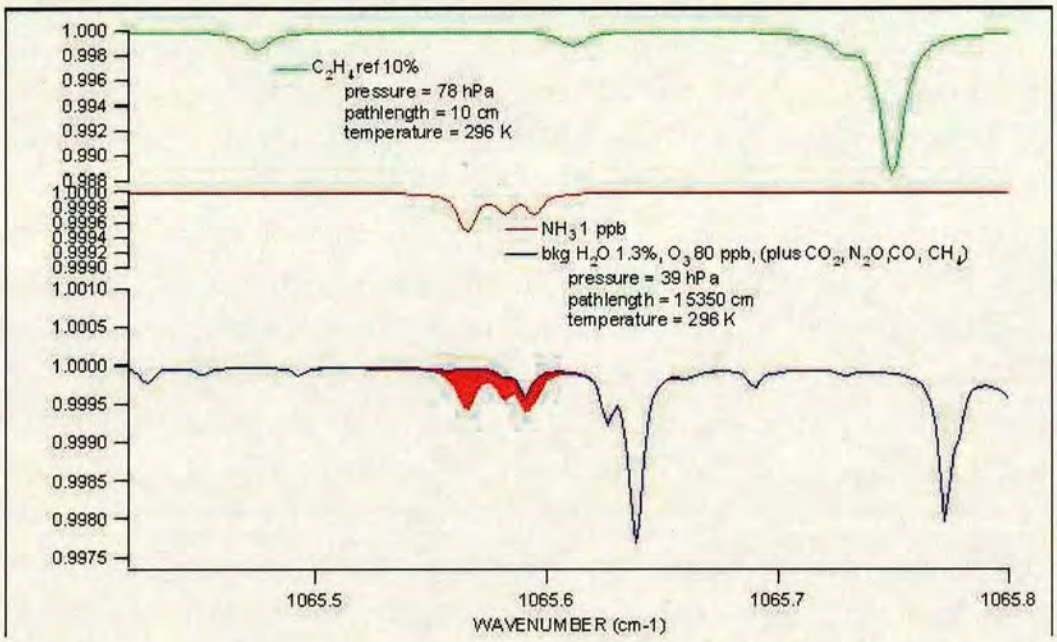

Figure 4.3: Absorption spectra for (from top to bottom): ethylene, ammonia (red), and background in the operational region of the used diode laser.

Current control and modulation systems

The tuneability of the frequencies emitted from the diode can be achieved by changing the diode temperature, which is controlled by the current flowing through the diode.

The laser emission has a narrow elliptical shape, with nominal wave number 1065 cm^{-1}; this corresponds to the centre of an emission range of about 200 cm^{-1}.

The instrument uses a low-pressure (10 hPa), stainless steel reference cell with quartz windows containing a low-pressure sample of ethylene to automatically lock onto the line positions and eliminate frequency drift.

Once the diode temperature is stable, the scan of the emission range is typically at a step of about 5×10^3 cm^{-1} mA^{-1}, which requires current stability better than 0.05 mA to obtain a spectral resolution in the order of magnitude of 10^5 cm^{-1}. A modulation waveform of sufficient amplitude to tune the laser across the absorption feature is applied to the laser current and is repeated at frequencies of about 10 kHz. All these functions are executed by a model L5830 TDL Controller (Laser Components Instrument Group, Inc.) which is a micro-processor-controlled temperature and current controller designed for use with the L5600 series TDL

(Aerodyne Research Inc.).

Optical bench

The purpose of the optical module is to transport the light from the infrared laser diodes, housed in the LN_2 Dewar, into a narrow beam, to direct the light into a sample cell which provides the long absorption path, and then direct the light leaving the cell to a detector. This is achieved by means of a 2 m by 1.22 m optical bench shown in figure 4.4.

The "collection" segment of the instrument includes microscope objectives, dichroic beam-splitters and a pinhole. A parallel visible optical system aids alignment and setup of the optical assembly. A red visible (678 nm) "trace" diode laser beam passes through a dichroic beam-splitter and thus is co-aligned with the infrared beam associated with it, as guaranteed by focussing both visible and infrared beams through the common input aperture (200 μm pinhole).
Following the input aperture, the beams are refocused and aimed into the multi-pass sampling Herriott cell, then recollected to the detector, located in the Dewar as the diode lasers. A reflection of the beam from the entrance hole of the cell is directed via more mirrors through sealed cells filled with reference gases, at low pressure (<6.6 hPa), and then directed to other detectors in the Dewar. Light passing through these cells will have strong absorption features that are used to identify the spectral line positions and can also be used to lock the laser diode emission wavelength.

Multi-pass absorption cell

The laser beam is directed into a cell, where the absorption by the gaseous molecules takes place. Multi pass absorption cells are widely used as a means of providing long optical absorption paths in a compact volume. There are several factors to be considered in the evaluation of a multi-pass cell design, the first of which is the total available path length.
The signal-to-noise ratio (SNR) in an absorption measurement increases with the path length, up to a limit where loss from the many reflections becomes important. Another, and often the most important, factor limiting the effective SNR at long path lengths is the appearance of optical interference fringes. These fringes, which are due to scattering in the cell, can have a free spectral range close to the frequency width of molecular absorption lines. Thus, fringes tend to obscure the

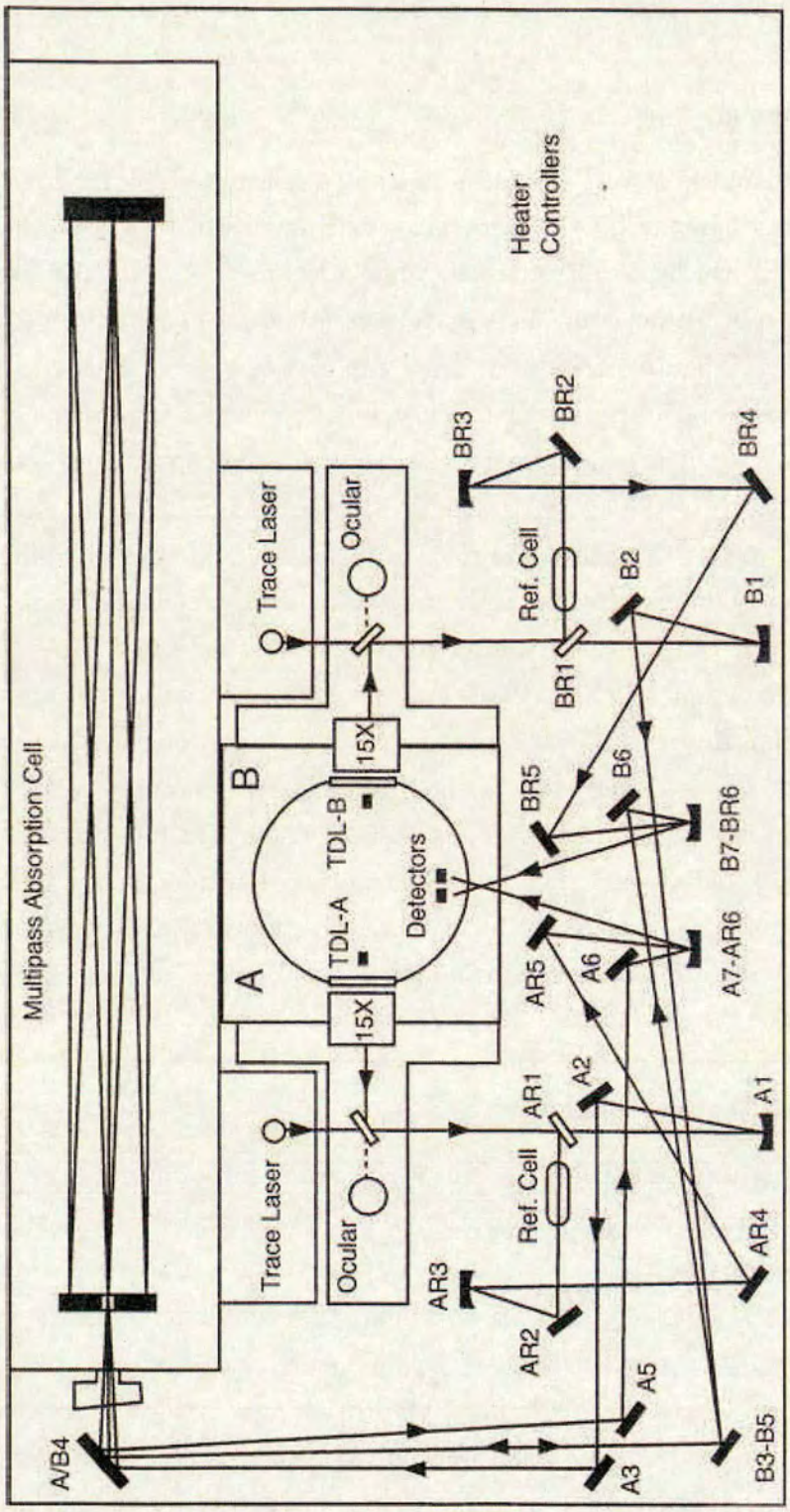

Figure 4.4: Optical bench layout of the dual TDL (from [McManus J.B., 2001])

spectral features of interest. Finally, the volume of the cell for a given path length is a limiting factor in the measurement response time.

The cell used in the measurements at Easter Bush is an astigmatic Herriott cell that consists of two astigmatic mirrors placed at the bases of a glass cylinder. The optical beam is injected through a hole in one mirror in an off-axis direction, and is reflected 174 times on a base length of 88.2 cm, providing a total path length of 153.5 m, before exiting through the coupling hole, fig.4.5.

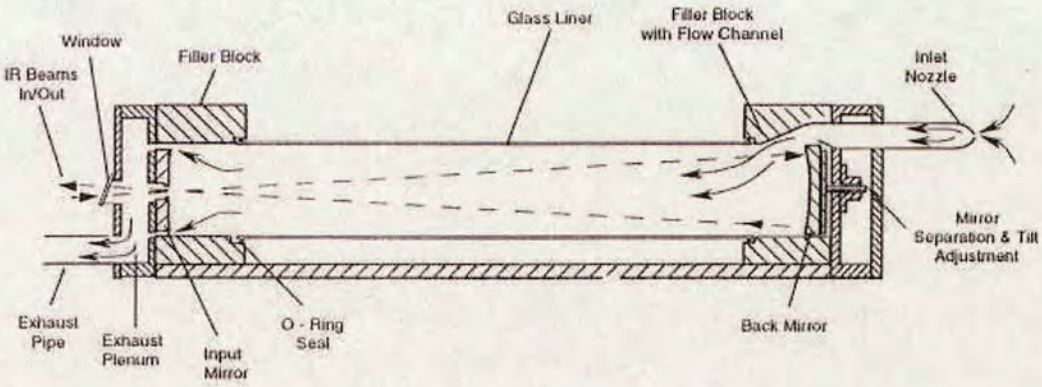

Figure 4.5: Multi-pass absorption cell ([Zahniser et al., 1995]).

The different horizontal and vertical radii of curvature produce beam spots on the mirrors which form a Lissajous pattern (fig.4.6), and the volume of the cell is optimised for fitting in the desired optical path ([Zahniser et al., 1995], [Zahniser et al., 1997]).

Detector

Once the beam has left the absorption cell, it is directed to the detector, a semiconductor placed in the Dewar operating at cryogenic temperatures. The detectors used are photodiodes which can be photovoltaic indium antimonide (InSb) elements for short wave detection, or photoconductive mercury cadmium telluride (HgCdTe) elements for detection of wavelengths longer than 4 μm. The difference between the two, apart from the different wavelengths detected, is that in a photoconductive detector change in internal resistance is measured as an effect of an external reverse bias voltage, whereas a photovoltaic detector is used without bias, and the generated photo voltage or current is measured. Photovoltaic operation requires the presence of an internal potential barrier such as a p-n junction in the

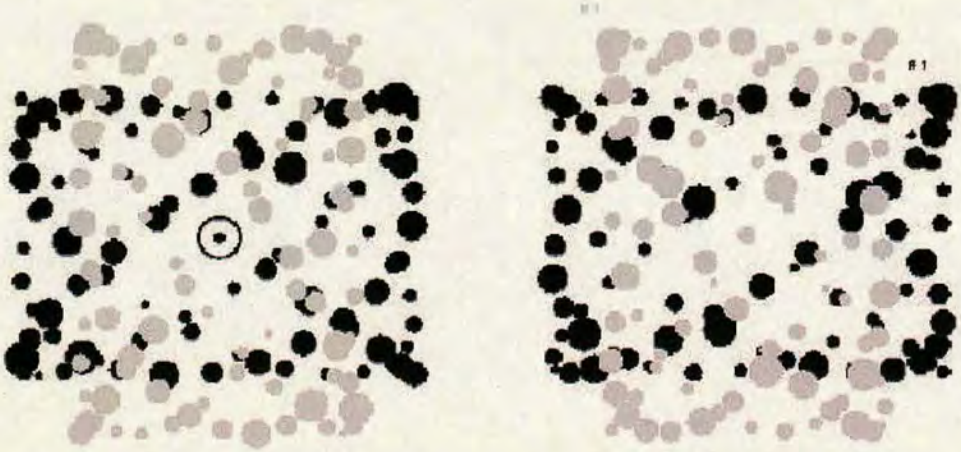

Figure 4.6: Calculated mirror beam spots for two patterns, each with 182 passes propagating in an astigmatic Herriott cell. The two different wavelengths are shown as different shades, and spot diameters are largest for the earliest reflections. Similar discrete patterns with 174 passes were used in the Easter Bush deployment.

photodiode to separate the photo-generated charge carriers in the absence of external bias. The light revealed by the detector is converted into a signal which goes through an analogue-to-digital card and subsequently is processed by a computer.

Signal processing and computing

The TDLAS measures absorption spectra directly using rapid scan sweep integration. Information on the unabsorbed laser power is retained, allowing direct, spectroscopic determination of concentration using predetermined line strengths, positions and broadening coefficients. The result is an absolute measurement of the concentration of the trace gas.

The problems encountered with TDL operation are primarily due to limitations in stability of the laser output frequency, mainly due to the sensitivity of the laser to fluctuations in operating temperature. These are reflected in the reproducibility of the spectra, which in turn affects the determination of both transition frequencies and line shapes.

The laser current is saw-tooth modulated at approximately 20 Hz circa, and phase-locked to the signal averager. Laser temperature, current and modulation ampli-

tude, are adjusted to sweep the desired spectral interval. The result is a spectrum in which all points are integrated simultaneously and which may be scanned for any period of time sufficient to reduce the noise to an acceptable level. Once the laser mount temperature reaches equilibrium with the average injection current, it generally remains stable over periods much longer than the scan time, so that the spectrum is reproducible, and no smearing of lines occurs during a scan [Jennings, 1980].

The control module sweeps the current in order to vary the wave number over a typical range of 0.2 cm^{-1}, and it acquires a distinctive "fingerprint" for the trace gas. In fig. 4.7 is shown an example of absorption feature for the ammonia line of wave number 1065.6 cm^{-1}; the transmitted signal intensity is displayed in the ordinate axis, while in the abscissae axis is displayed the channel number, which corresponds to the step of wave number (reciprocal of the wavelength).

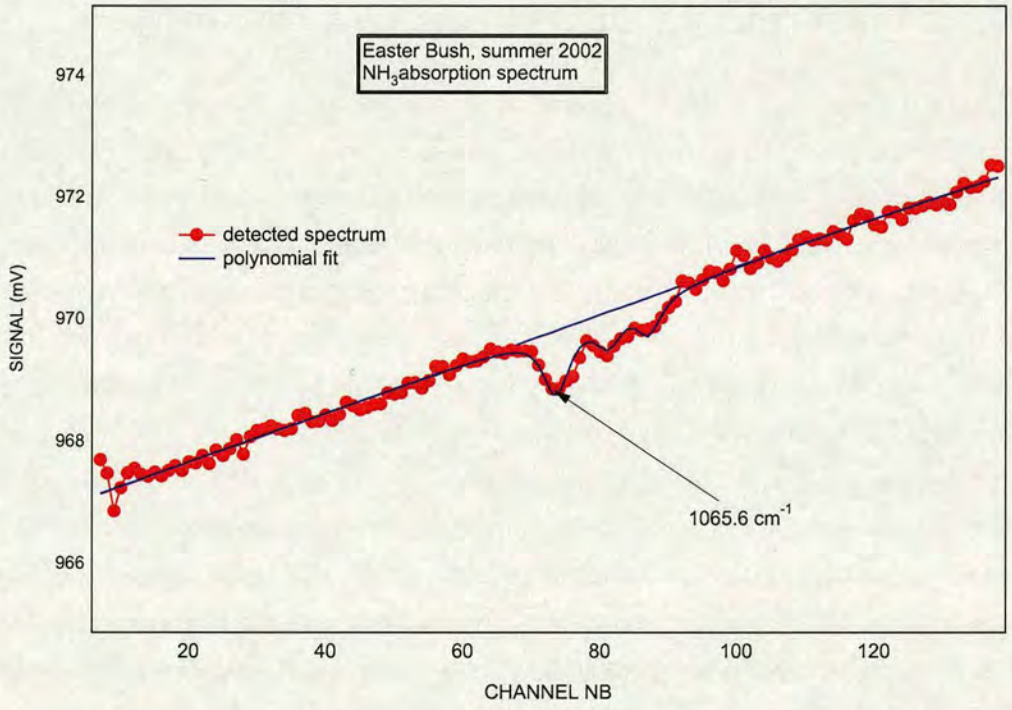

Figure 4.7: Absorption features for ammonia in the spectral region of the diode used in the Easter Bush campaign. The channel numbers in the abscissas axis correspond to wave numbers of the laser light.

Compared to monitoring at a single absorbing wavelength, this approach makes the retrieved concentrations less susceptible to potential interferences from other

species absorbing in the same spectral region, as well as those of weak interference fringes inherent to the optical system.
Fingerprint fits are performed with an iterative nonlinear least squares minimisation routine, which computes the Voigt profile for each line in the spectrum, using the HITRAN spectral database line parameters, temperature and pressure in the cell [Rothman, 2004]. The TDL software developed by Aerodyne Research allows up to 45 individual lines to be used in the fingerprint fit for each species and can fit up to 4 species in each spectrum. The analysis of spectra is executed in real time and resulting concentrations are saved to disk as well as sent by means of a serial cable to a separate logging unit [Horii et al., 1999]. A PC provides access to all laser control, spectrum fitting and data archiving functions.

4.2 Measurement of NH_3 concentration

The output data are divided in different files, containing a time string and concentration data, as well as spectral data. The signals coming from the TDL and sonic anemometer are converted and processed synchronously by using a Labview (National Intruments Inc.) program. In Fig.4.8 is shown a typical concentration data output from the TDL system measuring ammonia in the lab at a frequency of 1Hz.

The information about the retrieved spectrum (see fig.4.9) are used to check the quality of the measurements. By observing the polynomial fit, the range of the signal, the position of the absorption line on the prescribed channel (i.e. wave number), it is possible to ensure a good operation of the instrument.
In order to avoid interferences from absorption lines belonging to other species, it is advisable to inject "scrubbed" air at the end of the multi-pass cell orifice until the cell has been flushed for a few times and then record a "background" spectrum. This spectrum can then be subtracted to the sampling air spectrum and contribution of lines other than the analysed species will be removed. The "scrubbing" process has proved difficult for ammonia: several set-ups were tried before and during the Easter Bush field campaign, but none of those was fully satisfactory. The first attempt was done using a sealed column containing dried rock-wool impregnated of a solution of citric acid dissolved in methanol, to scrub NH_3, put in series with charcoal to adsorb water molecules. Air would be pushed

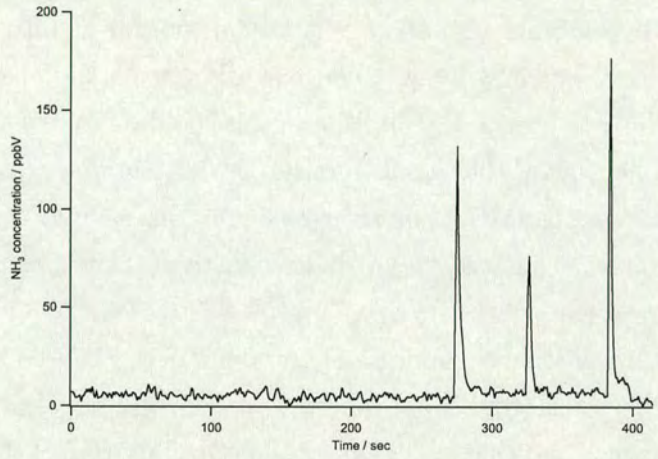

Figure 4.8: Concentration of ammonia measured in the lab at CEH Edinburgh: the three peaks in concentration are the answer to waving a source of ammonia in front of the inlet at a distance of about 20cm.

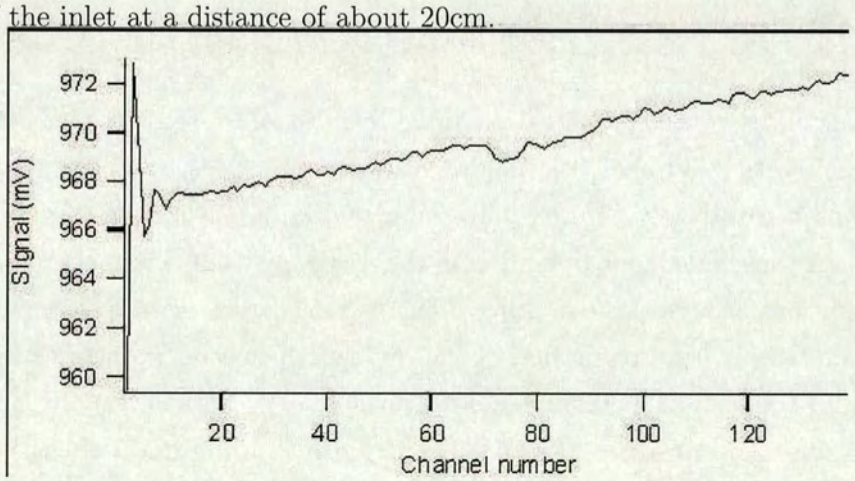

Figure 4.9: The detected signal shows a spectral portion of 0.2 cm^{-1} circa centred on the line of absorption chosen for the measurement (in this case, 1065 cm^{-1} corresponding to channel nb.78).

through the column by means of a pump and the outlet connected near the critical orifice (see Fig. 5.1. The system worked in the lab, but after a short while in the field it got contaminated with humidity, and this compromised the scrubbing action. In a second attempt a Perma-Pure tube was used, and again it proved efficient in the lab, but got contaminated in the field.

The subtraction of the background signal is a very useful tool for quality control on the data: for instance over low-ammonia concentration areas the absorption peak is not always so strong to ensure a good fit, and this could be source of errors on the signal. At the same time, if the signal is noisy the subtraction of one signal to another can cause noise amplification, as the two signals, air sample and background, are not synchronous: thus the noise fringes can either cancel each other out or sum up, increasing the error in the signal.

The noise present in the absorption signal is partly random, partly caused by scatter of the beam in the absorption cell, beam clipping on the mirrors' edges,interferences between the two laser beams operating at the same time. Optimisation of the range helps to increase the signal to noise ratio, which in optimum conditions was of 10^4.

The laser light output can be unstable, presenting variable range and fringes: this is due to the temperature fine regulation on the diode and can vary with time of operation of the diode.

The uncertainty in the concentration values can be addressed to signal noise and interference with additional laser modes overlapping in the same spectral subrange of the chosen absorption feature (multi-mode operation). It is necessary to periodically check the single mode operation of the diode, by using a monochromator: in field conditions though this can prove difficult, as the opening of the insulated box upsets the temperature regulation of the optical bench, and wetness can damage the electric connections. Single mode operation can be verified also by observing a strong absorption feature in proximity of the measuring line: when the shape of the strong absorption line changes, it is very likely that another frequency is overlapping, and the concentration calculation will take into account both contributions, the one from the measured species and the other from an unknown species.

During the field measurements at Easter Bush, a measure over one minute periods at an aquisition rate of 5 Hz of a constant source of ammonia from a cylinder gave a standard deviation of 2%. When the aquisition rate is decreased to 1 Hz the standard deviation becomes on average 0.02%.

Chapter 5

Measuring fluxes of ammonia by eddy covariance using tunable diode laser absorption spectroscopy

Parts of the contents of this chapter have been published in Water, Air, Soil Pollution: Focus **4***: 151-158, 2004.*

5.1 Introduction

Gaseous ammonia plays an important role in the processes of eutrophication and acidification of vegetation, and it is the main contributor to the total N deposition in the UK [Fowler et al., 1998b]. To assess the impact of atmospheric ammonia on vegetation, it is necessary to quantify its deposition rather than its concentration in the air. This study demonstrates the applicability of a novel eddy covariance flux measurement system based on Tunable Diode Laser Absorption Spectroscopy (TDLAS) to measure ammonia exchange fluxes over grassland. Grassland has been chosen as it represents one of the major ecosystems in terms of land cover throughout Europe: specifically for Great Britain, managed grassland covers about 27% of land [Fuller et al., 1994], and when rough grazing and the uplands are included the value approaches 50% of the UK.

Micrometeorological measurements of ammonia fluxes provide valuable insight into processes regulating the ammonia exchange between vegetation and the atmosphere, averaged over 10 to 30 min. Measurements of NH_3 concentrations have proved challenging in the past, and the first studies on NH_3 fluxes were made in the 1990s, e.g. [Sutton et al., 1993b], where fluxes were calculated using the aerodynamic flux gradient method. Vertical concentration profiles were initially measured by filter pack or manual denuder methods, and later with continuous wet-chemistry analysers such as the AMANDA (Ammonia Measurement by ANnular Denuder sampling with on line Analysis). While gradient techniques rely on empirical parameterisations and derive a flux which is averaged over the height range of the measurements, the lack of fast NH_3 sensors has until recently prevented the application of the more direct eddy correlation techniques to NH_3. In fact, to obtain a measure of the actual flux using the eddy covariance method, an analyser must be able to detect the fluctuations in the concentration signal of all frequencies typical of the turbulence in the surface layer.

In the first study on ammonia fluxes measured with the eddy covariance technique, [Shaw and Spicer, 1998] used a tandem mass spectrometer to measure the concentrations of NH_3.

Recent improvements on TDLAS now allow the measurements of NH_3 concentration at a time resolution (>1 Hz) suitable for the application of eddy covariance. Data presented in this chapter show typical features of the fluxes and concentration for the summer season. NH_3 concentration and flux values are in a similar

range as previous studies using flux gradient methods at the same field site, although the particularly wet season reduced the concentration of NH_3 in the air. For an example day, measured NH_3 fluxes ranged between -11 and 44 ng m^{-2} s^{-1} with an average value of 3.78 ng m^{-2} s^{-1} indicating a small net emission from the vegetation. Spectral analysis executed on the data show the percentage of flux carried by the small eddies (from 0.3 to 2 m) suggesting that high detection frequency instruments are particularly suitable for estimating NH_3 fluxes between atmosphere and vegetation.

These data demonstrate the ability of the TDL system coupled with sonic anemometry to measure NH_3 fluxes by eddy covariance and show fluxes in the typical range of NH_3 emission over grassland [Milford et al., 2001]. There are many concerns for the applicability of eddy covariance methods in various situations, such as night hours, due to low wind speed conditions, or non stationary conditions, due to e.g. the presence of local sources.

However, such problems are common to all micrometeorological techniques, and the high frequency of acquisition used in eddy covariance provides information on the underlying turbulent structure and on the contributions of the different eddies to the turbulent transport.

This chapter reports on the application of the eddy covariance method for NH_3 flux measurement at the same field site used for earlier NH_3 flux measurements by aerodynamic gradient methods. The objective of this chapter is to show the suitability of the eddy covariance method using TDLAS for NH_3 flux and report a set of turbulent fluxes measured during a summer season in Southern Scotland.

5.2 Fast sampling of NH_3 concentrations with TDLAS

TDLAS has been used in the past to measure NH_3 at small concentrations with success, e.g. [Schiff et al., 1987], [Lachish et al., 1987], [Silver et al., 1991]. The time response of the systems used was long (up to a few minutes) compared to the time scales that characterise the turbulent surface layer, and these methods were not suitable for micrometeorological flux measurements. The challenges related to fast detection of NH_3 are not only connected to the ability of the instrument to

sample, analyse and compute the concentration from the air, but also to the reactive nature of gaseous NH_3. As seen in chapter 1, the residence time of ammonia in atmosphere is heavily influenced by relative humidity of the air and wetness of the vegetative surface. Water drops can accumulate on surfaces of both instrument and vegetation, either by precipitation or by condensation in cool conditions; this film of water can capture gaseous NH_3 from the air sampled by the analyser, altering in this way the estimate of the ambient concentration of NH_3. Also temperature provides an important control over NH_3 emissions from vegetation. The factors that regulate the frequency response of the TDL system for NH_3 measurements are the flow rate, the shape, length and material composition of the inlet tube.

5.2.1 Attenuation of the signal through the inlet

The detection of simultaneous, fast fluctuations of wind speed and scalar concentration of an air parcel is necessary for the application of eddy covariance. The air parcel analysed by the scalar sensor and the sonic anemometer has to be the same, therefore the inlet tube connected to the chemical analyser must sit close to the sonic transducers. Using a length of tubing to transport the air sample to the analyser reduces the obstruction to the air flow caused by the analyser itself, but also affects the concentration signal.

The sampling tube introduces a delay, between the time when the sample of air enters and leaves the tube (time lag). This is not constant, as it depends e.g. on wind speed, and on the chemical properties of the measured compound. The sampling tube also acts as a high frequency filter, higher frequencies being attenuated more rapidly than low ones: such attenuation of concentration fluctuations leads to potential underestimates in the flux, see e.g. [Leuning and Moncrieff, 1990]. Therefore properties of the inlet tube must be considered when estimating the time response of an analyser.

The factors regulating the attenuation are: the tube radius, material and length, the flow rate, wind speed, measuring height. The mean flow through a tube isn't uniform along the radial axis, and the fluctuations of the gas concentration are smeared as they advect along the tube. Both radial diffusion and differential advection are caused by the deformation of the fluid as it flows through the tube as a result of friction. If the motion through the tube is laminar, the velocity of the flow has a parabolic profile, whereas in the case when the flow is turbulent the velocity profile is more uniform throughout the tube, see

e.g.[Lenschow and Raupach, 1991], [Massman, 1991].

The concentration is more likely to be affected in the laminar flow case, where concentration fluctuations are attenuated along the length of the tube. Attenuation of the concentration fluctuations occurs for all gases, but for reactive gases also the composition of the sampling tube has to be taken into account, as the surface is likely to absorb the gas. The choice of the material of the inlet tube is crucial as gaseous NH_3 has a "sticky behaviour".

In a study by [Goretty, 1998], different materials were tested for sampling tubes for NH_3 detection with a TDL system: the results of that study show that clear polyethylene gave the best time response, followed by Pyrex and stainless steel. The same tests revealed that turbulent flow and short inlet tubing optimise the time response, as expected. Since ammonia has a high affinity for water, it is desirable to minimise the presence of water along the lines: low pressures decrease the amount of water molecules on the walls (as in the TDL absorption cell) reducing the number of sites to which ammonia can adsorb.

The inlet tube used during the field campaign at Easter Bush in 2002 was clear polyethylene (PE), 2.5 m long, with an outer diameter of 1/2" (12.7 mm) and an inner diameter of 3/8" (9.6 mm): as shown in fig.5.1.

The flow rate at the critical orifice of the TDL glass inlet (see §4.1.2) was 10 ℓ/min, and an additional pump was connected at the bottom of the PE inlet tube to keep the flow through the tubing turbulent. The flow rate at the inlet end was 42 ℓ/min: with this flow rate, the flow inside the inlet was fully turbulent, with a Reynolds number value of $Re = 8158$.

The measurements in the field showed that humidity is a critical factor as it increases the time response of the same system: to minimise this effect it is advisable to keep the inlet at a higher temperature, to prevent, or at least reduce condensation on the inlet walls. This is in agreement with the previous studies, see e.g. [Goretty, 1998].

An evaluation of step concentration changes from adding higher concentrations of NH_3 from a cylinder has been made in the lab, in order to measure the inlet extension response time (see fig. 5.2). After the removal of the source from the inlet, an exponential decay is noticeable in the concentration strip chart; the exponential decay time constant τ found for the setup described above was ranging between 0.65 s and 1.35 s. The median of these results is a value of $\tau = 0.9$ s.

When operating in the field, the ammonia loss at the inlet showed different

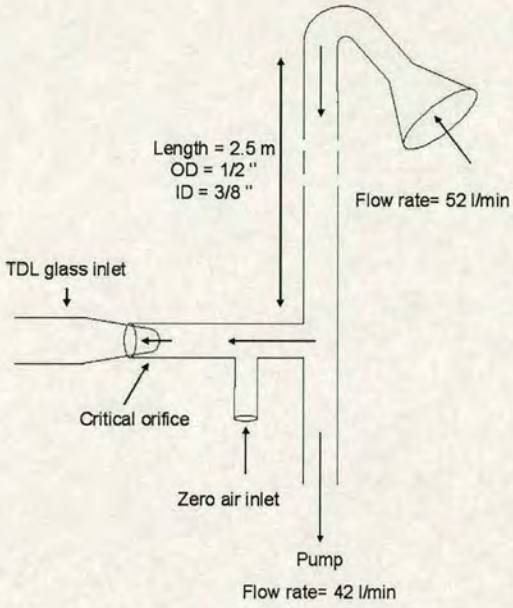

Figure 5.1: Inlet schematic view.

behaviours from the lab conditions; τ was on average longer, and depended on the air humidity and wetness conditions of the surface. In fig. 5.3 some examples of time response measured in the field in different atmospheric conditions are shown. The values of τ ranged between 0.9 s in fairly dry conditions to 7.5 s in very wet conditions. This longer time response of the inlet jeopardizes the application of eddy covariance as the higher frequecies are not resolved with such time response.

Heating the inlet proved useful in improving the time response, and for most of the time while the TDL was operating at Easter Bush the atmospheric conditions allowed a value of τ in the range 0.9 s to 1.8 s, with a median value of 1.3 s.

An evaluation of the attenuation of the flux depending on the response time of the TDL sensor has been done following the method from [Horst, 1997]. The fraction by which the eddy flux is underestimated because of the relatively slow response of a scalar sensor is a function of both the response characteristics of the sensor and the distribution of the eddies contributing to the flux. It can be expressed as:

$$\frac{F_m}{F} = \frac{1}{1 + (2\pi n_m \tau_c \overline{u}/z)^{\alpha}} \tag{5.1}$$

where, for neutral and unstable stratification:
$z/L \leq 0$, $\alpha = 7/8$, $n_m = 0.085$

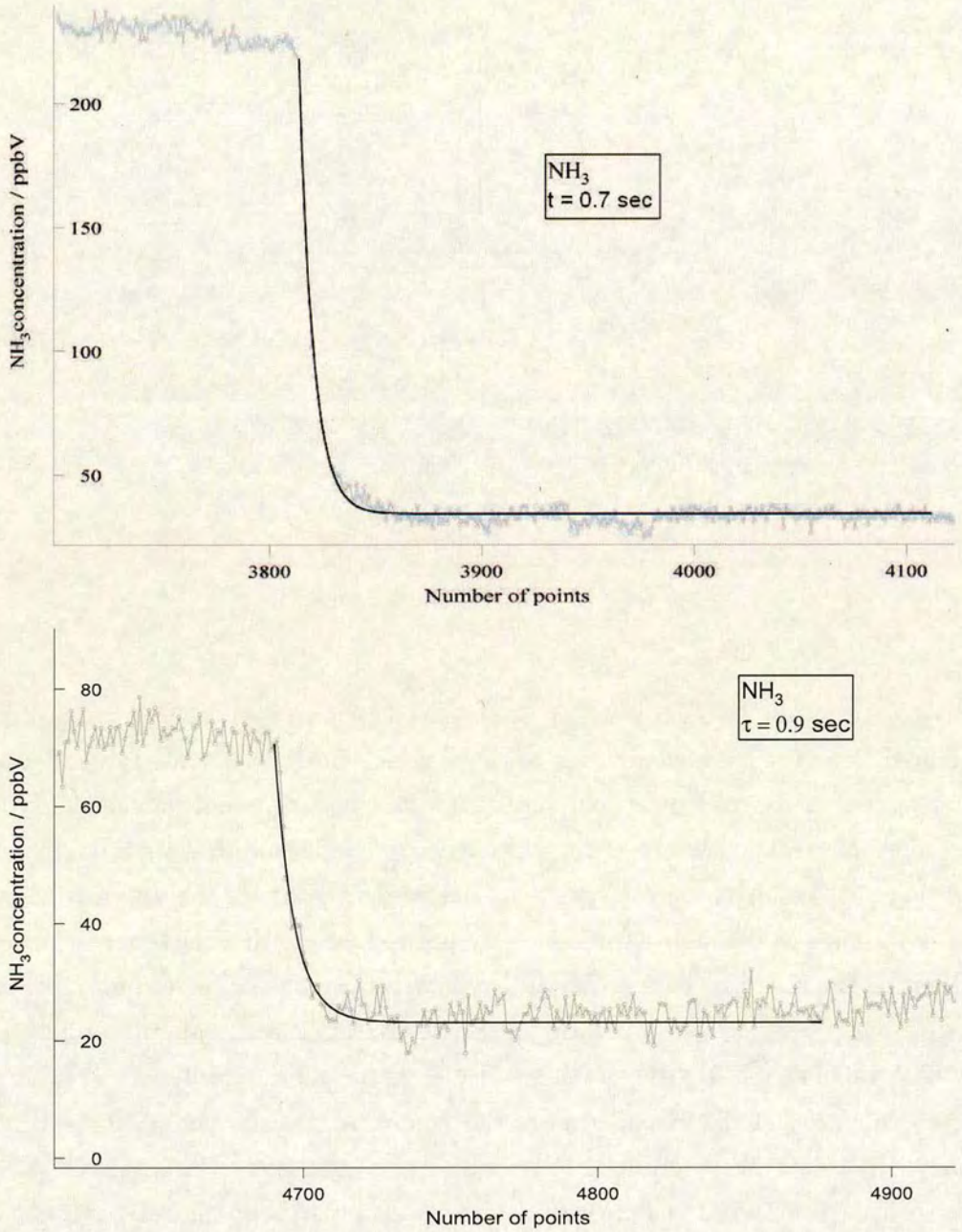

Figure 5.2: TDL responses to a step change in NH_3 gas flow at the inlet, using PE tubing. The top chart refers to higher NH_3 concentrations used for producing the change in step, the bottom chart to lower concentrations; the exponential decay time constant τ has a median value of 0.9 s.

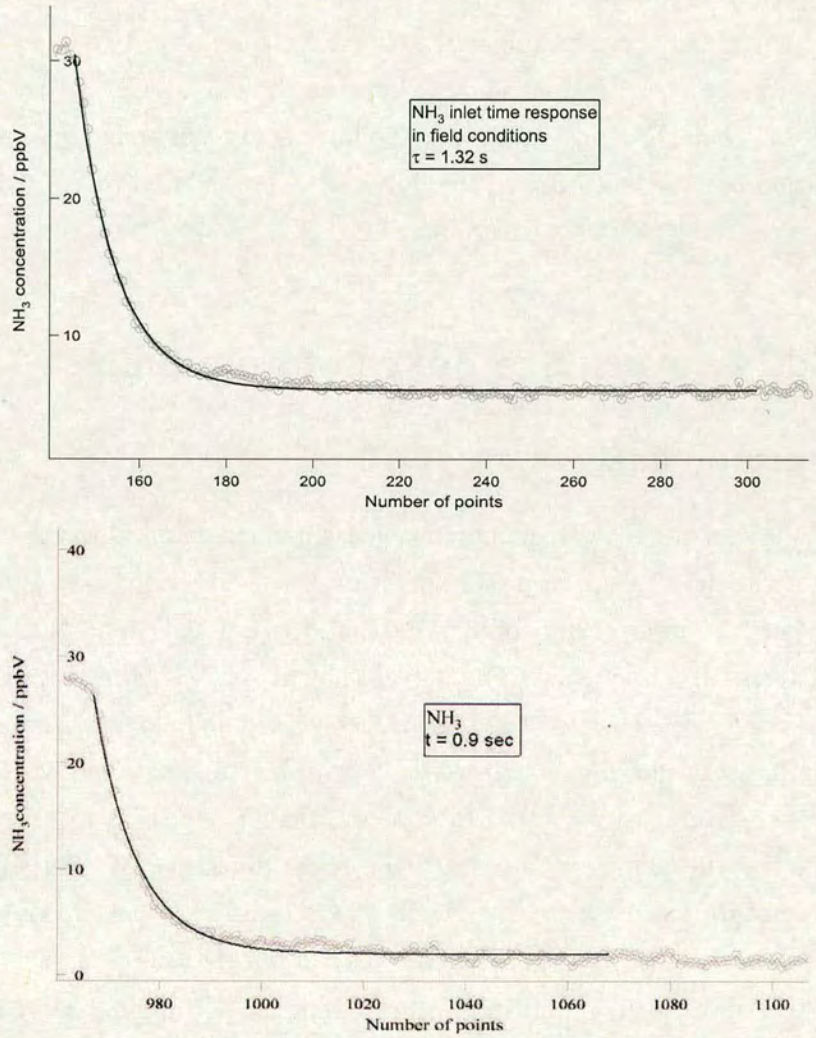

Figure 5.3: Dual TDL responses to a puff of NH_3 measured at Easter Bush. The exponential decay time constant τ has different values according to humidity.

and for stable stratification:

$z/L > 0$, $\alpha = 1$, $n_m = 2 - 1.915/(1 + 0.5\,z/L)$.

In the above formula, F_m is the measured eddy flux, and F is the actual eddy flux; τ_c is the response time characteristic for the sensor, z is the measurement height, L the Obukhov length, $\overline{u}$ the mean horizontal wind speed, n_m is the normalised frequency of the co-spectral peak.

The results from the field campaign at Easter Bush showed that on average the flux loss was of a 32% factor, ranging between 23% and 46%. In particularly wet conditions, when the response time of the instrument was strongly affected by the attenuation of the concentration the flux loss was calculated to be up to 72%, and the data were rejected as a consequence.

5.3 Eddy covariance fluxes of ammonia

5.3.1 Spectral analysis

Spectral analysis of the high frequency flux measurement data allows the component parts of the flux turbulent power spectrum to be quantified (see §2.3.2). In fig.5.4 the spectral power of horizontal wind speed (u), T, CO_2 and H_2O with w, are plotted versus the frequency. The curves show a typical shape for cospectra, with a decreasing slope towards the high frequencies that follows a slope of -4/3 showing the inertial subrange energy cascade from big to smaller eddies (§2.3.2). These values are averages of 3660 × 15 min-covariances.

By examining the contribution to the fluxes of the different frequencies for wind speed, temperature and scalar concentrations (CO_2 and H_2O), it is evident that most of the flux is carried by eddies in the 0.002 to 0.5 Hz range.

An example of co-spectrum of NH_3 is shown in figures 5.5 and 5.6; the cospectra shown represent a covariance calculated over half an hour period. In fig. 5.5 the normalised cospectra of temperature and NH_3 concentrations are plotted together, their shapes are similar and they follow a slope of -4/3 as well as the cospectra in fig. 5.4.

The percentage of ammonia flux carried by eddies smaller than 2 m (corresponding to frequencies >1 Hz with a wind speed of 2 m/s, as it was on average at Easter Bush during the measuring period) was on average 18.4%, and this value has been calculated from daily cospectra during the measuring season.

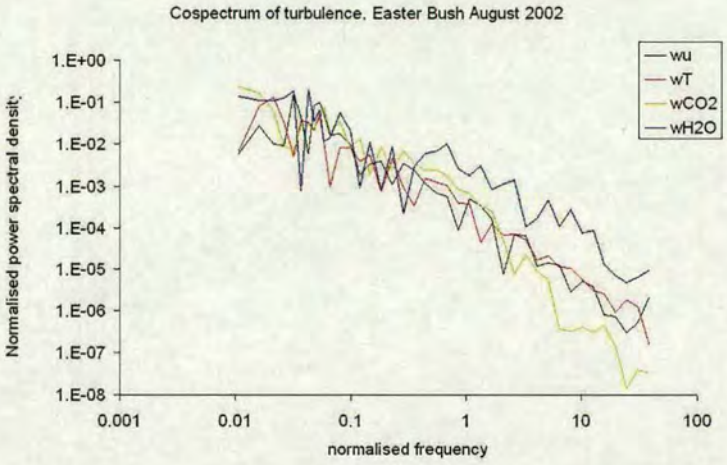

Figure 5.4: Cospectra of wind speed u (black line), temperature (red), CO_2 concentration (green) and H_2O concentration (blue) with vertical wind speed w, averaged over 15 min period covariances recorded at Easter Bush.

This percentage suggests that the contribution of small scale turbulence is important in the estimate of NH_3 fluxes, and therefore fast response sensors such as TDL can provide very useful information about the exchange dynamics between surface and atmosphere.

5.4 The field site

Measurements were made at the Easter Bush field site (NT245641, lat. 55°52', long. 3°2', elevation 190 m above sea level), located south of Edinburgh. The Pentland Hills (AMSL max 580 m) lie close to Easter Bush and characterise the wind field of the area. The measuring site is an intensively managed grassland, covered by more than 90% with *Lolium Perenne* and with a minor presence of *Phleum Pratense* and *Ranunculus repens, Poa Annua, Trifolium Repens* as shown in fig.5.7. The field is used for silage production, cattle and sheep grazing. Surrounding the field site is a mixture of woodland (mixed, maximum height 15 m), roads, rough grazing land and farms as shown in fig.5.8.

The instrumentation was placed on the boundary between two fields with similar management, as shown in fig.5.9, providing more than 200 m of fetch in the two most common wind directions, namely SW and NE, which were determined

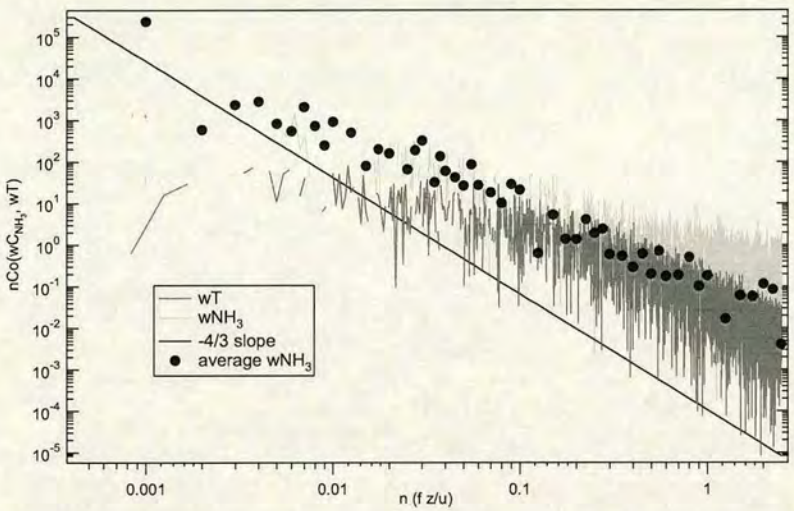

Figure 5.5: Co-spectra of ammonia (grey line), temperature (dark grey line) and vertical wind speed for a 30-min sample of data. The dots refer to the NH_3 cospectrum block-averaged to result evenly spaced. Covariance values are plotted vs non-dimensional frequency n and compared with the theoretical -4/3 slope.

during previous years measurements.

The field measurements started in July 2002 and continued until mid-October 2002, providing a total of 915 hours of data. The measurements provided fluxes of NH_3, momentum, CO_2, sensible and latent heat, as well as a full set of meteorological variables as wetness, rainfall (see fig.5.9) to help the interpretation of the data. During the growing season, farming activities went on at Easter Bush: the south field was fertilised, the grass was cut, and animals (both cattle and sheep) were grazing in the north portion of the field.

Both the fertilisation of the field and the animals provide sources of ammonia, but their impacts are different. For this reason it is important to evaluate the contributions to the ammonia fluxes relative to the two areas of the field. This can be achieved by sorting the contributions according to wind direction.

5.4.1 Footprint and fetch study

An estimate of the fetch (see § 2.4) has been calculated by using the model of Kormann and Meixner (2001). An example is shown in fig. 5.10, where the Cumu-

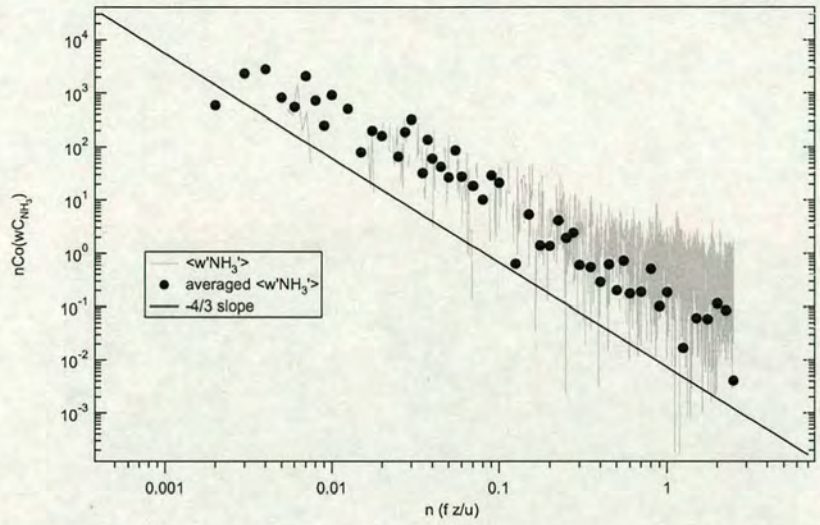

Figure 5.6: Co-spectrum of ammonia and vertical wind speed for a 30-min sample of data. Covariance values are plotted vs adimensional frequency n and compared with the theoretical -4/3 slope.

lative Normalised contribution to the Flux (CNF) is plotted against the distance from the sonic anemometer. This result refers to a half hour period, on August 25^{th} from 12:30 to 13:00 as an example in which an ellipse with a long axis of 215 m described the fetch that contributed 90% of the flux.

In fig.5.11 are shown the average characteristics of the fetch during the measuring period in 2002 at Easter Bush: in the 95% of the cases, the fetch was extending to a distance from the sonic between 175 m and 250 m. A plot of the CNF values is shown in relation to the wind direction: in this chart it is possible to visualise the capture of the flux according to the direction of the wind. Along the main wind field (NE-SW) it is logical to find the majority of the events, including very high horizontal wind speed that stretch the footprint far beyond the fetch, and therefore causing the loss of flux capture. A very interesting information is given by each point of this plot as it characterises the event in terms of flux capture according to the wind direction and therefore the location that originated that contribution.

Figure 5.7: Example of vegetation on the Easter Bush field site.

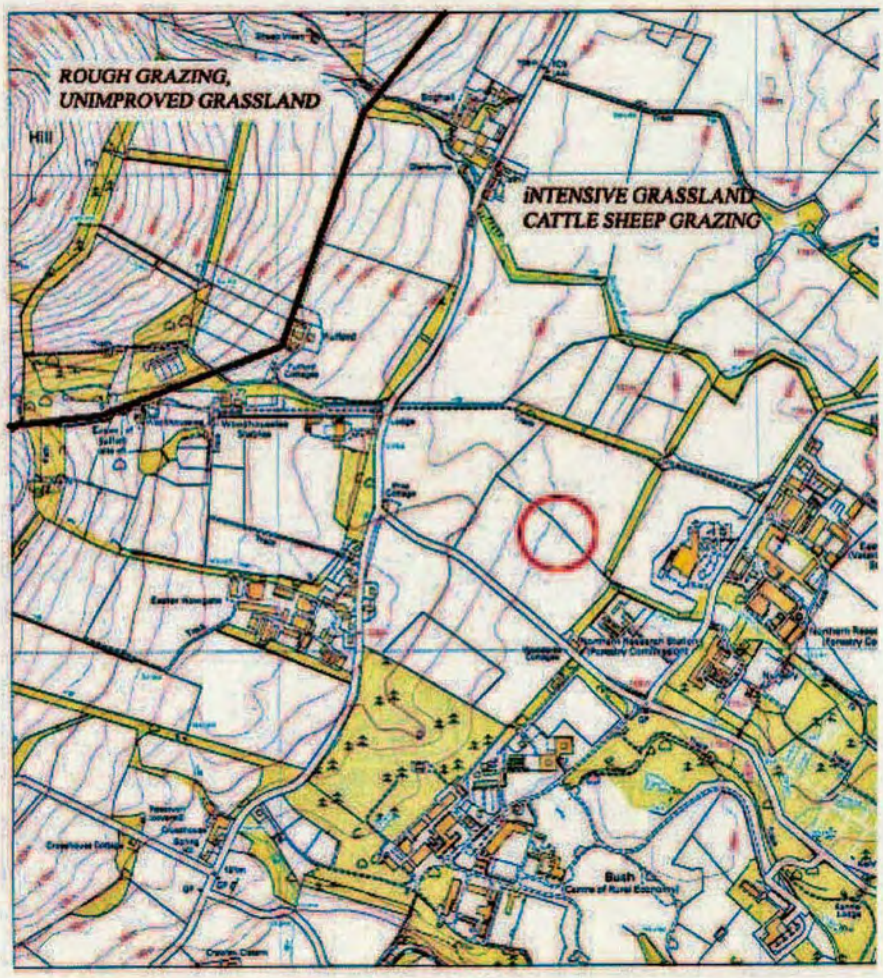

Figure 5.8: Easter Bush topography (from Ordnance Survey map).

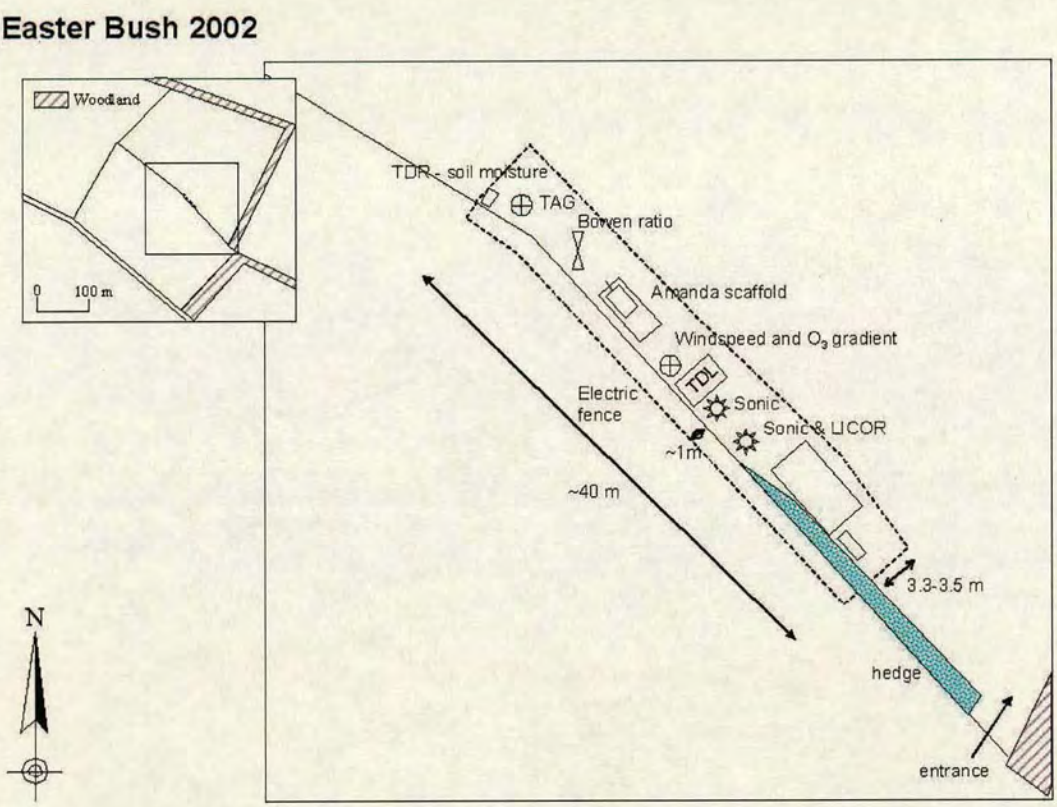

Figure 5.9: Map of the Easter Bush site, with instruments lined up on the fence between the north field, mainly used for grazing, and the south field, mainly used for silage production.

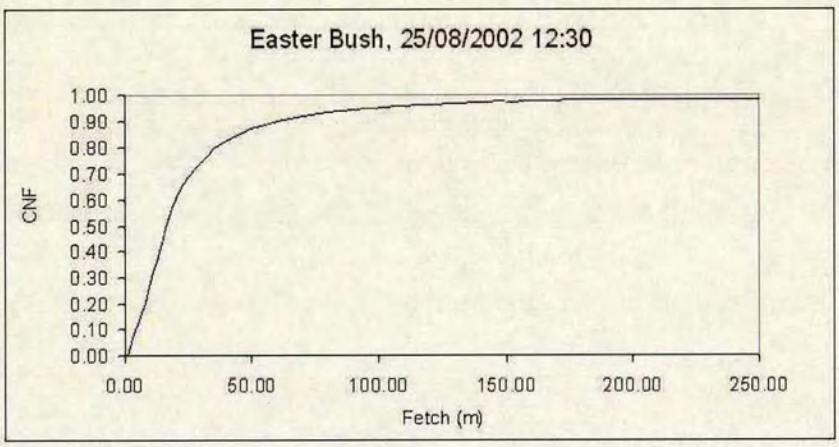

Figure 5.10: Cumulative Normalised Function calculated with the method by Kormann and Meixner at the Easter Bush field site on August, 25^th 2002.

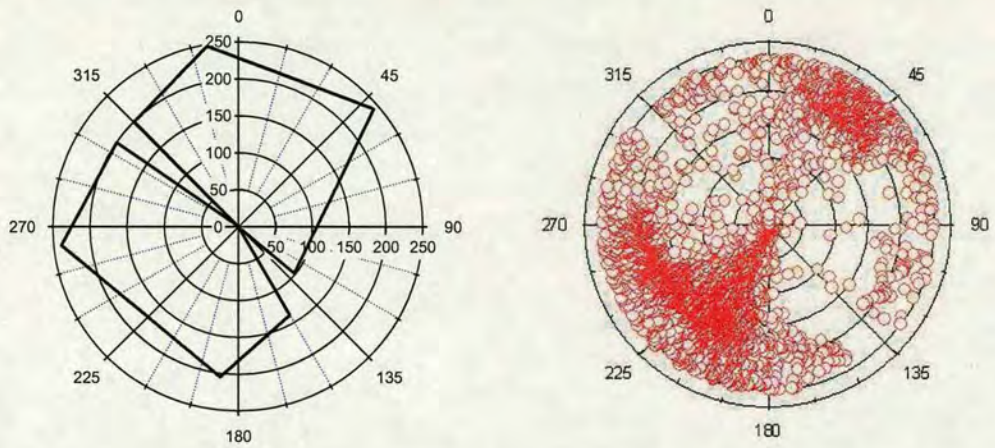

Figure 5.11: *Left:* Dimensions of the average fetch recorded at Easter Bush during the period from July to October 2002 (distances are expressed in m, 0 degrees correspond to North). *Right:* Distribution of CNF according to the wind direction; the values on the radius axis are normalised to 1, and represent the fraction of flux captured from the fetch.

5.5 The system deployment on the field site

An ultrasonic anemometer (USA-1, METEK GmbH, Elmshorn, Germany) was used to measure the three components of turbulence *u'*, *v'*, *w'* at a frequency of 10 Hz, and was coupled with a TDL system (Aerodyne Research Inc.) to measure eddy covariance fluxes (see § 4).

Tuneable diode laser spectrometers (TDL) can provide mixing ratio values of atmospheric trace gases up to 10 Hz frequency; their high spectral resolution (typical values span between $2\text{x}10^{-5}$ cm^{-1} and $1.7\text{x}10^{-2}$ cm^{-1}) allows a good selectivity between the spectral contribution of the different species. The novel version of TDL used during the field campaign is a dual system, and has a detection limit of up to a few hundreds of pptV; this high sensitivity, together with high selectivity, resolution and fast response time, make TDL systems suited for the observation of processes on the small temporal and spatial scale (typically involving turbulent eddies from 0.3 m to 2 m dimension), ideal for application of the eddy covariance technique.

The sonic anemometer was mounted on a 2.5 m tall mast, and a 2.5 m long inert 1/2" OD PE tube was placed 0.2 m below the centre of the ultra sonic trans-

ducers (fig.5.12). The flow through this tube was high to minimize wall effects and maximize response time, as discussed before. A sub sample of 10 l min^{-1} was taken from the air stream through the inlet tube driven by a pump, to the short glass inlet of the TDL system (see fig.5.1), which was enclosed in an aluminium shell, surrounded by foam insulation and a weatherproof polyethylene case situated just beneath the ultra sonic anemometer. A photograph of the system is shown in fig. 5.12.

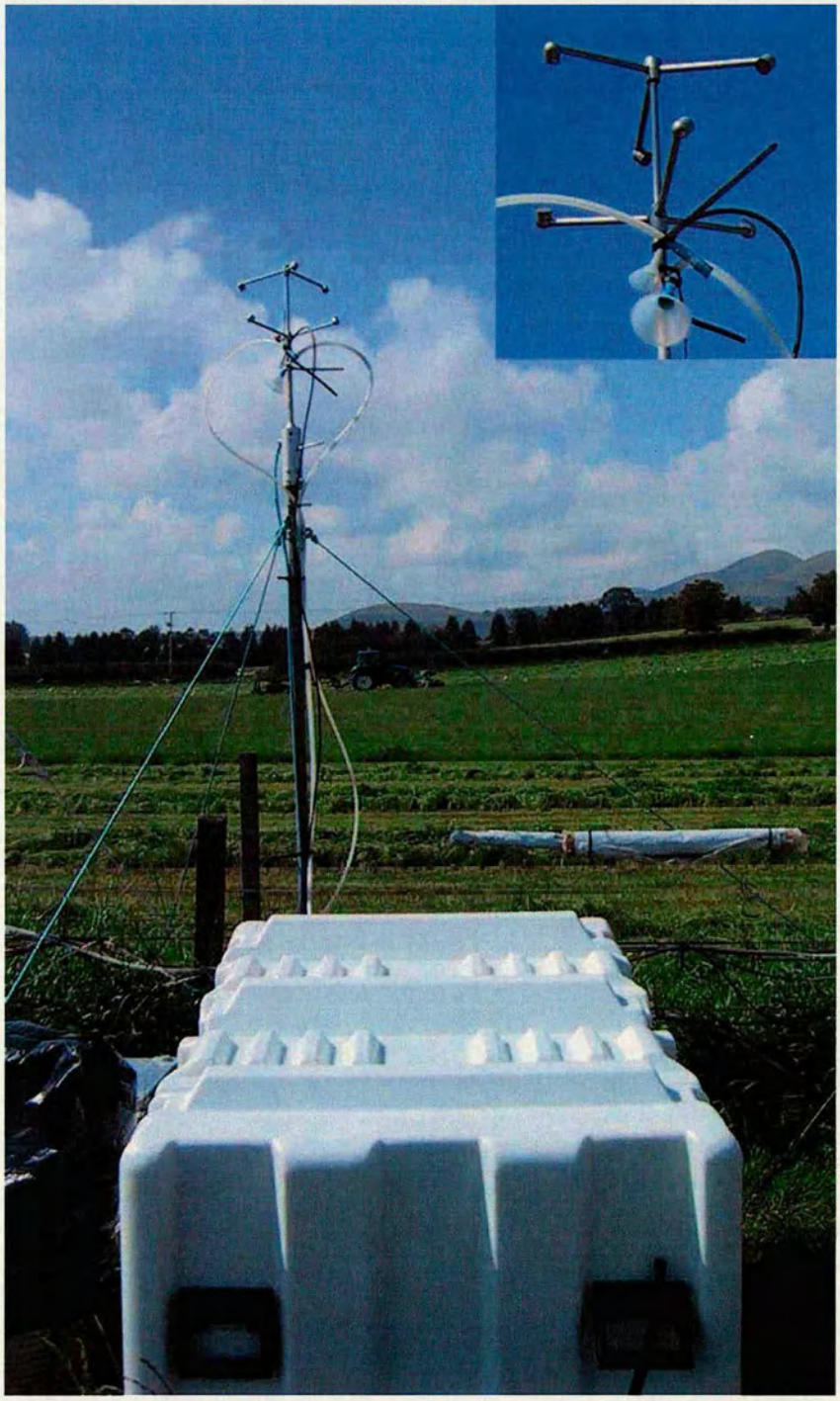

Figure 5.12: Dual TDL system and sonic anemometer at Easter Bush. On the top right, detail of sonic transducers and inlet tubing for TDL and LICOR.

5.6 Measurements results: some case studies

Data from wind sectors disturbed by the nearby cabin and other pieces of equipment, corresponding to an angular portion between 80°C and 120°C have been removed from the dataset, as the changing flow would upset the turbulent fluxes. The signals from anemometer and spectrometer are acquired at a frequency of 5 Hz, and logged on to a PC synchronously by means of serial connections.

A program written in LabVIEW^{TM} (National Instruments) performs the acquisition as well as on line calculation of fluxes and storage of raw data. The instantaneous values of vertical wind speed component and gas concentration are used to calculate the covariances over a period of 15 min; in the analysis process, the wind components, temperature and chemical concentration were routinely scanned to remove noise spikes.

In the flux calculation, raw data from closed path sensors (e.g. LICOR and TDL) were offset by the observed time lag, that is defined as the time it takes to the air parcel to go through the inlet of the instrument, i.e. the phase delay time between the data recorded by the sonic anemometer and the concentration measured by the analyser. It depends on the length and radius of the tube, on the flow rate, on the tube material composition (see § 5.2.1) and on the atmospheric turbulent conditions. Lag times were calculated from the maximum covariances of w and χ for each measured compound.

Examples of the application of the technique are given in the following paragraphs.

5.6.1 $10^{th} - 11^{th}$ July 2002

In figure 5.13 the concentration of ammonia recorded at the field site on the 10^{th} of July 2002 shows a range between 0.35 ppbV and 7.5 ppbV: these values were typical of an average behaviour at Easter Bush during summer 2002; in fact, the range has been between 0 and 20 ppbV, with an average value of 7 ppbV during the day. The NH_3 concentration is not particularly stable, due to the patchy source contribution. In figure 5.13 the eddy flux values range between -14 and 67 ng $m^{-2}s^{-1}$. The fluxes are mainly of emission, during the day, then small deposition fluxes can be seen during the night. The net contribution is predominantly emission, and a daily structure seem to appear: the role of vegetation is evident as a source during the light hours, when the stomata are open, and therefore release NH_3, and as a sink

when the stomata activity is inhibited.

In figure a 5.14 the values of u_* are shown to range between 0.1 and 1.6 m s^{-1}, having an average value of 0.47 m s^{-1}, which again is quite typical for a summer day on Easter Bush. From the chart it can be seen the convective conditions starting increasing in the morning and decreasing in the evening hours.

On the 10^{th} of July 2002, the convective layer of the atmosphere was well developed at Easter Bush. These conditions can be seen in the heat fluxes charts (figures b and c, 5.14) as well, where typical daily cycles are recognisable. The quantities displayed in all the charts have been sorted according to the wind direction, which was mainly in the SW-NE portion, and this allowed the fetch conditions to be satisfied. Similarities can be seen between the behaviour of heat fluxes as well as momentum fluxes and ammonia fluxes.

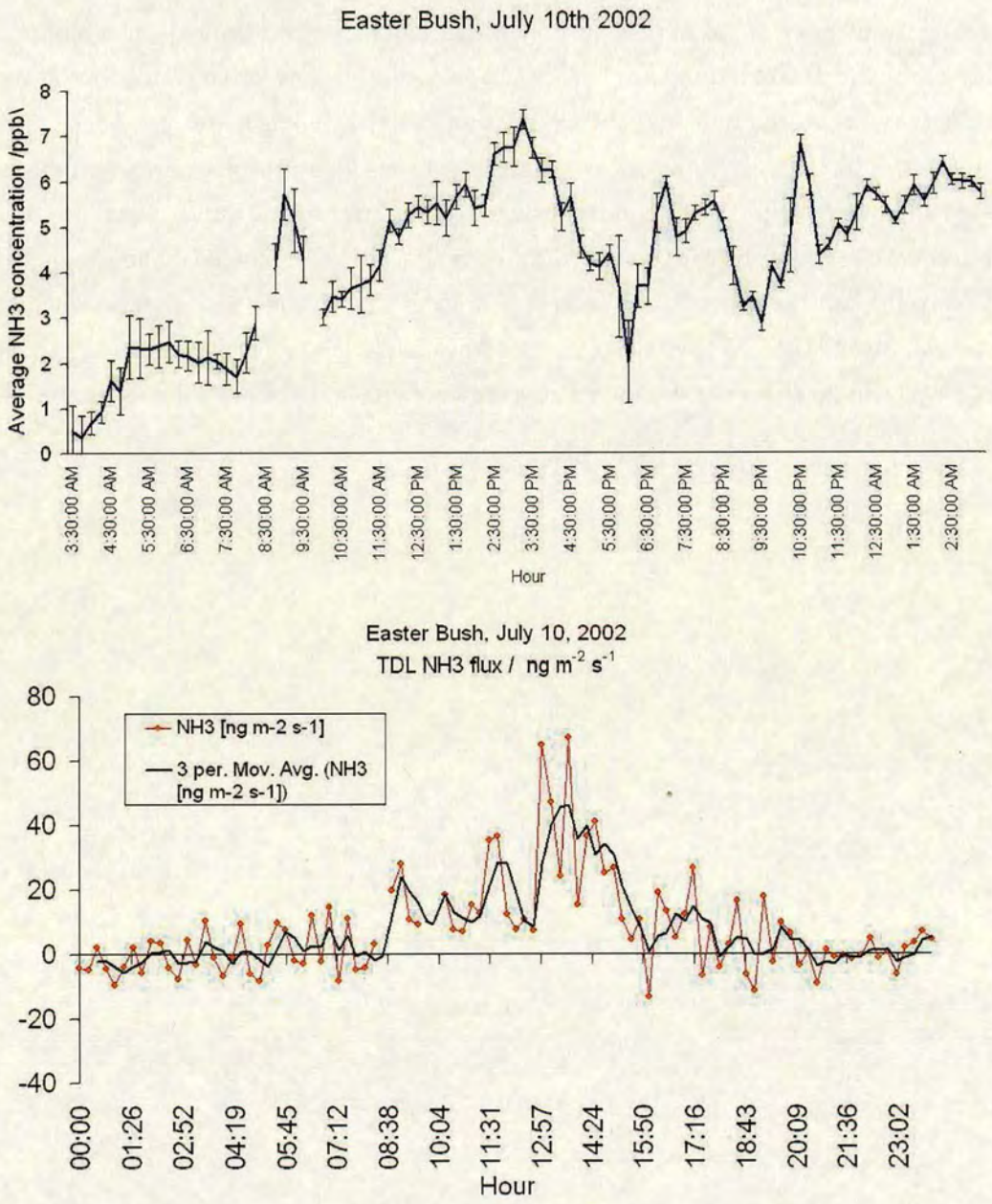

Figure 5.13: Top chart: concentration values of ammonia averaged over a 15-min period; the error bars refer to the relative standard deviation values. Bottom chart: values of 15-min fluxes (red line) and moving average per 3 values (thicker black line).

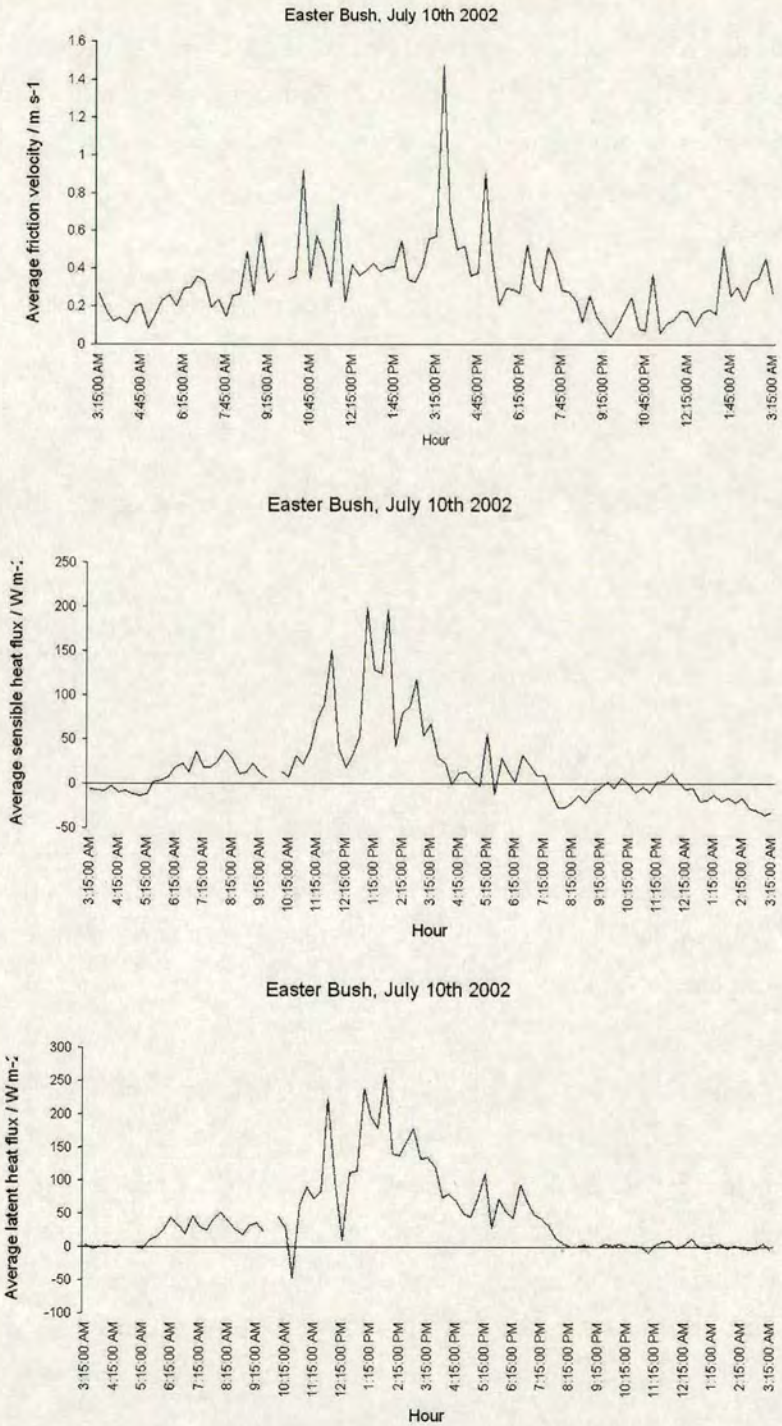

Figure 5.14: Values of friction velocities (top), fluxes of sensible heat (middle) and fluxes of latent heat, measured with a LICOR 7500 coupled with the sonic anemometer (bottom), averaged every 15 min.

5.6.2 $10^{th} - 11^{th}$ August 2002

Fertiliser (50 kg N ha^{-1} as NPK) was applied on the 10^{th} of August on the southern field; the emission fluxes from the vegetation following this application were still evident after a few weeks from the fertilisation, as can be seen in fig.5.17.

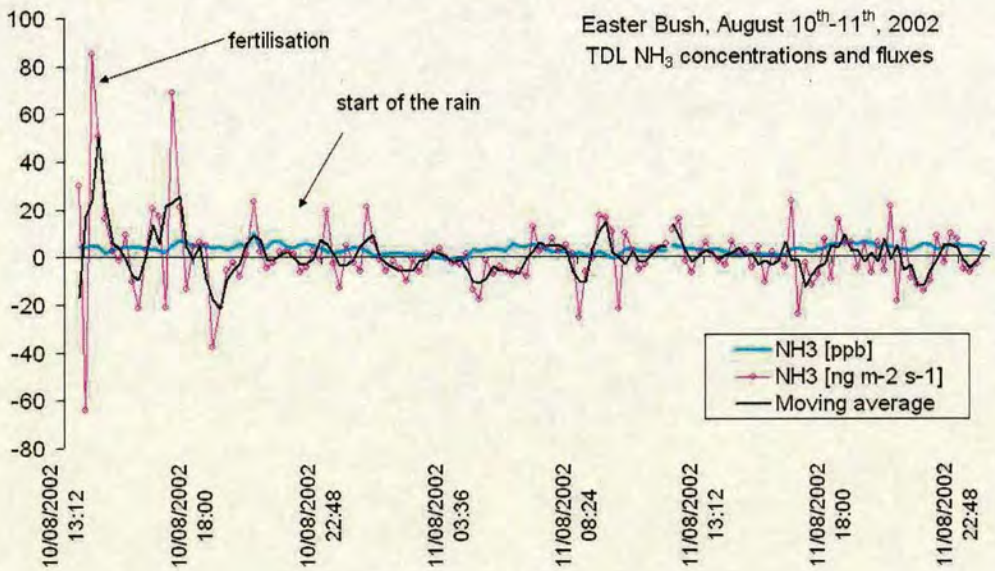

Figure 5.15: NH_3 concentration (pale blue line) and flux (pink line) values over $10^{th} - 11^{th}$ August 2002 at Easter Bush. The black trace corresponds to a moving average of the flux.

In figure 5.15 is plotted the time series for NH_3 fluxes and concentrations for a two-days period. The southern field (see fig.5.9) was fertilised on the 10^{th}, and an emission flux is noticeable and it can be attributed to the volatilisation of the fertiliser being spread. During the evening hours of the 10^{th} it started to rain, and it continued intermittently in the following days, with a rainfall of 18.5 mm over two days. In both days the average wind speed was of 1.3 m/s, and the average concentration of ammonia was of 4.8 ppbV on the first day and 3 ppbV on the second day: the fluxes averaged 6.7 ng $m^{-2}s^{-1}$ on the 10^{th} and -0.23 ng $m^{-2}s^{-1}$ on the 11^{th}. The average air temperature dropped off 2^oC from the first to the second day, as well as net radiation (5.4 MJ m-2 day-1 to 3.45 MJ m-2 day-1) and solar total radiation (81.2 MJ m-2 day-1to 5.8 MJ m-2 day-1).

In fig.5.16 are shown the turbulent fluxes for the same period. On the 11^{th} a

problem occurred with the LICOR and the values of H_2O concentration had to be removed (window of missing values in the chart during the afternoon hours). The convective mixing was quite developed in both days, and the main difference between the two cases was in humidity and surface wetness. No significant emission fluxes were observed on the 11^{th}due to uptake of ammonia by water on the surfaces and the scavenging in the air by rain.

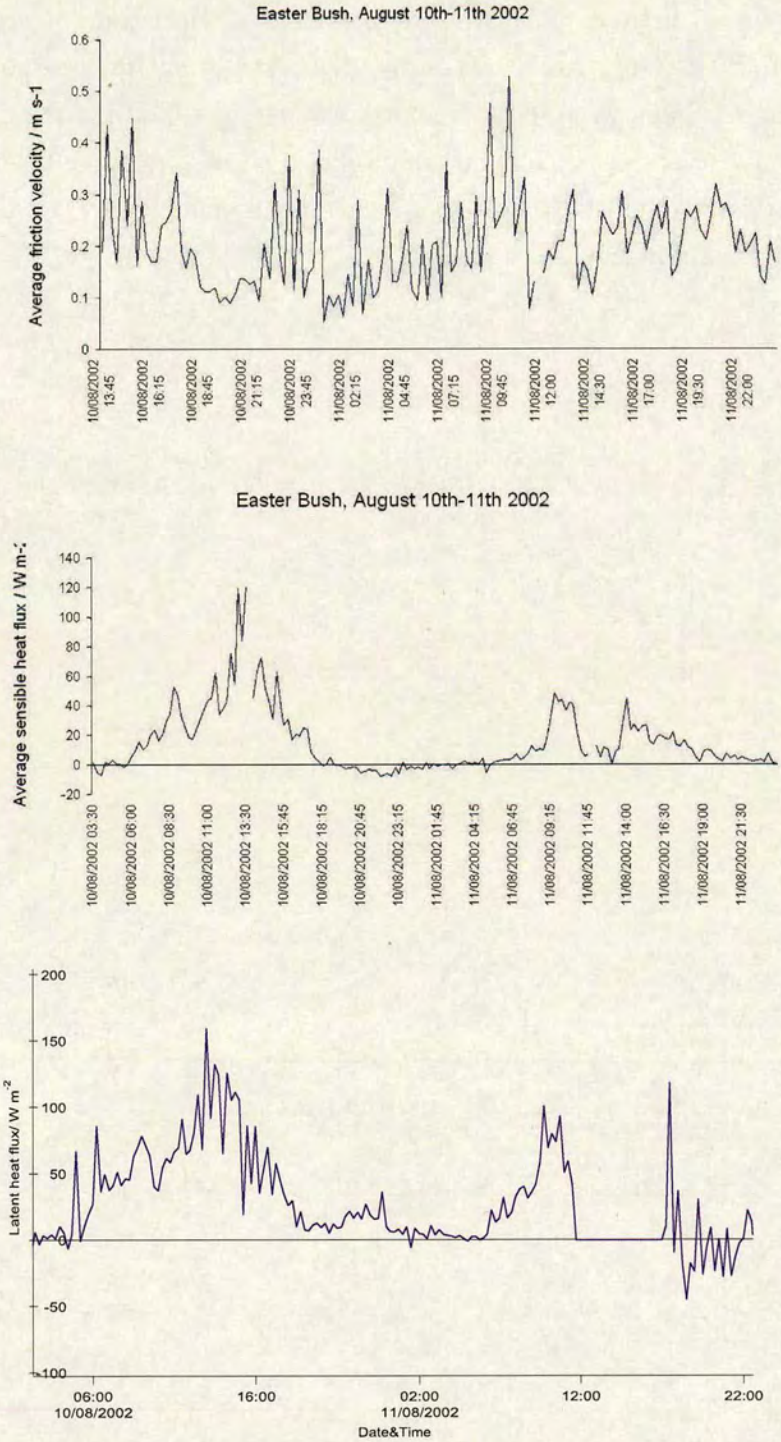

Figure 5.16: Values of friction velocities (top), fluxes of sensible heat (middle), fluxes of latent heat, measured with a LICOR 7500 coupled with the sonic anemometer (bottom) averaged over 15 min. Shown values were recorded at Easter Bush field site from 10^{th} August at 3:30, until 11^{th} of August at 21:30.

5.6.3 $24^{th} - 26^{th}$ August 2002

Values of u_* to range between 0.02 and 0.97 m s^{-1}, with an average of 0.35 m s^{-1}, which is slightly lower than the typical value for a summer day on Easter Bush, of around 0.5 m s^{-1}. Strongly positive sensible heat fluxes during the day (fig. 5.17) show that convection was well developed during the daytime. On the 25^{th} of August 2002, the sky at Easter Bush was clear, it was warm and sunny, and the convective layer was well developed. These conditions are reflected in the heat fluxes shown in fig. 5.17. Observing the charts for the 24^{th} of August, the latent heat flux shows very similar values to the 25^{th}, while the sensible heat flux, u_* and CO_2 fluxes show the same tendencies, but with smaller amplitude due to the wetter conditions of the 24^{th}, where water vapour pressure values were on average 1.6 kPa, whereas on the 25^{th} the average value was 1.3 kPa. The net radiation on the 24^{th} ranged from -12 W m^{-2} to 505 W m^{-2}, while on the 25^{th} from -6 W m^{-2} to 530 W m^{-2}; in the early afternoon of the 24^{th} a sharp decrease in net radiation flux is noted, due to cloud cover, with an average value of 130 W m^{-2}. By contrast, on the 25^{th}, the average flux was 152 W m^{-2}, with a larger value during the afternoon.

The diurnal cycle in NH_3 emission correlates positively with u_* and the heat fluxes, and negatively with the CO_2 flux, as can be clearly observed in fig. 5.17. The cause for this is the photosynthetic activity: when the stomata open, they release ammonia from the ammonium contained in the apoplast, while starting assimilating CO_2.

The set of measurements taken between the 24^{th} and the 26^{th} of August 2002 show the typical range of summer emission fluxes, when compared to previous field studies on the same field site. By contrast, during cooler, especially winter conditions, NH_3 fluxes are predominantly deposition [Milford et al., 2001].

NH_3 Concentrations: mean value of 5.9 ppbV with a standard deviation of 2.6 ppbV, with a range between 0.35 ppbV and 13.5 ppbV: these values were typical of an average behaviour on Easter Bush during the summer of 2002; the typical daily range was 0 to 20 ppbV, with an average value of 7 ppbV during the day. The concentration value is highly variable, due to the reactive nature of NH_3, and the sensitivity of sources and sinks to surface temperature and surface wetness, respectively [Flechard and Fowler, 1998], [Sutton et al., 2000].

NH_3 Fluxes: emission fluxes were observed on the 24^{th} up to 25.3 ng m^{-2} s^{-1}, with a mean value of 4.3 ng m^{-2} s^{-1} during daytime. On the 25^{th} the flux showed

Figure 5.17: Values of NH_3 concentration, flux, friction velocity, sensible heat flux, latent heat flux, CO_2 flux (from top to bottom). Shown values were recorded at Easter Bush field site from 24^{th} August at midnight, until 26^{th} of August at 9 in the morning.

a clear diurnal cycle, with values between - 7 ng m^{-2} s^{-1} and 44 ng m^{-2} s^{-1} and an average value of 11.1 ng m^{-2} s^{-1} during the day.

The fluxes represent mainly emission during the day, but small deposition fluxes can be seen at night. This behaviour is consistent with stomatal emission from the vegetation during the day, which is controlled by solar radiation and surface temperature [Sutton and Burkhardt, 1995]. By contrast, at night time, when stomata are closed, the vegetation provides a sink for ammonia, which depends on humidity and wetness.

5.7 Summary of the eddy covariance flux measurements during 2002

Table 5.1 provides a summary of the main meteorological variables statistics, to characterise the Easter Bush field site during the measurement period.

The wind field (fig. 5.18) was for the 80% of the time in the prevailing direction of the wind flow, SW-NE, as previously assessed by long term studies on the same field, see e.g. [Milford et al., 2001]. The horizontal wind speed had a median value of about 2 m/s, which is typical for the site over the summer season; the low values of H and relatively higher λE show that in 2002 the summer season was particularly wet, as can be noticed as well from the value of rainfall, which amounted to circa 275 mm of rain over 3 months and a half, higher in comparison to the average value over the same period of the year of 208 mm.

Some basic statistics on the whole dataset for concentrations and fluxes of NH_3 are shown in Table 5.2: concentration averages take into account night hours, leading to lower values if compared to daytime conditions.

The data have been separated into 2 categories: dry and wet. A sensor placed in the Bowen ratio system, provided the wetness conditions. It records the wetness conditions as a boolean information rather than providing a quantification, so every half hour (period of operation of the Bowen ratio system) the information "dry" or "wet" will be recorded.

Geometric mean values for NH_3 concentrations show rather smaller values than the arithmetic average and the median. The geometric mean has been chosen to describe the values of NH_3 concentrations as NH_3, like all wind despersed pol-

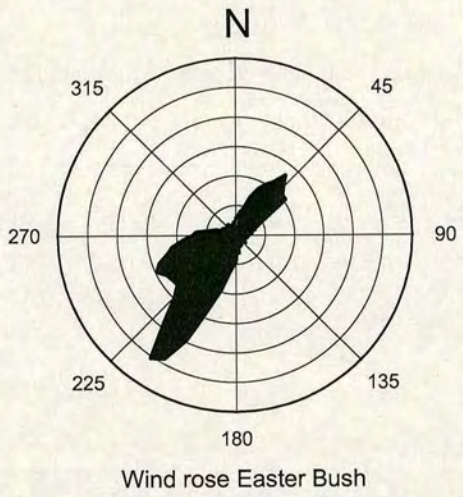

Figure 5.18: Wind field recorded at Easter Bush during the period from July to October 2002.

Variable	Units	Mean	Median	Min	Max	Std. Dev.
Rn	W/m^2	72.52	16.13	-213.50	625.70	120.10
Soil T	^oC	14.33	14.56	9.44	17.95	1.46
Rainfall	mm	0.03	0.00	0.00	41.06	0.50
G	$[W/m^2]$	-0.16	-1.61	-38.48	57.85	11.37
St	$[W/m^2]$	209.24	156.40	0.00	976.00	192.30
Air T	^oC	11.73	11.66	0.64	21.80	2.90
Wind speed	$m\ s^{-1}$	2.26	1.92	0.01	8.40	1.48
u_*	[m/s]	0.30	0.27	0.00	1.47	0.16
H	$[W/m^2]$	12.14	0.97	-92.45	290.82	38.64
CO_2 flux	$[\mu mol\ m^{-2}\ s^{-1}]$	-0.86	0.01	-49.83	49.03	8.36
λ E	$[W/m^2]$	31.35	7.90	-149.34	289.37	51.71

Table 5.1: Fundamental statistics of the main meteorological variables and turbulent fluxes of momentum, sensible heat, latent heat flux, and CO_2 calculated over 30 min. For the rainfall, the value in the first column is the total rainfall for the whole period from July to October 2002 at Easter Bush.

lutants, show log-normal frequency distribution. The analysis shows that in dry conditions the concentration values are smaller, whereas the flux values are considerably larger. This could be explained by the scavenging effect that water has on ammonia: the stomatal emission would be neutralised by the presence of water at the surface as it would take up the ammonia. The higher concentrations in wet periods could be explained by the fact that generally, close to the ground, rather stable conditions of the atmosphere associated with low pressure regimes present a development of the convective layer that is small in comparison to dry, high pressure conditions, where convective motion is promoted by buoyancy: this is confirmed by the values of u_* and H, which show lower values for wet conditions in comparison to the dry ones. Values of wind speed as well were lower in wet conditions and the same can be said about temperatures. The lack of mixing could just cause an accumulation of gas in the surface layer. The maxima of the flux were following the fertilisation event.

The net flux shows that emission from grassland was greater (55% of the events), but the particularly wet season caused deposition events to be more frequent than usual, as can be seen from fig.5.19. The values ranged from -139.55 ng m^{-2} s^{-1} to 197.68 ng m^{-2} s^{-1}: dividing this range in two sub intervals, the contribution of each event can be identified as emission or deposition. When dividing the dataset for dry and wet conditions, a slight shift towards emission happens in dry periods, as can be seen from fig. 5.19. The frequency curve for dry conditions presents a clearer division between emission and deposition episodes, and an increased percentage of emission fluxes, 58% versus the 53% found in wet conditions.

Fig. 5.20 shows dependencies of NH_3 flux and concentration values on the wind sector. In the left chart the values of median concentration of ammonia show higher values in direction of the south field (where silage production took place, i.e. fertilisation and grass cutting), although the difference between north and south field is rather limited, on average up to 2 ppbV. Looking at the fluxes values on the right chart, two very high values can be seen coming from the north field, dedicated to cattle and sheep grazing, with no fertilising activity, which would suggest lower emission ability. By looking at the wind frequency chart (see 5.18) though, it is evident that the majority of the contribution to the total flux came from the south field, whereas in the north field were recorded fewer episodes (28% of the coverage), therefore its characterisation results are less accurate than the

Variable	Units	Geomean	Mean	Median	Min	Max	Std dev
NH_3 flux	ng $m^{-2}s^{-1}$	***	1.24	1.50	-139.55	106.99	13.77
NH_3 conc	ppbV	2.62	4.79	5.31	0.00	24.73	3.78
Dry							
NH_3 flux	ng $m^{-2}s^{-1}$	***	2.90	2.59	-85.26	197.68	17.28
NH_3 conc	ppbV	2.84	5.38	5.16	0.06	19.15	2.67
T	^oC	***	13.34	13.44	4.64	21.80	2.81
U	m/s	***	2.74	2.51	0.02	8.40	1.61
u_*	m/s	***	0.34	0.33	0.02	1.47	0.16
H	W m^{-2}	***	31.31	18.36	-68.17	290.82	49.83
Wet							
NH_3 flux	ng $m^{-2}s^{-1}$	***	0.94	0.86	-121.91	106.99	12.95
NH_3 conc	ppbV	4.05	6.15	5.10	0.05	24.73	3.95
T	^oC	***	10.63	10.66	0.64	18.18	2.49
U	m/s	***	1.97	1.66	0.03	7.02	1.34
u_*	m/s	***	0.26	0.23	0.01	0.92	0.14
H	W m^{-2}	***	2.58	-0.18	-92.45	163.73	24.70

Table 5.2: NH_3 fluxes and concentrations statistics for the season between July and October 2002 at Easter Bush.

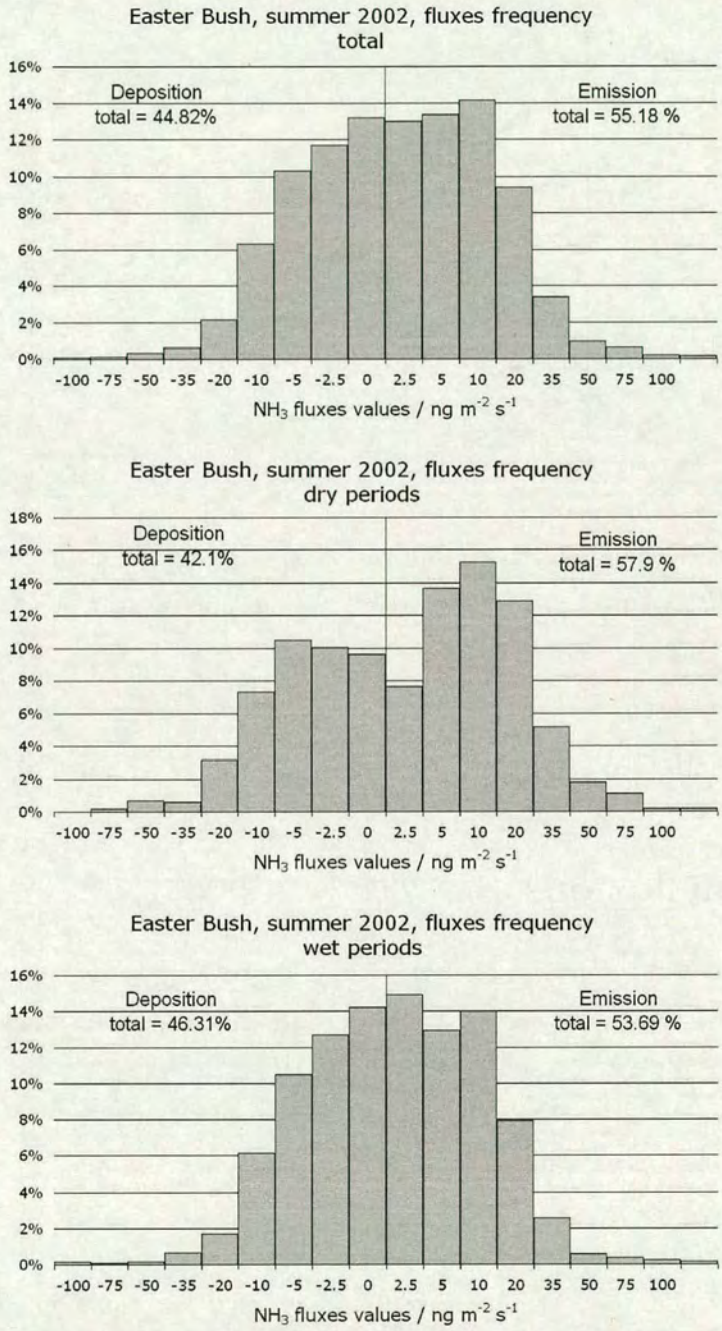

Figure 5.19: a)NH_3 flux values measured during the summer season in 2002 at Easter Bush are divided in two sub intervals and the percentage contribution is shown for each category. b) Percentage contribution to NH_3 fluxes during dry periods. c) Percentage contribution to NH_3 fluxes during wet periods.

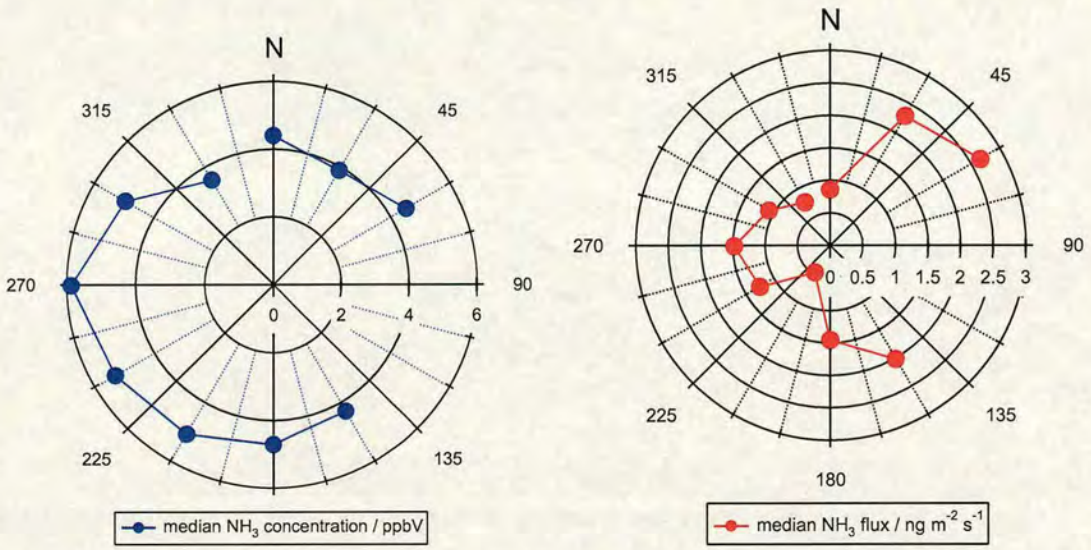

Figure 5.20: Values of :a) NH_3 concentration, b) NH_3 fluxes and recorded for each wind sector at an interval of 30^o, during the summer season in 2002 at Easter Bush.

one for the south field (72%).

5.8 Conclusions

Field measurements of NH_3 fluxes using an eddy covariance technique were made for a total of 60 days between July to October 2002 at an intensively managed grassland in Southern Scotland. The collected data demonstrate the suitability of a Tuneable Diode Laser Absorption Spectroscopy (TDLAS) system coupled with a sonic anemometer for eddy covariance measurements.

Eddy covariance usign TDLAS provides 15 min mean fluxes in ambient concentrations of NH_3 averaging to 5ppbV; the average flux recorded on the field was 1.24 ng m-2 s-1, meaning that the Easter Bush field site contributed as a source to the total NH_3 exchange between vegetation and atmosphere over the measuring priod.

The results show agreement with the previous long-term meaurements of ammonia conducted on the same field site with continuous annular denuders using the aerodynamic flux gradient method. The dataset provides a seasonal description of ammonia fluxes over grassland and it proved its suitability for any field experiment

on terrestrial ecosystems.

Particular problems for eddy flux measurements of NH_3 are due to the solubility and reactivity of NH_3: special care was required in setting up the inlet system in order to minimise the response time of the TDL spectrometer.

Chapter 6

The role of long term measurements of reactive trace gas fluxes in defining the UK deposition climate

6.1 Introduction

The measurements of long-term fluxes of pollutants has a great potentiality in the validation of deposition models, both on the regional and on the local scale. To date, very little comparison between measured data sets and model outputs has been done. Particularly, the deposition models would greatly benefit from the measurements for validation purposes.

The existing monitoring networks provide a very useful tool for concentration maps validation and wet deposition information; but very little information can be found in terms of dry deposition. The high costs for instrumentation maintenance and data analysis involved with the deposition measurements prevented a widespread application of long term measurements of deposition fluxes of pollutants.

The introduction of the TAG system (for a detailed description, see chapter 3) provides the potential for deposition monitoring networks, because of its low cost, compared to the micrometeorological instrumentation currently used by the scientific community. The instrument provides long term data series on deposition (or emission) fluxes, deposition velocities, resistances, concentrations, wind speed and direction and temperatures. The data provided by this instrument can be used in the development of process-based models as well as in the validation of long-range transport models.

6.2 Estimating deposition on the UK scale

The first studies of air pollutant deposition in the UK date back to the 19^{th} century, with the work at Rothamsted [Lawes et al., 1883], providing annual deposition estimates based on wet deposition measurements. The role of dry deposition became evident later, when in a study about the mass balance of SO_2 over the UK, Meetham estimated a deposition of more than half the total SO_2 emissions through processes other than rainfall [Meetham, 1950]. In the 1970's the first field measurement campaigns allowed the direct quantification of dry deposition of SO_2 to crops, e.g. [Garland et al., 1973, Fowler and Unsworth, 1979]. These studies showed the importance of dry deposition processes and led to an improved understanding of the underlying atmospheric dynamics; dry deposition processes could account for the removal from the atmosphere of half the sulphur emitted.

The acid deposition problem is a regional rather than a local issue, as pollu-

tants travel long distances from their sources. Sulphur and oxidised nitrogen have atmospheric residence times of 2-3 days and typical transport distances about 1500-3000 km [Brimblecombe, 1996].
The nitrogen-based air pollutants acquired importance in the wider picture of air pollutants in Europe at a later stage than sulphur compounds (see Chapter 1); processes involving N-compounds transported over long distances can be modelled in a similar way to SO_2.

The first modelling step in this direction quantified dry deposition of air pollutants using a fixed value of deposition velocity to the landscape, [Fisher, 1978], later field studies showed that deposition rates varied according to the season, to the daily conditions and to the vegetation type.

A model approach commonly used at present for dry deposition processes is the "big leaf" approach: the vegetation structure is described by means of a single leaf that represents the whole canopy and that covers the whole area considered in the model, see [Monteith and Unsworth, 1990, Hicks et al., 1987]. In order to take into account the differences between vegetative cover, the physiological processes are parameterised for each vegetative category, and then inserted in the model. Currently there are a variety of "big leaf" models being used for different environments, adjusted specifically to the conditions that characterise the area described by the model. Different countries in Europe present different land-cover, meteorology and chemical climate: all these factors interact in different ways making it difficult to find a universal modelling tool that is able to estimate the deposition dynamics over wide continental scale in Europe.

The "big leaf" model used in this study (see § 6.3) is a process-based model of deposition for several atmospheric compounds, including SO_2 and NH_3, that has been thoroughly described in [Smith et al., 2000]. It uses a resistance analogy and focuses on the description of the deposition dynamics that take place in UK conditions, providing a quantification of the annual UK input for different species at a resolution of 5 km $\times$ 5 km. The application of the model is constrained by measurement data such as gas concentration, wind speed, land use, temperature, rainfall and vapour pressure, that are available at the national scale; the approach is therefore measurement-based.

Another model used currently to assess deposition maps over the UK is the FRAME model, Fine Resolution Atmospheric Multi-pollutant Exchange, a long-term statistical trajectory model used over the UK with a resolution of 5 km x

5 km. It was developed from the TERN model [ApSimon et al., 1994]. It is a Lagrangian model which describes the main atmospheric processes (emission, deposition, diffusion and chemistry) in a column of air extending from the ground to a maximum altitude of 2500 m, [Singles et al., 1998], that moves along straight-line trajectories according to the wind direction and speeds specified.

The advantages of Lagrangian approaches are the relative simplicity and the low computational costs [Fournier et al., 2004]; FRAME has been created to be used as a statistical atmospheric transport model. Its main purpose is to describe an average long-term behaviour of atmospheric pollutants, specially NH_3, at a national scale, and to describe the spatial distribution of annually averaged surface concentrations and annual deposition fluxes.

6.3 The UK "big leaf" model

The model uses a resistance analogy to the electrical current flow through a network of resistances to simulate the flow of air pollutants through the resistances of the surface layer, such as aerodynamic resistance , canopy resistance, that can be divided into stomatal component and non-stomatal component (uptake at the surface). A diagram with the resistances is shown in Fig. 6.3.

Emission of gases such as NH_3 can occur through stomata, or during the evaporation of the thin water films on the leaf surface, as for SO_2 and NH_3 [Fowler et al., 2001], or from the soils, as for NO. These emission processes can alter the deposition estimate of the model. In order to take into account these processes, a compensation point (see Chapter1) approach is adopted to assess NH_3 stomatal emission [Smith et al., 2000].
The deposition rate D is calculated as the product of the concentration χ of the gas under consideration and the deposition velocity V:

$$D(z) = \chi(z) \cdot V(z) \tag{6.1}$$

The resistance to deposition in total is the sum in series of the stomatal and non stomatal canopy resistances (r_c), boundary layer resistance (r_b) and aerodynamic resistance (r_a), as shown in Fig. 6.3. The deposition velocity is the inverse to the total resistance, and therefore:

$$D(z) = \frac{\chi(z)}{r_a(z) + r_b + r_c} \tag{6.2}$$

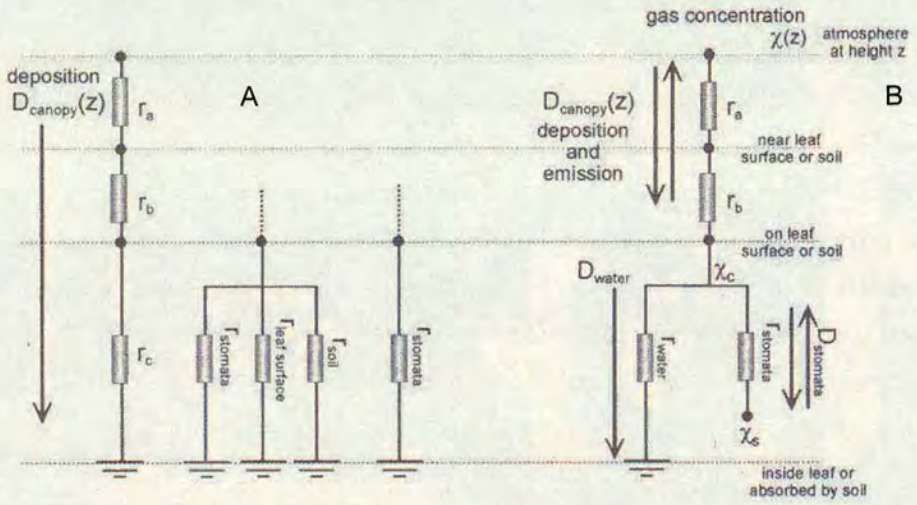

Figure 6.1: Resistance components used in the deposition processes description, from [Smith et al., 2000]. Illustrating a)the deposition and in b) the bi-directional approaches.

When considering vegetative surfaces, the canopy resistance is the sum (this time in parallel) of the stomatal resistance, the soil and the leaf surface resistances. For different gases these three factors are important in different ways, e.g. for SO_2 they are all included in the calculation of r_c, but for NO_2 the stomatal resistance is prevalent and the others can be ignored, for HNO_3 the canopy resistance is zero, as it is a very reactive gas and "sticks" very rapidly to the majority of the surfaces; for NH_3 the exchange is bi-directional, as discussed in Chapter 1, and needs a different approach.

Defining a stomatal compensation point $\chi_{stomata}$ as a threshold value of NH_3 concentration at the stomatal surface, emission occurs when the air concentration of ammonia is lower than $\chi_{stomata}$, vice versa deposition when air concentration is larger than $\chi_{stomata}$. This has been inserted in the model to assess the rate of exchange of NH_3 (denoted with D), with the introduction of a canopy compensation point (χ_{canopy}), and by using a non-stomatal resistance r_{water} for uptake by leaf and soil surfaces through water films:

$$D_{canopy} = \frac{\chi(z) - \chi_{canopy}}{r_a(z) + r_b} \tag{6.3}$$

The total deposition rate in the canopy is the sum of stomatal and non-stomatal

(water-film surfaces) contributions:

$$D_{water} = \frac{\chi_{canopy}}{r_{water}} \tag{6.4}$$

$$D_{stomata} = \frac{\chi_{canopy} - \chi_{stomata}}{r_{stomata}} \tag{6.5}$$

Sice the mass needs to be conserved, deposition to the canopy (or the ground) equateds to the total deposition wiithin the canopy, so:

$$D(z) = D_{canopy}(z) = D_{stomata} + D_{water} \tag{6.6}$$

By substituting χ_{canopy} using Eq. 6.3-6.6, it is possible to eliminate it and obtain:

$$D(z) = \frac{\chi(z)}{r_a(z) + r_b} - \frac{\chi(z)/(r_a(z) + r_b) + \chi_{stomata}/r_{stomata}}{1 + (r_a(z) + r_b) \cdot (\frac{1}{r_{water}} + \frac{1}{r_{stomata}})} \tag{6.7}$$

To calculate the canopy compensation point for ammonia or the bulk canopy resistance for the other compounds, information on solar radiation and stomata is needed to determine the stomatal activity status. An algorithm used by [Weiss and Norman, 1985] calculates the radiation that is physiologically active for the plants, both for the direct and the diffuse beam ($R_{beam}, R_{diffuse}$) at the top of the boundary layer, calculating the position of the sun with respect to the "leaf". The actual direct and diffuse radiation hitting the leaf ($S_{beam}, S_{diffuse}$) is extrapolated from R_{beam}, taking into account the cloud cover and the pressure effects.

The effective Leaf Area Index, i.e. the LAI concerning the leaves exposed to radiation, is not equal to the LAI of the whole canopy. The LAI used in the model distinguishes for contribution from the shade leaves (diffuse radiation receivers) and contribution from the sun-lit leaves, [Hicks et al., 1987]. Stomatal resistance is then calculated for sunlit and shade leaves, taking into account the different molecular diffusivities for the different gases modelled [Smith et al., 2000].

During the development of the model, the measurement data input played an important role in the quantification of the parameters. In fact, the different land covers that the model is able to describe, i.e. moorland, grassland, forest, agricultural land and urban areas, have been parameterised in the model in terms of resistances, LAI, and meteorological variables, by collating environment-specific data from the literature.

The input data for land cover and altitude were taken from the Countryside

Information System database, which include satellite information with surveys for land usage; the meteorological data are monthly mean values, including rainfall, temperature, vapour pressure from a 30-years series and interpolated according to the altitude. The cloud cover was estimated from [Weston, 1992].The pollutant concentrations were derived from: an interpolation of measurement data with an urban enhancement from urban areas monitoring [RGAR, 1997]; the NH_3 concentration map was derived from an emission inventory processed through a multi-layer atmospheric transport model, FRAME (see following paragraph), calibrated by measures from a rural monitoring network of over 60 sites.

The main output of the model provides deposition maps for the compounds including: NO_2, NO_3^-, NH_3, NH_4^+, SO_2, SO_4^{2-}, Ca, Mg, and Cl. The deposition rates are expressed in keq (kiloequivalents) ha^{-1} $year^{-1}$, in order to provide a universal unit of measure, that can be readily converted in kg ha^{-1} $year^{-1}$. These compounds can deposit to the surfaces either via dry or wet processes; combining the wet and dry deposition maps provides a total deposition map for the UK at 5 km x 5 km for the main contributors to air pollution, S and N.

The model has been run over the UK domain considering as input the data for the years 1998 to 2000. In Fig. 6.2 a map of deposition of total oxidised S (SO_2, SO_4^{2-}) is shown; the highest values for depositions are found in the area that goes through the Midlands of England to the South and East Coast, and on the west coast along the whole country, from Cornwall through Wales and the west coast of Scotland. The deposition on the coastline to the total S deposition is due to the wet deposition, whereas the Midlands-south east coast contribution is due to highly populated urban areas that are characterised by high dry deposition rates of S. In Fig. 6.3 the same total oxidised S maps are shown, but differentiating by the contribution of forest and moorland: the definition of the land class for the territory, and the representativeness of the land cover for each 5 km x 5 km square is important in defining the different distribution of deposition rates between the two land covers.

In Fig. 6.4 the map for total reduced N (NH_3, NH_4^+) deposition for the UK for the years 1998-2000 is presented. The deposition rates in this case reflect a variation on a smaller scale, due to the nature of the sources (mainly agricultural activities) and to the short travelling distances of reduced nitrogen compounds in comparison to, for example, oxidised S that leads to large deposition values near to the areas of high emission.

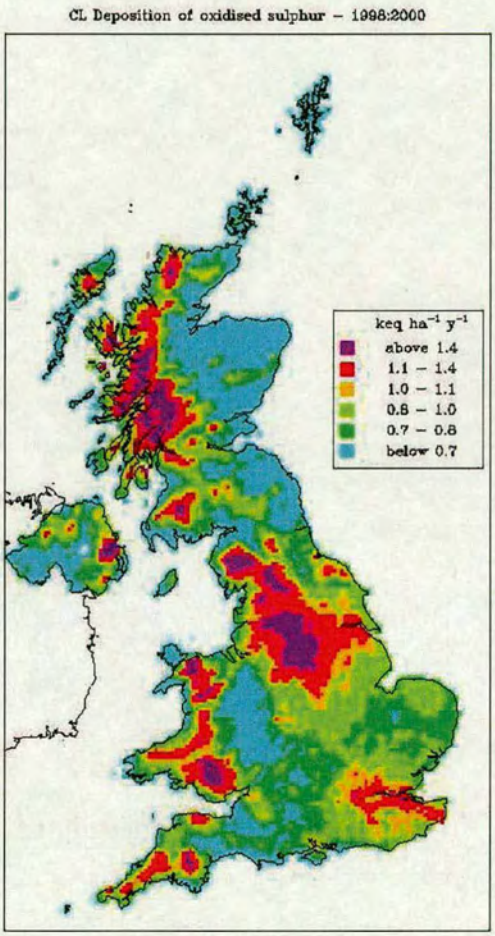

Figure 6.2: Total oxidised sulphur deposition map for years 1998-2000 over the UK (from the process-based, big-leaf model for deposition inventories of the UK).

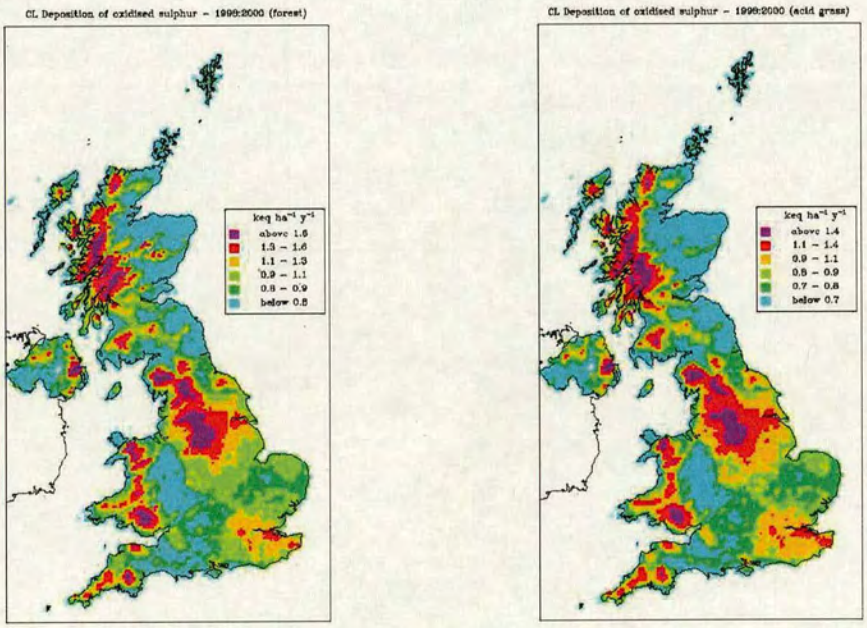

Figure 6.3: Total oxidised S maps, on the left the contribution of forest and on the right the contribution of moorland to deposition, for years 1998-2000 over the UK.

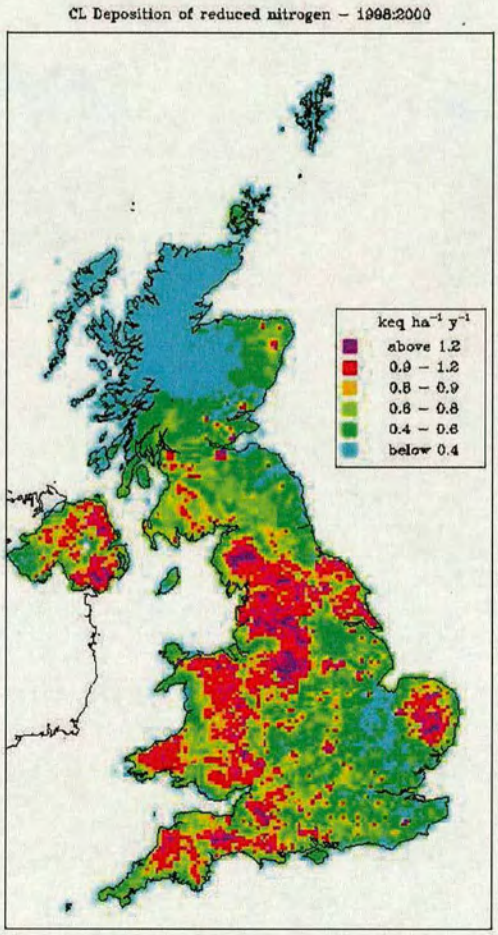

Figure 6.4: Total reduced nitrogen deposition map for years 1998-2000 over the UK.

Figure 6.5: Map of the field sites where the TAG systems were set: Auchencorth Moss, Easter Bush, Plynlimon.

6.4 Application of direct measurements of the flux using micrometeorological methods

Long-term measurements of deposition fluxes provide valuable information for model validation purposes. The introduction of the TAG system (see Chapter 3) allowed the collection of data series covering years over three different sites characterised by different land cover. The data provided by the TAG instrument are useful for both meteorological characterisation of an environment (wind speed and temperature), and chemical climate determination; the fluxes are inferred from vertical profiles by using the aerodynamic gradient method. The three locations in the UK are shown in Fig. 6.4.

The first experimental site for the TAG instrument has been a moorland site, Auchencorth Moss (AM), in the Uplands in South Scotland. The site is a blanket bog covering a flat area of approximately 1000 ha, with a regular fetch of about

1 km, characterized by weather typical of British Upland environments, being generally wet, windy and cool (for a description of the site, see Chapter 3). The species measured were SO_2 (five years series) and NH_3 (three years series).

Easter Bush (EB) is located south of Edinburgh (southern Scotland), close to the Pentland Hills. The field site is an intensively managed grassland, covered by more than 90% with Lolium perenne: it is used for sileage production and cattle and sheep grazing. The monitored species was NH_3 (for a characterisation of the field site, see Chapter 5).

The third TAG instrument installed at Plynlimon (PL) was located at SN 806853, and had been set up to sample NH_3 and SO_2. The remote location and foot and mouth problems have limited the quantity of data recorded at the site during the first year of operation, but the measurements show satisfactory performance of the micrometeorological aspects of the instrument. The data are very valuable for the provision of site-specific deposition data for Plynlimon, but they have the addition value in proving appropriate data for application to the large areas of upland vegetation throughout western Britain.

In Table 6.1 are presented the values of annual deposition output from the UK model described previously for NH_3 and SO_2 for the three sites. The model run simulated an average year between 1998 and 2000. The annual datum from the three sites is an average annual deposition value calculated from each dataset.

The experimental data provide a tool for validation of the method used by the model, and a site-specific check for the parameterisation. It emerges from this exercise that the UK model is overestimating the deposition rates, both for NH_3 and SO_2.

The NH_3 deposition flux at Easter Bush estimated by the model predicts the 5 km x 5 km square is a sink, whereas the measurements consider a field that is intensively managed (see Chapter 5) and contributes to an annual budget as a source of ammonia (the negative value in the flux means emission, as the model works in deposition rates). The annual average of the NH_3 flux measured with the TAG instrument compares well with other measurements made on the same field site by continuous measurements with micrometeorological techniques [Milford et al., 2001], which estimate the net contribution of the field as a source of NH_3. The land cover in the modelled grid square is mixed between managed and rough grassland, whereas the footprint of the TAG system is limited to an intensively managed grass field, and this could be a cause of the big discrepancy.

Site	Meas.	Mod.
NH_3	kg N $ha^{-1}y^{-1}$	kg N $ha^{-1}y^{-1}$
PL (2002)	0.63 ± 2.02	7.28
PL(2003)	1.21 ± 2.72	
AM (2002)	3.22 ± 2.7	9.1
AM (2003)	4.1 ± 3.1	
EB (2001)	-0.3 ± 5.1	14.98
EB (2002)	-0.51 ± 4.6	
SO_2	kg S $ha^{-1}y^{-1}$	kg S $ha^{-1}y^{-1}$
PL (2001)	1.32 ± 1.05	4.96
PL (2002)	1.04 ± 1.23	
AM (1999)	1.2 ± 3.9	5.92
AM (2000)	1.34 ± 2.7	
AM (2001)	1.19 ± 3.4	
AM(2002)	1.02 ± 3.3	
AM (2003)	1.38 ± 3.9	

Table 6.1: Output of the UK deposition model in comparison with measured deposition annual rates for three sites using the TAG data recorded in the listed years.

At Auchencorth Moss, the NH_3 deposition flux measured with the TAG is almost a factor of 3 smaller than the modelled flux. Comparing the NH_3 deposition rate measured by the TAG with previous measurements made on the same field site with a continuous annular denuder system [Flechard, 1988], again the TAG shows good agreement. The land cover of the square can be considered moorland for the major part of it.

In the case of Plynlimon, the TAG measured a flux of NH_3 that is a factor 10 smaller than the modelled one. From a previous study, [Reynolds et al., 1997], annual deposition fluxes were derived for N and S compounds for the Plynlimon site: the NH_3-N contribution was estimated 10.1 kg $ha^{-1}year^{-1}$, value that is certainly closer to the 7.28 kg $ha^{-1}year^{-1}$ estimated from the model than the 0.63 kg $ha^{-1}year^{-1}$ measured by the TAG system. The difference between the measurement techniques used in the study by Reynolds et al. and the TAG application has to be considered as a source of error.

For what concerns the SO_2 deposition data, the modelled deposition rate at Auchencorth Moss is bigger than the measured deposition by on average a factor 5; a comparison with previous measurements done with micrometeorological methods at the field site [Flechard, 1988] that estimated the annual average flux as 0.44 kg S $ha^{-1}y^{-1}$ shows that the TAG system is in good agreement with the previous measurements.

At the Plynlimon site, the TAG measured a deposition rate for SO_2 that is smaller than the modelled one by almost a factor 4. The value reported from the previous study by Reynolds is 4.3 kg S $ha^{-1}y^{-1}$, showing good agreement with the modelled value.

This comparison shows that further investigation is needed to assess the impact of different monitoring techniques for the concentration and deposition ; further work is required to improve the response of the model according to the measurements. The mapped values are weighted by land use in the grid square; this is a very important aspect that needs to be taken into account when comparing experimental data with model outputs. In order to aid the interpretation of the data when using the maps of deposition from the UK model, it is advisable to choose the measurements sites in squares where the land cover is reasonably uniform, to be able tocompare it with the model output, or the prediction will be biased. A larger network of deposition measurements would help greatly in the improvement of the parameterisation of this process-based model, and this is a possibility with

the application of the TAG system on a larger scale.

Comparison of the measured fluxes of NH_3 with mapped and site specific 5km x 5km grid square values

The model described above has been adapted to the small scale to simulate an annual cycle over one 5 km × 5 km square. The purpose of this exercise was to provide a simple tool, with low computing requirements that can be used as a comparison with the field data acquired with different techniques. The availability of long term series of deposition data provides the tool that is needed to validate this model.

The model has been adjusted to take as input the field-scale data provided by the TAG system and applied to the grid square containing Auchencorth Moss; again, it uses resistance analogy but in the case of ammonia it considers a zero resistance that only makes it possible to simulate deposition and not emission events.

The TAG experimental data were fed as input into the model, and monthly averaged values of deposition rate were output from this model, allowing a comparison with the TAG experimental results.

The land cover was considered uniform over the 5 km × 5 km domain, as moorland. LAI and cloud cover information were taken from the same sources used in the national model. The model was run every half-hour of the days in the year.

The input data provided by the TAG system consisted of half hourly data of: wind speed, temperature, concentration of the species of interest at one reference height (in this case 1 m), canopy height, and additional information on solar radiation and wetness were provided by a Bowen ratio system that was operating in parallel on the same field site during the TAG operation. The dataset chosen for NH_3 at Auchencorth Moss was recorded during year 2003, and for SO_2 the data were recorded in 2000. In Fig. 6.6 is shown a correlation plot between the modelled data and the TAG measurements for the NH_3 fluxes values recorded at Auchencorth Moss during year 2003.

The output values from the model for the NH_3 fluxes recorded in 2003 have a poor correlation coefficient ($r^2 = 0.37$), however there remains a degree of agreement between the two sets of data; the measured values show a greater variability than the modelled values, as it would be expected, while the model seem to be

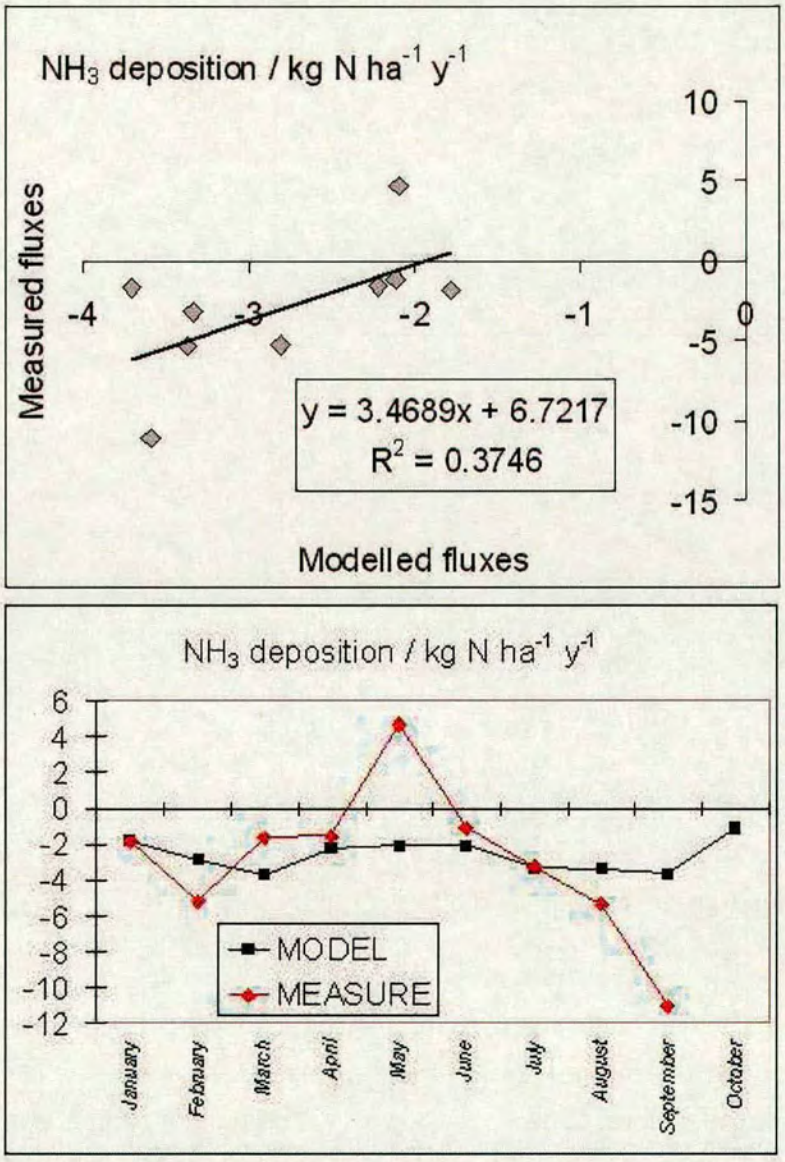

Figure 6.6: Linear regression and comparison of modelled values versus measured values of NH_3 fluxes for Auchencorth Moss 2003.

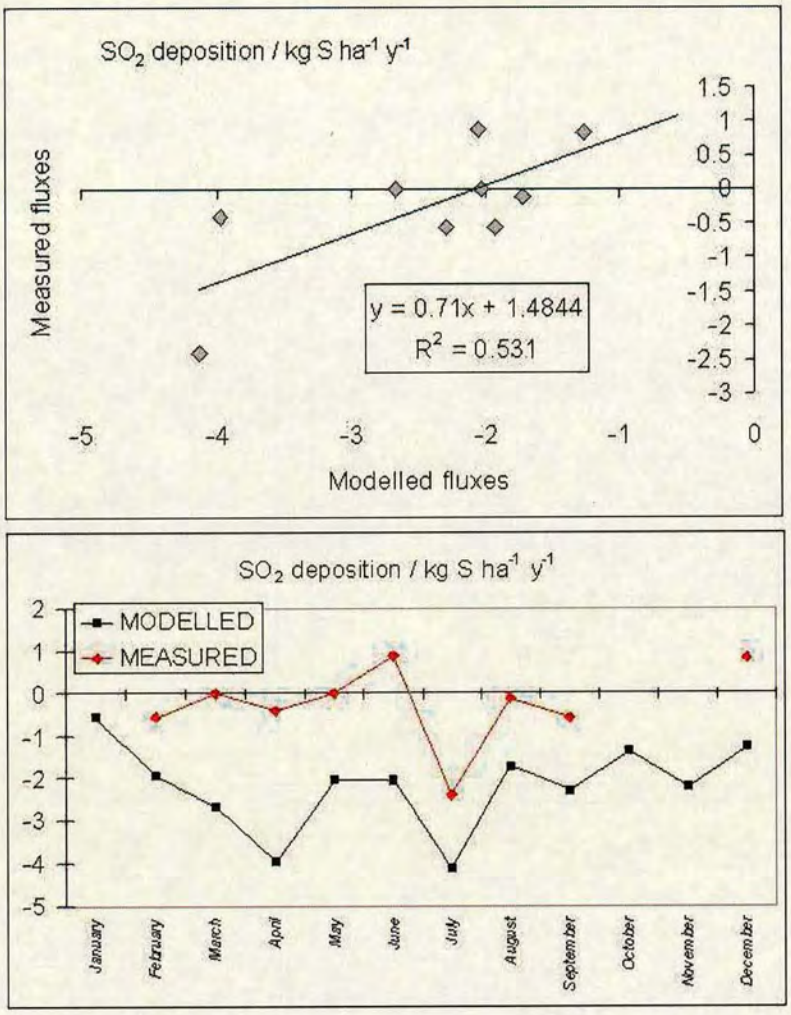

Figure 6.7: Linear regression and comparison of modelled values versus measured values of SO_2 fluxes for Auchencorth Moss 2000.

under-estimating the flux. This could be partially due to the presence of emission episodes in the measurements, that are not included in this simpler version of the model. This will need further work, in order to provide a valid tool for comparison between model and measurements.

Comparison of the measured fluxes of SO_2 with mapped and site specific 5km x 5km grid square values

The scatterplot in Fig. 6.7 shows a better correlation in comparison with the NH_3 dataset, with an r^2 value of 0.53. As in the NH_3 case, the measured values show

more scatter, but the measured values seem this time to be underestimating the deposition relative to the model. This discrepancy could be attributed to the TAG protocol (for a discussion, see Chapter 3), but it is difficult to pinpoint the causes of such discrepancy.

6.5 The FRAME model

The FRAME model is a Lagrangian model that uses a multi-layer (33 levels of variable depth, from 1 m to 100 m) scheme to describe vertical diffusion in the atmosphere, coupled with an emission database of NH_3 for the UK at a resolution of 5 km $\times$ 5 km. To account for different ecosystems effects on NH_3, FRAME relies on a land-use database applying different canopy resistances and deposition velocities according to the land cover class.

The first version of the FRAME model [Singles et al., 1998] had a range that covered Great Britain, but the domain of the model has recently been extended to Ireland, as described in [Fournier, 2003].

The vertical mixing inside the Lagrangian moving column is described by means of the vertical diffusivity for momentum (K_m). It is defined as a function of the height z, atmospheric stability and friction velocity (see Eq.2.10) and therefore is dependent on the time of the day. K_m is modelled to increase linearly with height, starting from the bottom layer value up to a specified height, and then it is fixed constant up to the top of the mixing layer.

$$\frac{\partial \chi}{\partial t} = \frac{\partial}{\partial z}\left(K_z \frac{\partial \chi}{\partial z}\right) \tag{6.8}$$

The pollutant emissions are introduced into the column at different heights, according to the chemical considered. NH_3 emissions enter the column at the surface level, whereas oxidised sulphur and nitrogen enter the column at a higher level (depending on the source characteristics).

Wet deposition is modelled by using "washout" coefficients: in the model the wet removal includes the scavenging from the surface, considering the material scavenged by precipitation, with no differentiation between in-cloud processes and the low-cloud processes. The atmospheric pollutants are removed from the column according to concentrations and rainfall rate. As the emissions are considered to have a constant rate in the input, also the rainfall is treated as in conditions of constant precipitation rate.

The height of the mixing layer is determined following a model of [Carson, 1973] which considers the input heat flux in the column for day time, and during the night time by using stability classes from Pasquill.

Dry deposition is described by an average value of deposition velocity for each chemical species, and can be written in function of atmospheric resistances as

follows:

$$V_d = (r_a + r_b + r_c)^{-1} \tag{6.9}$$

For NH_3, a land-use database is used to to create a set of V_d depending on the land cover; for SO_2 and NO_2 the values of V_d are derived from the dry deposition model of [Smith et al., 2000] described earlier.
The resistances r_a and r_b are calculated following the method by [Garland, 1977], whereas the values for r_c are taken from the literature and have different values according to the type of land cover considered [Sutton et al., 1993e, Sutton et al., 1994].
The transboundary import of foreign material is modelled using a set of concentration profiles for the edge of the domain, which is used to initialise the trajectories of the moving column of air. These profiles have been created using the TERN model, [ApSimon et al., 1994], that was modified by [Singles et al., 1998] to create this boundary conditions for the UK using EMEP emissions.

As each column moves along its trajectory, chemical interactions take place according to the source distribution and land cover. The species considered in the current version of the model are: NH_3, NH_4NO_3, $(NH_4)_2SO_4$, NO, NO_2, HNO_3, PAN, NO_3^-, SO H_2SO_4 and H_2O_2 [Fournier et al., 2004]. The model has coupled chemistry for SO_2, NH_3 and NO_x: this includes the main reactions for oxidised nitrogen and sulphur and reduced nitrogen in the lower level of the atmosphere.

The emissions inputs for the UK are taken from various databases, SO_2 and NO_x are provided by the National Atmospheric Emission Inventory for the UK, by EMEP for Ireland; for NH_3, FRAME uses a database of emissions with a resolution of 5 km $\times$ 5 km [Dragosits et al., 1998]. The rainfall data are annual rainfall fields, taken from 30-year (1961-1990) averages from the Meteorological Office database.

The surface concentrations of certain pollutants, such as NH_3, can vary greatly over the short range of a few hundred metres, therefore over a square unit of 5 km x 5 km there might be a lot of variations that cannot be reproduced by the model. When comparing the model output specific for a square with measurements from a site located in the same square, this diversity has to be taken into account; an ideal measurement location would lie in a square where the land cover is uniform. However, this is not the case in most real situations and an evaluation of the impact of the different land covers and sources in the square has to be quantified in order to compare model and measurements.

6.5.1 The application of long-term measurements for comparison with the FRAME model output

The long-term measurements operated with a TAG system can also be used for comparison with the Lagrangian model for long distance transport of air pollutants. A simulation of the national NH_3 and SO_2 emissions and air concentration has been done using the FRAME model, version 5.4 [Vieno, 2005]. The model has been run considering the inputs for year 1999.

In Fig. 6.8 FRAME output maps of air concentrations of NH_3 and SO_2 for the UK are shown. It is evident from these maps the importance of the different sources, that for NH_3 appear more scattered and for SO_2 more intensive around a few source areas.

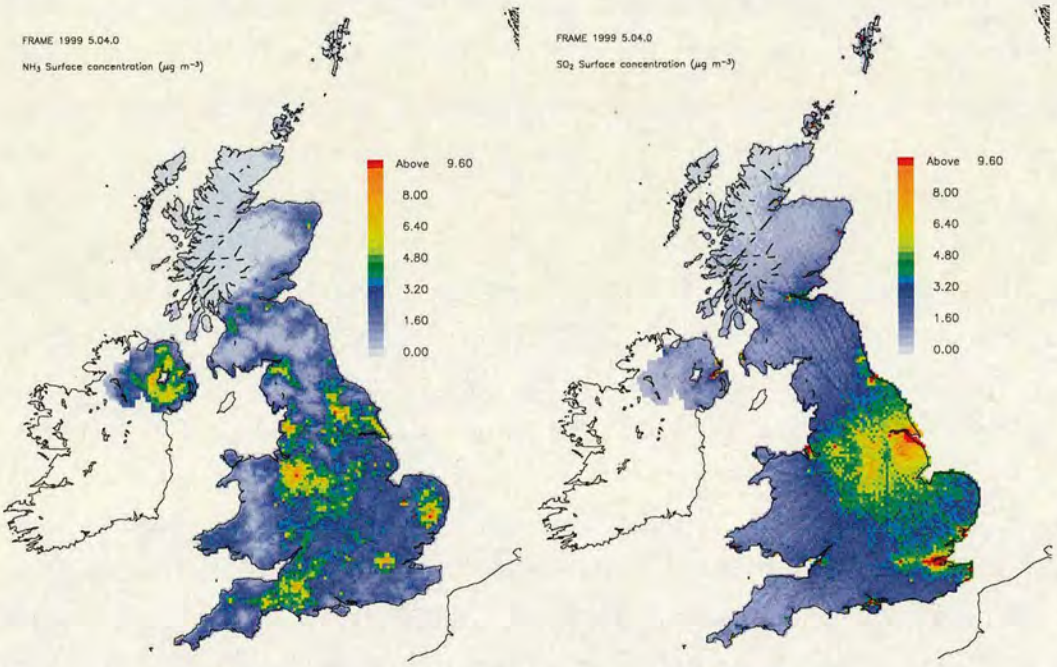

Figure 6.8: UK maps of air concentrations of NH_3 (on the left) and SO_2 (on the right) modelled by FRAME for year 1999.

A comparison between the modelled air concentrations and the emission rates for NH_3 and SO_2 and long-term measurements from the TAG system has been done over three sites. The field sites where the TAG was operated are: Auchencorth Moss, a moorland site located in Southern Scotland (see Chapter 3) (AM), Easter Bush, an intensively managed grassland south of Edinburgh (see Chapter 5) (EB)

Site	Meas.	Mod.	Meas.	Mod.
NH3	μg N m^{-3}	μg N m^{-3}	kg N ha$^{-1}y^{-1}$	kg N ha$^{-1}y^{-1}$
PL	0.4 $\pm$ 0.21	0.81	0.73 $\pm$ 1,52	1.84
AM	0.63 $\pm$ 0.29	2.01	3.01 $\pm$ 2.82	4.7
EB	1.51 $\pm$ 0.72	1.74	-0.38 $\pm$ 4.7	2.9
SO2	μg S m^{-3}	μg S m^{-3}	kg S ha$^{-1}y^{-1}$	kg S ha$^{-1}y^{-1}$
PL	0.29 $\pm$ 0.13	0.6	1.22 $\pm$ 0.98	1.6
AM	0.31 $\pm$ 0.28	0.95	1.12 $\pm$ 2.9	2.45

Table 6.2: Values of air concentration and deposition fluxes of NH_3 and SO_2 measured at three field sites in the UK compared with concentration and deposition fields modelled by FRAME (version 5.4) for the squares containing the field sites for year 2002.

and Plynlimon, an upland grazed land in Wales (PL).
In Table 6.2 is a summary of the concentration and deposition (exchange) values for an average year for the three sites: NH_3 and SO_2 were measured at Plynlimon and Auchencorth Moss, NH_3 was measured at Easter Bush.

The values of NH_3 and SO_2 concentration and fluxes are annual averages over year 2002 recorded at each of the sites. The variability of the values presented in the table is expressed by means of the standard deviations from the averages. The modelled and measured values of the fluxes are of the same order of magnitude for every case, and the modelled values fall in an interval of 1 standard deviation around the average value. Concentrations of NH_3 seem to be overestimated by the model, and the same can be said about deposition rates. In the case of Easter Bush, the square presents variability in the land use: although most of the 5 km $\times$ 5 km area is covered by rough grassland, the presence of farms and intensive management for silage production could explain the overestimate of the model in comparison to the measured values, where the fertilising practices make of the field site a net source for NH_3.

For SO_2, again the concentration seem to be overestimated by the model, but the deposition rates are closer, and the modelled values fall in an interval of 1

standard deviation around the average value.

6.5.2 The introduction of measured meteorological parameters in the FRAME model

The FRAME model uses a constant initial value of K_m that is interpolated through the different heights in the column; this value is changing according to time of the day and atmospheric stability [Fournier et al., 2004].
According to the results shown in the previous section, and moreover according to comparison between model output and the national NH_3 monitoring network carried out so far, NH3 concentrations estimated by FRAME are larger than the measured values. In order to investigate possible reasons for this over-estimate (in particular close to source areas), an exercise of sensitivity analysis on the FRAME model has been done by using the eddy diffusivity for momentum as a test parameter.
Values of eddy diffusivity for momentum were input to the model from measurements by the TAG system placed at Auchecorth Moss. Values of K_m were measured with reference at two heights, 1 m and 2 m. The values of K_m were calculated half-hourly, and then averaged for each half-hour of the day for a whole year, to give the average day behaviour in K_m values. In Fig.6.5.2 are shown half-hourly values of K_m averaged over a year, and an example of daily trend of measured values of K_m. The run of FRAME using measured K_m values interpolated starting from 1 m gave an output for the air concentration of NH_3 that underestimates the concentrations in comparison to the base model run.
A second run of FRAME used K_m values measured at two heights, starting the vertical interpolation for the rest of the column beginning at 2 m. The ratio plots between the base run and the measured-K_m runs are shown in Fig. 6.10. The second run (K_m measured at 1 m and 2 m) shows a smaller difference with the base run of FRAME in comparison to the first run (K_m measured at 1 m).
The differences between the base run of FRAME and the measured-K_m run of FRAME on the total values in the output are listed as follows: -4% for NH_3 concentration; -2.6 % for NH_3 deposition; +1.7% for SO_2 concentration; and +1.9% for SO_2 deposition. The maximum variation in the output caused by a different K_m parameterisation was for the concentration of NO, that changed by a factor of

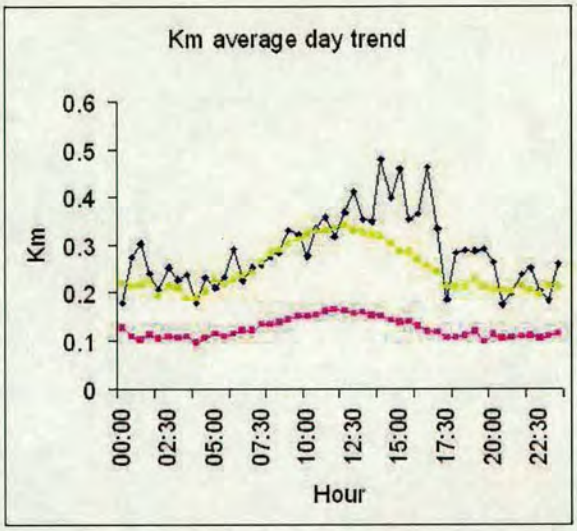

Figure 6.9: Average daily cycle of the momentum eddy diffusivity measured at Auchencorth Moss by the TAG system. The pink line refers to K_m calculated at 1m, the yellow line at 2m, and the blue line is a non-averaged daily trend example taken on a 19 October 1999.

-18%.

In Fig. 6.11 the scatterplots between the modelled and measured (from the national network for NH_3 emissions) values of NH_3 concentration for the year 1999 over the UK show that the introduction of measured K_m did not modify the correlation coefficient, but changed very slightly the regression coefficient, from 1.18 to 1.13, indicating that an approach towards the measured values is given by the use of measured K_m values input.

Such a difference in output is not sufficient to explain the discrepancies between the model estimates of deposition and concentration for ammonia with the field measurements. The parameterisation of K_m does not therefore seem to be the cause of the discrepancy, which requires other sources of error to be explained. However, a 4% difference in air concentration of NH_3 could be relevant in terms of local policies regarding critical levels in areas where the concentration of NH_3 is close to the fixed threshold, and this exercise shows how crucial the sensitivity analysis on model parameters is. Long term measurements of meteorological parameters, concentration and deposition (exchange) are a very valuable tool to provide the means for comparison and validation of such models, as well as better input parameters for the development stage of the models.

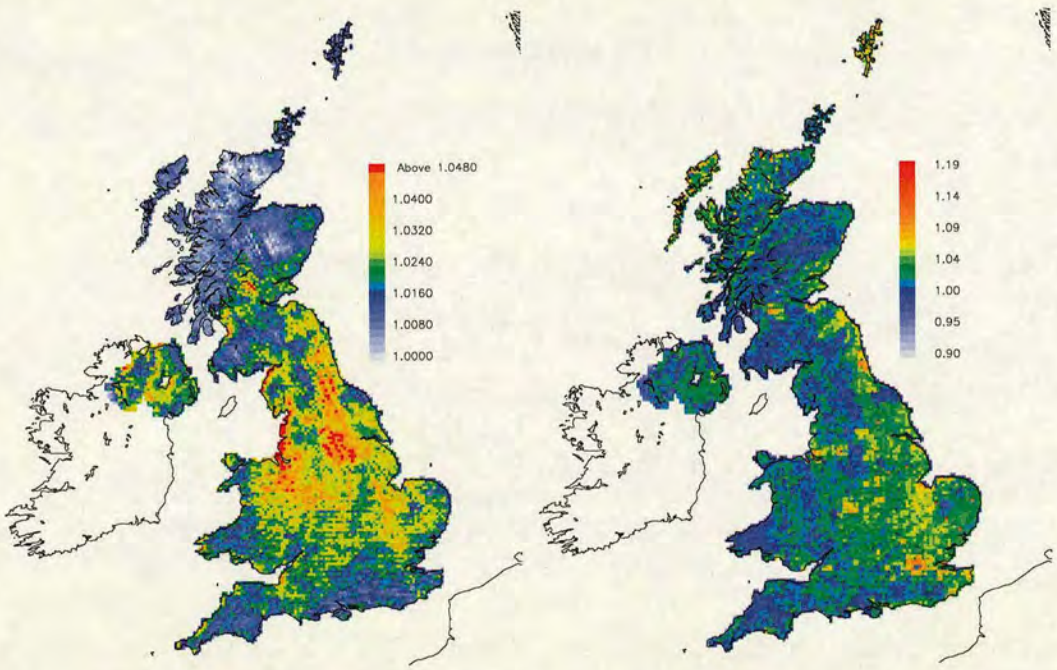

Figure 6.10: Ratio plots between NH_3 surface concentrations modelled with FRAME-constant-K and FRAME-measured-K. On the left, value of K_m measured at 1 m, on the right, value of K_m measured at 2 heights, 1 m and 2 m.

6.6 The potential application of TAG or other micrometeorological measurement approaches to validate mapped deposition values

The application of a modified version of the UK deposition model presented in § 6.4 is a possible use of the data collected with the TAG instrument. The possibility of validating a process-based model with site-specific inputs is very important in terms of improvements in the understanding of the deposition dynamics to be implemented in the long-range transport models for atmospheric pollutants.

The TAG system has considerable potential to provide long-term datasets of deposition of various trace gases. The same principle can be applied to a wide variety of gases, as well as aerosols. In fact, a field campaign using a modified version of the TAG system (more similar to the Easter Bush model presented in Chapter 3) is ongoing at Auchencorth Moss. This new version of the instrument has a more extended height in order to increase the footprint area, and measures

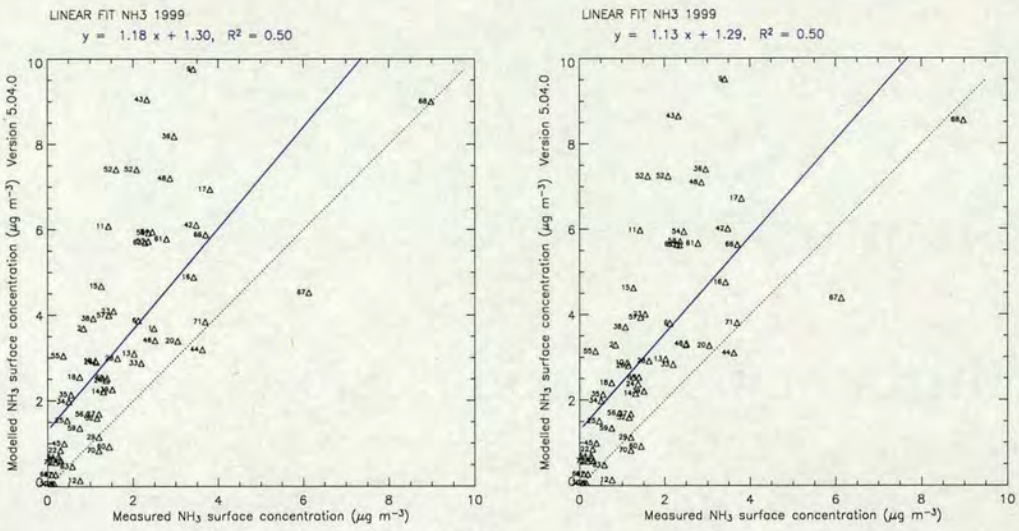

Figure 6.11: Scatter plots between measured (x axes) and modelled (y axes) values of NH_3 concentrations at the surface. On the left hand side, the output of FRAME considers constant K_m, on the right the measured values of K_m are input.

a variety of chemical species: NH_3, SO_2, HNO_3 for the gaseous phase, and NH_4^+, NO_3^-, NO_2^-, SO_4^{2-} for the aerosols, plus cations as Cl^-, Ca^{2+}, Mg^{2+}, Na^+.

With such an input of experimental data, it would be possible to test new versions of process-based models, greatly extending the exercise in this work. The application of the new TAG measurements would help to understand the interactions between the chemicals measured; this information input in the model would improve the parameterisation of models used for long-range transport when considering total S or N contribution and not the only contribution of one species.

The implementation of a site-specific model to reproduce on the small scale the regional scale version of the UK model would provide a simple validation tool, applicable to a wide range of environments and for a wide range of air pollutants. The input inserted in this model could include more measured variables.

Chapter 7

Summary and conclusions

This thesis project focussed on the measurement of NH3 and SO_2 fluxes between different kinds of vegetation and the atmosphere, using two very different micrometeorological techniques.

7.1 Long-term surface-atmosphere NH_3 and SO_2 flux measurements

For most site specific studies there are no direct measurements of dry deposition, mainly because the techniques developed for measurement are suitable only for micro-meteorologically ideal sites, with extensive, uniform fetch. Even at such locations the methods applied are generally suitable only for campaign measurements over a few hours or days, because of the costs of instruments capable of continuous monitoring of atmospheric concentrations and the excessive work required for their maintenance. The overall concept of a low cost instrument able to provide long term measurements of deposition follows from the consideration that in principle, a long-term averaged vertical gradient of concentrations measured with simple methods would substitute for the expensive continuous monitoring techniques

The first part of the work involved the development of a low-cost system able to provide long-term fluxes of NH_3 and SO_2 at remote sites, starting from a prototype implemented during the EU LIFE project.

By sampling continuously over an extended period, the large vertical gradients generated by high stability would lead to an over-estimate of the actual flux. It is therefore necessary to develop techniques which avoid the bias due to these processes. To overcome this problem, the time averaged gradient system (TAG) works in a conditional sampling mode, by selecting only the periods during which the neutral flux-gradient theory applies for the gas sampling, while continuously sampling the micrometeorological conditions at the site.

The first model of the TAG had a vertical profile of 3 denuder tubes at 3 different heights to measure the air concentrations of SO_2, a wind speed and a temperature sensor, a wind vane. The sampling conditions of this system were determined by the wind sector and wind speed (exclusion of flow-disturbed area of the fetch, low wind speeds), and by using the gradient Richardson number as

an indicator of atmospheric stability, choosing a "window of neutrality" (included between -0.02 and +0.02) for sampling. The first version of the instrument relied on the presence of a sonic anemometer for the assessment of the stability parameters. This system was setup at the Auchencorth Moss field site, and it was later modified to a second version, with the addition of NH_3 denuder placed in series with the SO_2 denuders, more wind and temperature sensors to provide vertical profiles of wind speed and temperature to allow independent on-line calculation of the stability parameters that determined the sampling conditions.

This system recorded deposition data from 1999 until 2003 fortnightly at Auchencorth Moss, an extended area of moorland in Southern Scotland. The data coverage for the whole data series was of 95%, and the conditional sampling of the chemistry data led to a time coverage of 60%, excluding stable and highly unstable conditions. A characterisation of the site in terms of wind field, temperatures, and chemical climate is provided by the TAG, giving information about the seasonal features of the exchange processes for the extensive area of surrounding environment.

The data reveal the windy exposed nature of the site, with some daily average wind speeds in excess of 10 m s^{-1}. The friction velocities are correspondingly large. In the absence of gradient data these measurements provide sufficient information to model the dry deposition of NH_3 and SO_2 to the catchment using concentrations provided by the national monitoring data.

The same version of this instrument was reproduced and placed at Plynlimon, an upland environment in Wales, where it sampled SO_2 and NH_3 from 2000 to 2003, in order to characterise inputs to this grazed acid grass environment at higher altitudes. The data coverage for this site was 85%, the data losses due to the occurrence of the "foot and mouth" disease spread, that prevented access to the site for a few months. The SO_2 concentrations at the site are small, in the range 0.1 to 1 μg m^{-3} and yet the measured fluxes are clear in the data with values averaging 10 ng $SO_2 \mu$g $m^{-2}s^{-1}$. These deposition fluxes are consistent with large deposition velocities, in the range 20 to 35 mm s^{-1} and consequently very small surface or canopy resistances, in the range 2 to 20 s m^{-1}. The results from this field site are not discussed in detail in this thesis, however the annual averaged results were used to compare with the output of UK scale models.

A third version of the instrument was implemented with more temperature, wind speed sensors and denuders in order to improve the quality of the vertical

profiles and reduce the rejection of the data for poor gradients. This TAG system was placed for testing at Easter Bush field site, an intensively managed grassland, and it operated from 2001 to 2003, measuring NH_3 exchange fluxes. The results from the field show that the data coverage improves and the data rejection, particularly for the chemical gradients data, which is reduced from 39%, in the Auchencorth Moss dataset, to 21%.

In order to assess the validity of the fluxes obtained from the TAG system, omitting the stable and the highly unstable conditions from the measurements, a simulation of the TAG sampling system has been achieved using the data collected at Auchencorth Moss with a continuous analyser for SO_2 coupled with a sonic anemometer. The results of the simulation show that the TAG instrument is in good agreement with the continuous gradient system, as the correlation coefficient shows that for the 75% of the cases the 2 protocols (TAG and continuous flux gradient) agree in the estimate of the turbulent fluxes of sensible heat, momentum, and chemical species. The correlation coefficients for both sets of data regarding u_* and H show a very good agreement (above 87% in both cases) between TAG protocol and continuous system suggesting the removal of stable conditions from the sampling period does not greatly modify the evaluation of the turbulent fluxes, although it introduces a bias. The SO_2 fluxes calculated omitting stable conditions under-estimate the fluxes of SO_2 measured by the continuous system by providing fluxes that are the 78% of the values estimated with the continuous system. The correlation coefficient shows that for the 75% of the cases the 2 protocols (TAG and continuous flux gradient) agree. The SO_2 concentration values averaged over times omitting stable conditions give smaller (77%) values in comparison to the continuous monitoring, and this is because of the removal of non-mixed air in the surface layer typical of stable atmospheric conditions. The comparison between the two analytical methods (UVF for continuous monitoring and ion chromatography for the TAG denuders) showed that the denuders were measuring smaller concentrations for SO_2, 87% circa of the values mesured by the continuous UVF analyser. This issue requires further investigation, as the quality of the chemistry data have shown to be the main concern regarding the operation of the TAG system. The percentage of rejected chemistry data was 40% during year 2000 at Auchencorth Moss: this could be due to the fact that the concentrations of background SO_2 are very close to the detection limit of the denuder technique.

To tackle the issue of background sites, where concentrations are very low and

close to detection limits of the techniques used to detect them, a new setup of the TAG instruments has increased vertical distance between the sensors, by increasing the height of the whole system. Larger space gaps between sensors allow larger differences of chemical concentrations, due to the atmospheric stratification. In this way, the rejection of gradients is reduced, by providing more defined vertical profiles.

7.2 Eddy covariance Measurements of NH_3 fluxes using TDLAS

This part of the work focussed on the implementation of an eddy-covariance measurement system using Tunable Diode Laser Absorption Spectroscopy. The eddy covariance technique applied to NH_3 flux measurement is a novelty, as NH_3 sensors were unable to acquire data at the high frequencies required by the eddy covariance method.

In the first stage, laboratory tests were conducted to assess the setup of the system for the measurement of atmospheric ammonia concentrations. These involved: characterisation of the laser diode and optimisation of the measuring conditions of the system for operation on the field, tests on response time of the system and tests of NH_3-free air production devices. The system used a 2.5 m long polyethylene sampling tube in extension to the TDL glass inlet attached to the sampling cell, and tests on the time response of this extension tube showed that the system had a time response of 0.9 s in the lab, but this figure changed in the field, where on average the time response was estimated to be 1.25 s, probably due to humidity and wall effects.

Measurements of surface-atmosphere exchange of ammonia were made for a period of over 3 months (July 2002 to mid-October 2002) over an intensively managed grassland in southern Scotland (Easter Bush) at a 15-minute time resolution. The TDL system was operated in conjunction with an ultra-sonic anemometer that provided the fast response wind speed and temperature needed to calculate the eddy-flux of NH_3.

The data collected in the field were analysed for their spectral characteristics: the percentage of ammonia flux carried by eddies smaller than 2 m (corresponding

to frequencies >1 Hz with a wind speed of 2 m/s, as it was on average at Easter Bush during the measuring period) was on average 8.4%, and this value has been calculated from daily cospectra during the measuring season. This percentage suggests that the contribution of small scale turbulence is important in the estimate of NH_3 fluxes, and that fast response sensors such as the TDL can provide very useful information on the exchange dynamics between surface and atmosphere.

A characterisation of the Easter Bush field site showed that the cumulative normalised contribution to the flux measurement was more than 70% in the 87% of the time covered by the measurements. During the measurement period, a part of the field was treated with fertiliser, and the other part of the field had cattle and sheep grazing. Both treatments affect the NH_3 exchange budget over the grassland area in consideration. The season was particularly wet and this affected the NH_3 exchange budget, decreasing the impact of emission caused by fertilisation and grazing. The Easter Bush field contributed as a source of NH_3 during the period July-October 2002, with an average net flux of 1.24 ng m^{-2} s^{-1}.

7.3 Comparison of long-term measurements with deposition models

Data collected by the TAG system over three different sites over the UK were used in a comparison with the output of a regional scale "big leaf" model, applied to the UK. The model uses land cover information at the national scale and provides concentration and deposition maps for a variety of pollutants. The comparison was made for NH_3 and SO_2 (data available from the long-term measurements).

The data collected with the TAG system at the three sites mentioned above are very valuable for the provision of site-specific deposition data for each site, but they have the additional value in proving appropriate data for application to the large areas of moorland (Auchencorth Moss), managed grassland (Easter Bush) and upland vegetation (Plynlimon) throughout the UK.

The comparison with the "big leaf" model showed an overestimate of the modelled data in comparison to the measurements: the causes of this discrepancy require further investigation, and this result shows that long term deposition information is crucial for the development of process based models, particularly for

improving the knowledge on the role of different land covers.

The comparison of the measurements with the long-range transport model FRAME showed that the data compare reasonably well, although substantial differences (up to a factor 3) between the model and the measurement were observed: for both concentrations and deposition rates, the model seems to be overestimating. This difference is mainly due to differences between land cover inside a square area where the model simulates the exchange processes and the footprint of the TAG system. It is necessary to consider that the measurements are representative of one point inside the grid square, and therefore unable to describe in an exhaustive way the processes over the whole grid square area, unless it is a perfectly uniform land cover.

A sensitivity test on FRAME has been made using measured values of K_m as an input, and the output showed little difference with the standard FRAME version: such a difference in output is not able to explain the discrepancies between the model estimates of deposition for ammonia with the field measurements, therefore the parameterisation of K_m does not seem to be the cause of the discrepancy.

A modified version of the "big leaf" model has been implemented in order to provide a small-scale comparison tool with the measurement data on the site specific grid square. A year of TAG measurements taken at Auchencorth Moss were fed as input data to the model, and the output was compared to the annual averaged values of the deposition fluxes measured on the field with the TAG system.

The monthly values extrapolated from the measurements show the same order ofmagnitude as the modelled monthly values, but the model is unable to describe the variabilty due to the seasonality of the square in exam. This is expected, as the model purpose is to provide annual deposition rates for the different compounds; when the annual averaged values are compared the agreement is satisfactory in both cases of SO_2 and NH_3. The results show better agreement for the SO_2 case than for the NH_3 case, however further comparison is needed to investigate the causes of the differences between measured and modelled values. There is evidence from other continuous measurements that the current model overestimates deposition of SO_2.

7.4 Recommendations for future work

Long term measurements of deposition fluxes of pollutants

- Further investigation of the comparison between the different methods used for the chemical analysis of SO_2 concentration in field conditions is required to optimise the data capture, which can prove difficult at background levels.
- More long-term measurements of NH_3 exchange fluxes are required, particularly over other key ecosystem types in Europe, to develop the understanding of the controls on trace gas exchange for model development and validation.

Eddy covariance measurements of NH_3 fluxes

- Further investigation of inlet materials for optimising the time response of the system in the field, and implementation of an ammonia-free air source to be used in the field.
- Measurements of ammonia run simultaneously with nitric acid to improve the understanding of the chemical balance between the two pollutants, a critical factor in the N exchange processes.
- Application of eddy covariance to measurements of ammonia exchange over different possible sources.

Validation of deposition models with experimental data

- In order to make an effective usage of the comparison between experimental and modelled data, it is necessary to further analyse the uncertainty of this process, by taking into account the coupling of uncertainties, of both the measurements and the models.
- Currently there is little independent validation for regional scale models, the main obstacle being the cost of the collection of deposition data in the fields. The TAG instrument can be a powerful tool of validation for such models and shows potential for application to a wide range of gaseous and particulate species.

Bibliography

[Allen et al., 1989] Allen, A. G., Harrison, R. M., and Erisman, J. W. (1989). Field measurements of the dissociation of ammonium nitrate and ammonium chloride aerosols. *Atmos. Environ.*, 23:1591–1599.

[Andersen et al., 1993] Andersen, H., Hovmand, M., Hummelshj, P., and Jensen, N. (1993). Measurements of ammonia flux to a spruce stand in Denmark. *Atmos. Env.*, 27A:189–202.

[ApSimon et al., 1994] ApSimon, H. M., Barker, B. M., and Kayin, S. (1994). Modelling studies of the atmosphericrelease and transport of ammonia - applications of the tern model to an emep site in england in anti-cyclonic conditions. *Atmos. Environ.*, 28:665–678.

[ApSimon et al., 1987] ApSimon, H. M., Kruse, M., and Bell, J. N. B. (1987). Ammonia emissions and their role in acid deposition. *Atmos. Environ.*, 21(9):1939–1946.

[Asman et al., 1988] Asman, W. A. H., Drukker, B., and Jansen, A. J. (1988). Modelled historical concentrations and depositions of ammonia and ammonium in Europe. *Atmos. Environ.*, 22:725–735.

[Asman and van Jaarsveld, 1992] Asman, W. A. H. and van Jaarsveld, H. A. (1992). A variable-resolution transport model applied for NH_x in Europe. *Atmos. Environ.*, 26A:445–464.

[Behra et al., 1989] Behra, P., Sigg, L., and Stumm, W. (1989). Dominating influence of NH_3 on the oxidation of aqueous SO_2: the coupling of NH_3 and SO_2 in atmospheric water. *Atmos. Env.*, 23:2691–2707.

[Benner et al., 1992] Benner, W., Ogorevc, B., and Novakov, T. (1992). Oxidation of SO_2 in thin water films containing NH_3. *Atmos. Env.*, 26(A):1713–1723.

[Bobbink et al., 1992] Bobbink, R., Boxman, D., Fremstad, E., Heil, G., Houdijik, A., and Roelofs, J. (1992). Critical loads for nitrogen eutrophication of terrestrial and wetland ecosystems based upon changes in vegetation and fauna. *Critical loads for Nitrogen*, pages 111–160.

[Breitenbach and Shelef, 1973] Breitenbach, L. P. and Shelef, M. (1973). Development of a method for the analysis of NO_2 and NH_3 by NO-measuring instruments. *J. Air Pollut. Control Assoc.*, 23:128–131.

[Brimblecombe, 1996] Brimblecombe, P. (1996). *Air composition and chemistry.* Cambridge University Press, Cambridge, second edition.

[Buijsman et al., 1987] Buijsman, E., Mass, H. F. M., and Asman, W. A. H. (1987). Anthropogenic NH_3 emissions in Europe. *Atmos. Environ.*, 21:1009–1022.

[Businger et al., 1971] Businger, J. A., Wingaard, J. C., Izumi, Y., and Bradley, E. (1971). Flux-profile relationships in the atmospheric surface layer. *Journal of Atmospheric Sciences*, 28:181–189.

[Carson, 1973] Carson, D. J. (1973). The development of a dry inversion-capped convectively unstable boundary layer. *Q.J.Roy. Met. Soc.*, 99:450–467.

[Cowell and ApSimon, 1998] Cowell, D. A. and ApSimon, H. M. (1998). Cost-effective strategies for the abatement of ammonia emissions from European agriculture. *Atmos. Environ.*, 32(3):537–580.

[Dragosits et al., 1998] Dragosits, U., Sutton, M. A., Place, C. J., and Bayley, A. (1998). 1998. *Environmental Pollution*, 102(S1):195–203.

[Duyzer et al., 1992] Duyzer, J., Verhagen, H., Weststrate, J., and Bosveld, F. (1992). Measurement of the dry deposition flux of NH_3 onto coniferous forest. *Env. Poll.*, 75:3–13.

[Dyer and Hicks, 1970] Dyer, A. J. and Hicks, B. (1970). Flux gradient relationships in the constant flux layer. *Q.J.R.Meteorol.Soc.*, 96:715–721.

[Erisman et al., 1996] Erisman, J., Mennen, M., Fowler, D., Flechard, C., Spindler, G., Grner, A., Duyzer, J., Ruigrok, W., and Wyers, G. (1996). Towards development of a deposition monitoring network for air pollution in Europe. Report 722108015, RIVM, Bilthoven, The Netherlands.

[Erisman et al., 1994] Erisman, J., van Pul, A., and Wyers, P. (1994). Parametrization of surface resistance for the quantification of atmospheric deposition of acidifying compounds and ozone. *Atmos. Env.*, 28:2595–2607.

[Farquhar et al., 1980] Farquhar, G., Firth, P., Wetselaar, R., and Weir, B. (1980). On the gaseous exchange of ammonia between leaves and the environment: determination of the ammonia compensation point. *Plant Physiol*, 66:710–714.

[Fehsenfeld et al., 2002] Fehsenfeld, F., Huey, L. G., Leibrock, E., Dissly, R., Williams, E., Ryerson, T. B., Norton, R., Sueper, D. T., and Hartsell, B. (2002). Results from an informal intercomparison of ammonia measurement techniques. *J. Geophys. Res.*, 107:4812.

[Ferm, 1979] Ferm, M. (1979). Method for the determination of atmospheric ammonia. *Atmos. Environ.*, 13:1385–1393.

[Finlayson and Pitts, 1986] Finlayson, B. J. and Pitts, J. N. (1986). *Atmospheric chemistry: fundamentals and experimental techniques.* Wiley.

[Finnigan, 2001] Finnigan, J. J. (2001). *Instrumentation II: vector wind sensors*, section 3.2. Advanced short course on agricultural, forest and micrometeorology. Universit degli studi di Sassari, Sassari.

[Fisher, 1978] Fisher, B. E. A. (1978). The calculations of long term sulphur deposition in Europe. *Atmos. Environ.*, 12:489–502.

[Flechard, 1988] Flechard, C. (1988). *Turbulentexchange of ammonia above vegetation.* PhD dissertation, University of Nottingham.

[Flechard and Fowler, 1998] Flechard, C. R. and Fowler, D. (1998). Atmospheric ammonia at a moorland site.I:The meteorological control of ambient ammonia concentrations and the influence of local sources. *Q.J.R.Meteorol.Soc.*, 124(547):733–757.

[Flechard et al., 1999] Flechard, C. R., Fowler, D., Sutton, M. A., and Cape, J. N. (1999). A dynamical chemical model of bi-directional ammonia exchange between semi-natural vegetation and the atmosphere. *Q.J.R.Meteorol. Soc.*, 125:1–33.

[Flechard, C. R. and Fowler, D., 1998] Flechard, C. R. and Fowler, D. (1998). Long term measurements of ammonia fluxes. Life report, CEH, Edinburgh.

[Fournier, 2003] Fournier, N. (2003). *Development of an atmospheric transport model simulating concentration and deposition of reduced nitrogen over the British Isles.* PhD dissertation, Edinburgh University.

[Fournier et al., 2004] Fournier, N., Dore, A. J., Vieno, M., Weston, K. J., Dragosits, U., and Sutton, M. A. (2004). Modelling the deposition of atmospheric oxidised nitrogen and sulphur to the united kingdomusing a multilayer long-range transport model. *Atmos. Environ.*, 38:683–694.

[Fowler, 2002] Fowler, D. (2002). *Pollutant deposition and uptake by vegetation*, section 4, pages 43–67. Air Pollution and Plant Life. John Wiley and Sons, Ltd., j.n.b. bell and m. treshow edition.

[Fowler and Duyzer, 1989] Fowler, D. and Duyzer, J. (1989). *Micrometeorological Techniques for the Measurement of Trace Gas Exchange*, pages 189–207. Exchange of Trace Gases between Terrestrial Ecosystems and the Atmosphere. John Wiley and Sons, Chichester, m.o. andreae and d.s. schimel edition.

[Fowler et al., 1991] Fowler, D., Duyzer, J. H., and Baldocchi, D. D. (1991). Inputs of trace gases, particles and cloud droplets to terrestrial surfaces. *Proc. Roy. Soc. Edinburgh*, 97B:35–59.

[Fowler et al., 1996] Fowler, D., Flechard, C., Milford, C., Hargreaves, K., Storeton-West, R., Nemitz, E., and Sutton, M. (1996). Towards development of a deposition monitoring network for air pollution in Europe: measurements of pollutant concentrations and deposition fluxes to moorland at Auchencorth Moss in Southern Scotland. LIFE project report 93/NL/A32/NL/3547, CEH Edinburgh, CEC, Brussels.

[Fowler et al., 1998a] Fowler, D., Flechard, C., Sutton, M., and Storeton-West, R. (1998a). Long-term measurements of the land-atmosphere exchange of ammonia over moorland. *Atmos. Env.*, 32:453–459.

[Fowler et al., 1995] Fowler, D., Hargreaves, K. J., Skiba, U., Milne, R., Zahniser, M., and Kaye, A. (1995). Measurements of CH_4 and N_2O fluxes at the landscape scale using micrometeorological methods. *Phil.Trans.Roy.Soc.London*, 351:339–356.

[Fowler et al., 2001] Fowler, D., Sutton, M. A., Flechard, C., Cape, J. N., Storeton-West, R., Coyle, M., and Smith, R. I. (2001). The control of SO_2 de[position on to natural surfaces by NH_3 and its effects on regional deposition. *Water, Air and Soil Pollution*, Focus 1:39–48.

[Fowler et al., 1998b] Fowler, D., Sutton, M. A., Smith, R. I., Pitcairn, C. E. R., Coyle, M., Campbell, G., and Stedman, J. (1998b). Regional mass budgets of oxidized and reduced nitrogen and their relative contribution to the N inputs of sensitive ecosystems. *Environ. Pollution*, 102:337–342.

[Fowler and Unsworth, 1979] Fowler, D. and Unsworth, M. H. (1979). Turbulent transfer of sulphur dioxide toa wheat crop. *Q.J.R.Meteorol. Soc.*, 105:767–783.

[Fuller et al., 1994] Fuller, R. M., Groom, G. B., and Jones, A. R. (1994). The land cover map of Great britain: An automated classification of Landsat thematic mapper data. *Photogramm. Eng. Remote Sens.*, 60:553–562.

[Garland, 1977] Garland, J. A. (1977). The dry deposition of sulphur dioxide to land and water surfaces. *Proceedings of the Royal Society of London*, 345(A):245–268.

[Garland et al., 1973] Garland, J. A., Clough, W. S., and Fowler, D. (1973). Deposition of sulphur dioxide on grass. *Nature*, 242:256–257.

[Genermont et al., 1998] Genermont, S. P., Cellier, P., Flura, D., Morvan, T., and Laville, P. (1998). Measuring ammonia fluxes after slurry spreading under actual field conditions. *Atmos. Environ.*, 32(3):279–284.

[Genfa et al., 1989] Genfa, Z., Dasgupta, P. K., and Dong, S. (1989). Measurement of atmospheric ammonia. *Environmental science and technology*, 23:1467–1474.

[Goodwin et al., 2000] Goodwin, J. W. L., Salway, A. G., Murrells, T. P., Dore, T. P., Passant, N. R., and Eggleston, H. S. (2000). UK emissions of air pollutants 1970 - 1998. *AEA Tachnology*, AEAT/R/EN/0270(ISBN 0-7058-1794-6).

[Goretty, 1998] Goretty (1998). *Development of an ammonia measurement and sampling system based on tunable diode laser spectroscopy.* PhD dissertation, University of Guelph, The Faculty of Graduate studies.

[Grace et al., 1995] Grace, J., Lloyd, J., McIntyre, J., Miranda, A., Meir, P., Miranda, H., Moncrieff, J., Massheder, J., Wright, I., and Gash, J. (1995). Fluxes of carbon dioxide and water vapour over an undisturbed tropical forest in south-west amazonia. *Glob. Ch. Biol.*, 1:1–12.

[Griffith and Galle, 2000] Griffith, D. W. T. and Galle, B. (2000). Flux measurements of NH_3, N_2O and CO_2 using dual beam FTIR spectroscopy and the flux-gradient technique. *Atmos. Environ.*, 34:1087–1098.

[Hicks et al., 1987] Hicks, B. B., Baldocchi, D. D., Meyers, T. P., Hosker, R. D., and Matt, D. R. (1987). A preliminary multiple resistance routine for deriving dry deposition velocities from measured quantities. *Water, Air and Soil Pollution*, 36:311–330.

[Hinkley et al., 1976] Hinkley, E. D., Ku, R. T., and Kelley, P. L. (1976). Techniques for detection of molecular pollutants by absorption of laser radiation. *Laser Focus: Tuneable lasers in the IR.*

[Horii et al., 1999] Horii, C. V., Zahniser, M. S., Nelson, D. D., McManus, J. B., and Wofsy, S. C. (1999). Nitric acid and nitrogen dioxide flux measurements: an application of tuneable diode laser absorption spectroscopy. *SPIE v.3758.*

[Hornung et al., 2002] Hornung, M., Ashmore, M., and Sutton, M. A. (2002). Environmental impacts of ammonia on semi-natural habitats. Technical report, DEFRA publication.

[Horst, 1997] Horst, T. W. (1997). A simple formula for attenuation of eddy fluxes measured with first-order-response scalar sensors. *Boundary Layer Meteorology*, 82:219–233.

[Jennings, 1980] Jennings, D. E. (1980). Absolute line strengths in ν_4, $12ch_4$: a dual-beam diode laser spectrometer with sweep integration. *Applied Optics*, 19(16):2695–2700.

[Kaimal and Businger, 1963] Kaimal, J. C. and Businger, J. A. (1963). A continuous wave sonic anemometer-thermometer. *J. Appl. Meteorol*, 2:156–164.

[Kaimal and Finnigan, 1994] Kaimal, J. C. and Finnigan, J. J. (1994). *Atmospheric Boundary Layer flows.* Oxford Univerity Press, New York, Oxford, second edition.

[Kaimal and Gaynor, 1991] Kaimal, J. C. and Gaynor, J. E. (1991). Another look at sonic thermometry. *Boundary Layer Meteorology*, 56:401–410.

[Kaimal et al., 1972] Kaimal, J. C., Wyngaard, J. C., Izumi, J., and Cote, O. R. (1972). Spectral characteristics of surface-layer turbulence. *Q.J.R.Meteorol.Soc.*, 98:563–589.

[Keuken et al., 1988] Keuken, M.P.and Schoonebeek, C. A. M., Van-wensveenlouter, A., and Slanina, J. (1988). Simultaneous sampling of NH_3, HNO_3, HCl, SO_2 and H_2O_2 in ambient air by a wet annular denuder system. *Atmos. Environ.*, 22(11):2541–2548.

[Kolmogorov, 1941] Kolmogorov, A. N. (1941). The local structure of turbulence in incompressible viscous fluid for very large reynolds numbers. *Doklady ANSSSR*, 30:301–304.

[Kormann and Meixner, 2001] Kormann, R. and Meixner, F. X. (2001). An analytical footprint model for non-neutral stratification. *Bound.-Layer Met.*, 99:207 – 224.

[Lachish et al., 1987] Lachish, U., Rotter, S., Adler, E., and Hel-Hanany, U. (1987). Tunable diode laser based spectroscopic system for ammonia detection in human respiration. *Review of Scientific Instrumentation*, 58(6):923–927.

[Lawes et al., 1883] Lawes, J. B., Gilbert, J. H., and Warrington, R. (1883). New determination of the ammonia, chlorine and sulphuric acid in the rainwater collected at rothamsted. *Journal of the Agricultural Society of England*, 19:313–331.

[Lenschow and Raupach, 1991] Lenschow, D. H. and Raupach, M. R. (1991). The attenuation of fluctuations in scalar concentrations through sampling tubes. *Journal of Geophysical Research - Atmosphere*, 96(15):15259–15268.

[Leuning and Moncrieff, 1990] Leuning, R. and Moncrieff, J. (1990). Sensitivity and damping of fluctuations in air sampling tubes. *Boundary Layer Meteorology*, 53:63–76.

[Lindsay, 1995] Lindsay, R. (1995). *Bogs: The Ecology, Classification and Conservation of Ombrotrophic Mires.* Scottish National Heritage, Perth.

[Massman, 1991] Massman, W. J. (1991). The attenuation of concentration fluctuations in turbulent flow through a tube. *Journal of Geophysical Research - Atmosphere*, 96(15):15269–15273.

[McManus J.B., 2001] McManus J.B., Nelson D.D., Z. M. (2001). *tunable diode laser system.* Aerodyne Research Inc., Billerica, MA, USA.

[Meetham, 1950] Meetham, A. R. (1950). Natural removal of pollution from the atmosphere. *Quarterly journal of the Royal Meteorological Society*, 76:359–371.

[Metek, 2001] Metek (2001). *USA-1 User Manual.* Metek GmbH, Elmshorn, Germany.

[Milford et al., 2001] Milford, C., Theobald, M. R., Nemitz, E., and Sutton, M. A. (2001). Dynamics of ammonia exchange in response to cutting and fertilising in an intensively-managed grassland. *Water, Air and Soil Pollution*, 1:167–176.

[Miranda et al., 1984] Miranda, A. C., Jarvis, P. G., and Grace, J. (1984). Transpiration and evaporation from heather moorland. *Bound.-Layer Met.*, 28:227–243.

[Misselbrook et al., 2000] Misselbrook, T., Van Der Weerden, T. J., Pain, B. F., Jarvis, S. C., Chambers, B. J., Smith, K. A., Philips, V. R., and Demmers, T. G. M. (2000). Ammonia emission factors for UK agriculture. *Atmos. Environ.*, 34:871 –880.

[Monin and Obukhov, 1954] Monin, A. S. and Obukhov, A. M. (1954). Basic laws of turbulent mixing in the ground layer of the atmosphere. *Trans. Geophys. Inst. Akad. Nauk. USSR*, 151:163–187.

[Monteith and Unsworth, 1990] Monteith, J. L. and Unsworth, M. H. (1990). *Priciples of environmental physics.* Edward Arnold, London, second edition.

[NEGTAP, 2001] NEGTAP (2001). Transboundary air pollution: acidification, eutrophication and ground-level ozone in the UK. Technical report, Centre for Ecology and Hydrology Edinburgh, Penicuik, Midlothian, UK.

[Nilsson and Grennfelt, 1988] Nilsson, J. and Grennfelt, P. (1988). Critical loads for sulphur and nitrogen. Report of the Skokloster workshop. Miljrapport 15, Nilsson, J. and Grennfelt, P. (Eds), Nordic Council of Ministers, Copenhagen.

[Nowak et al., 2002] Nowak, J. B., Huey, L. G., Eisele, F. L., Tanner, D. J., Mauldin, R. L., Cantrell, C., Kosciuch, E., and Davis, D. D. (2002). Chemical ionization mass spectrometry technique for detection of dimethylsulfoxide and ammonia. *J. Geophys Res.*, 107:4643.

[Panofsky, 1963] Panofsky, H. (1963). Determination of stress from wind and temperature measurements. *Q.J.R.Meteorol. Soc.*, 89:85–94.

[Panofsky and Dutton, 1984] Panofsky, H. A. and Dutton, J. A. (1984). *Atmospheric turbulence.* Wiley-Interscience, NewYork.

[Pitcairn et al., 1991] Pitcairn, C. E. R., Fowler, D., and Grace, J. (1991). Changes in species composition of semi-natural vegetation associated with the increase in atmospheric inputs of nitrogen. *Report to Nature Conservancy Council, Institute of Terrestrial Ecology, Edinburgh.*

[Pushkarsky et al., 2002] Pushkarsky, M. B., Webber, M. E., Baghdassarian, O., Narasimhan, L. R., and Patel, C. K. N. (2002). Laser-based photoacoustic ammonia sensor for industrial applications. *Applied Physics B special issue: Trends in laser sources, spectroscopic techniques and their application to gas detection*, 75:391–396.

[Reynolds et al., 1997] Reynolds, B., Fowler, D., Smith, R. I., and Hall, J. R. (1997). Atmospheric inputs and catchment solute fluxes for major ions in five welsh upland catchments. *J. Hydrol.*, 194:305–329.

[RGAR, 1997] RGAR (1997). *Acid Deposition in the United Kingdom 1992-94.* Fourth Report of the Review Group on Acid Rain. Department of the Environment, Transport and the Regions, London, UK.

[Rooth et al., 1990] Rooth, R. A., Verhage, A. J. L., and Wouters, L. W. (1990). Photoacoustic measurements of ammonia in the atmosphere - influence of water vapour and carbon dioxide. *Appl. Optics*, 29:3643–3653.

[Rothman, 2004] Rothman, L. S. e. a. (2004). The hitran molecular spectroscopic database: edition of 2000 including updates through 2001. *Journal of Quantitative spectroscopy and Radiative Transfer.*

[Schendel et al., 1990] Schendel, J. S., Stickel, R. E., A., V. C., Sandholm, S. T., Davis, D. D., and Bradshaw, J. D. (1990). Atmospheric ammonia measurement

using a VUV photo-fragmentation laser-induced fluorescence technique. *Appl. Optics*, 29:4924–4937.

[Schiff et al., 1987] Schiff, H. I., Harris, G. W., and Mackay, G. I. (1987). *Measurement of atmospheric gases by laser absorption spectroscopy*, volume 349 of *The Chemistry of acid rain: sources and atmospheric processes, ACS Symposium ser.*, chapter 24, pages 274–288. American Chemical Society, Washington DC, r.w. johnson and g.e. gordon edition.

[Schiff et al., 1994] Schiff, H. I., Mackay, G. I., and Bechara, J. (1994). *Air monitoring by spectroscopic techniques.* John Wiley and Sons, New York.

[Schmid., 2002] Schmid., H. P. (2002). Footprint modeling for vegetation atmosphere exchange studies: a review and perspective. *Agricultural and Forest Meteorology*, 113:159–183.

[Schuepp et al., 1990] Schuepp, P., Leclerc, M., MacPherson, J., and Desjardins, R. (1990). Footprint prediction of scalar fluxes from analytical solutions of the diffusion equation. *Bound.-Layer Met.*, 50:355–373.

[Shaw and Finnigan, 2001] Shaw, R. H. and Finnigan, J. J. (2001). *Atmospheric turbulence and diffusion*, section 1.4. Advanced short course on agricultural, forest and micrometeorology. Universit degli studi di Sassari, Sassari.

[Shaw and Spicer, 1998] Shaw, W. J. and Spicer, C. W. e. a. (1998). Eddy-correlation fluxes of trace gases using a tandem mass spectrometer. *Atmos. Environ.*, 32(17):2887–2898.

[Silver et al., 1991] Silver, J. A., Bomse, D. S., and Stanton, A. C. (1991). Diode laser measurements of trace concentrations of ammonia in an entrained-flow coal reactor. *Applied Optics*, 30(12):1505–1511.

[Singles et al., 1998] Singles, R., Sutton, M. A., and Weston, K. J. (1998). A multi-layer model to describe the atmospheric transport and deposition of ammonia in great britain. *Atmos. Environ.*, 32(3):393–399.

[Smith et al., 2000] Smith, R. I., Fowler, D., Sutton, M. A., Flechard, C., and Coyle, M. (2000). Regional estimation of pollutant gas dry deposition in the UK: model description, sensitivity analyses and outputs. *Atmos. Environ.*, 34:3757–3777.

[Soderlund and Svensson, 1976] Soderlund, R. and Svensson, B. H. (1976). *The global nitrogen cycle*, volume 22 of *Nitrogen, Phosphorus and Sulphur - Global cycles*, pages 23–73. Ecol. Bull., Stockholm.

[Sommer et al., 1995] Sommer, S., Mikkelsen, H., and Mellqvist, J. (1995). Evaluation of meteorological techniques for measurements of ammonia loss from pig slurry. *Agricultural and Forest Meteorology*, 74:169–179.

[Stull, 1988] Stull, R. B. (1988). *An introduction to boundary layer meteorology.* Kluwer Academic Publishers, Dordrecht.

[Sutton and Fowler, 1993] Sutton, M. and Fowler, D. (1993). *A model for inferring bi-directional fluxes of ammonia over plant canopies*, pages 179–182. Proceedings of the WMO conference on the measurement and modelling of atmospheric composition changes including pollution transport. World Meteorological Organization, Geneva, j.n.b. bell and m. treshow edition.

[Sutton et al., 1993a] Sutton, M., Fowler, D., and Moncrieff, J. (1993a). The exchange of atmospheric ammonia with vegetated surfaces. i: Unfertilized vegetation. *Quart. J. Roy. Met. Soc.*, 119:1023–1045.

[Sutton et al., 1993b] Sutton, M., Pitcairn, C., and Fowler, D. (1993b). The exchange of ammonia between the atmosphere and plant communities. *Adv. Ecol. Res*, 24:301–393.

[Sutton et al., 1995a] Sutton, M., Schjrring, J., and Wyers, G. (1995a). Plant-atmosphere exchange of ammonia. *Phil. Trans. Roy. Soc. London*, A351:261–278.

[Sutton et al., 1994] Sutton, M. A., Asman, W. A. H., and Schjoerring, J. K. (1994). Dry deposition of reduced nitrogen. *Tellus*, 46B:255–273.

[Sutton and Burkhardt, 1995] Sutton, M. A. and Burkhardt, J. K., e. a. (1995). Measurement and modelling of ammonia exchange over arable croplands. *Journal of Geophysical Research - Atmosphere*, 96(15):15259–15268.

[Sutton et al., 2000] Sutton, M. A., Dragosits, U., Tang, Y. S., and Fowler, D. (2000). Ammonia emissions from non-agricultural sources in the UK. *Atmos. Environ.*, 34:855–869.

[Sutton et al., 1993c] Sutton, M. A., Fowler, D., Hargreaves, K. J., and Storeton-West, R. L. (1993c). Interactions of NH_3 and SO_2 exchange inferred from simultaneous measurements over a wheat canopy. *General Assessment of Biogenic Emissions and Deposition of Nitrogen Compounds, Sulphur Compounds and Oxidants in Europe, Air Poll. Res. Rep*, 47:173–190.

[Sutton et al., 1993d] Sutton, M. A., Fowler, D., Moncrieff, J. B., and Storeton-West, R. L. (1993d). The exchange of atmospheric ammonia with vegetated surfaces. ii: Fertilized vegetation. *Quart. J. Roy. Met. Soc*, 119:1047–1070.

[Sutton et al., 1993e] Sutton, M. A., Fowler, D., Smith, R. I., Eager, M., Place, C. J., and Asman, W. A. H. (1993e). *Modelling the net exchange of reduced nitrogen*, volume 47 of *General assessment of biogenic emissions and depositions of nitrogen compounds, sulphur compounds and oxidants in Europe*, pages 117–131. CEC, Brussels, slanina, angeletti, beilke edition.

[Sutton et al., 1998] Sutton, M. A., Lee, D. S.and Dollard, G. J., and Fowler, D. (1998). Development of resistance models to describe measurements of bi-directional ammonia surface-atmosphere exchange. *Atmos. Environ.*, 32:473–480.

[Sutton et al., 2000] Sutton, M. A., Nemitz, E., Milford, C., Fowler, D., Moreno, J., San Jos, R., Wyers, G. P., Otjes, R. P., Harrison, R., Husted, S., and Schjoerring, J. K. (2000). Micrometeorological measurements of net ammonia fluxes over oilseed rape during two vegetation periods. *Agricultural and Forest Meteorology*, 105(4):351–369.

[Sutton et al., 1995b] Sutton, M. A., Place, C. J., Eager, M., Fowler, D., and Smith, R. I. (1995b). Assessment of the magnitude of ammonia emissions in the united kingdom. *Atmos. Environ.*, 29:1393–1411.

[Svensson and Ferm, 1993] Svensson, L. and Ferm, M. (1993). Mass transfer coefficient and equilibrium concentration as a key factor in a new approach to estimate ammonia emission from livestock manure. *Journal of agricultural engineering research*, 56:1–11.

[Tang et al., 2001] Tang, Y. S., Cape, J. N., and Sutton, M. A. (2001). Development and types of passive samplers for monitoring atmospheric NO_2 and NH_3 concentrations. *Scientific World*, pages 513–529.

[Thom, 1975] Thom (1975). *Momentum, mass and heat exchange of plant communities*, volume 1 of *Vegetation and the Atmosphere*, pages 55–79. Academic Press, London.

[Trebs et al., 2004] Trebs, I., Meixner, F. X., Slanina, J., Otjes, R., Jongejan, P., and Andreae, M. O. (2004). Real-time measurements of ammonia, acidic trace gases and water-soluble inorganic aerosol species at a rural site in the amazon basin. *Atmospheric Chemistry and Physics*, 4:967–987.

[Tuazon et al., 1978] Tuazon, E. C., Graham, R. A., Winer, A. W., Easton, R. R., Pitts, J. N., and Hanst, P. L. (1978). A kilometer path-length Fourier-transform infrared system for the study of trace pollutants in ambient and synthetic atmospheres. *Atmos. Environ.*, 12:865–875.

[Van Hove et al., 1987] Van Hove, L. W. A., Koops, A. J., Adema, E. H., Vrendenberg, W. J., and Pieters, G. A. (1987). Analysis of the uptake of atmospheric ammonia by leaves of Phaseolus-Vulgaris. *Atmos. Environ.*, 21:1759–1763.

[Vieno, 2005] Vieno, M. (2005). PhD dissertation, Edinburgh University, Institute of Atmospheric and Environmental Science.

[Warland et al., 2001] Warland, J. S., Dias, M. D., and Thurtell, G. W. (2001). A tunable diode laser system for ammonia flux measurem,ents over multiple plots. *Environ. Pollut.*, 114:215–221.

[Webb, 1970] Webb, E. (1970). Profile relationships: the log-linear range and extension to strong stability. *Q.J.R.Meteorol. Soc.*, 96:67–90.

[Weiss and Norman, 1985] Weiss, a. and Norman, J. M. (1985). Partitioning solar radiation into direct and diffuse, visible and near-infrared components. *Agricultural and Forest Meteorology*, 34:205–213.

[Werle, 1998] Werle, P. (1998). A review of recent advances in semiconductor laser based gas monitors. *Spectrochimica Acta Part A*, 54:197–236.

[Werle, 1999] Werle, P. (1999). Laser optical sensors in situ gas analysis. *Recent Research Developments in Optical Engineering*, 2.

[Weston, 1992] Weston, K. J. (1992). Objectivity analysed cloud immersion frequencies for the United Kingdom. *Meteorological Magazine*, 121:108–111.

[Wyers, 1998] Wyers, G.P.and Erisman, J. W. (1998). Ammonia exchange over coniferous forest. *Atmos. Environ.*, 32(3):441–451.

[Wyers and Slanina, 1993] Wyers, G.P.and Otjes, R. and Slanina, J. (1993). A continuous-flow denuder for the measurement of ambient concentrations and surface-exchange fluxes of ammonia. *Atmos. Env.*, 27(A):2085–2090.

[Wyngaard and Cote', 1972] Wyngaard, J. C. and Cote', O. R. (1972). Cospectral similarity in the atmospheric surface layer. *Quart.J.Roy. Meteor. Soc.*, 98:590–603.

[Zahniser et al., 1997] Zahniser, M. S., Nelson, D. D., and McManus, J. B. (1997). *A tuneable diode laser system for atmospheric trace gas flux measurements.* Aerodyne Research Inc., Billerica, MA, USA.

[Zahniser et al., 1995] Zahniser, M. S., Nelson, D. D., McManus, J. B., and L., K. (1995). Measurements of trace gas fluxes using tunable diode laser spectroscopy. *Philosophical Transactions of the Royal Society*, 351:371–382.